AD-A119 536 ITT GILFILLAN VAN NUYS CA F/G 17/9
FREQUENCY SCANNING RADAR CONCEPTS FOR ARMY HIGH ENERGY LASER WE--ETC(U)
APR 82 C BARFIELD, D EPPS, S HOWARD DAAH01-81-C-A782
UNCLASSIFIED NL

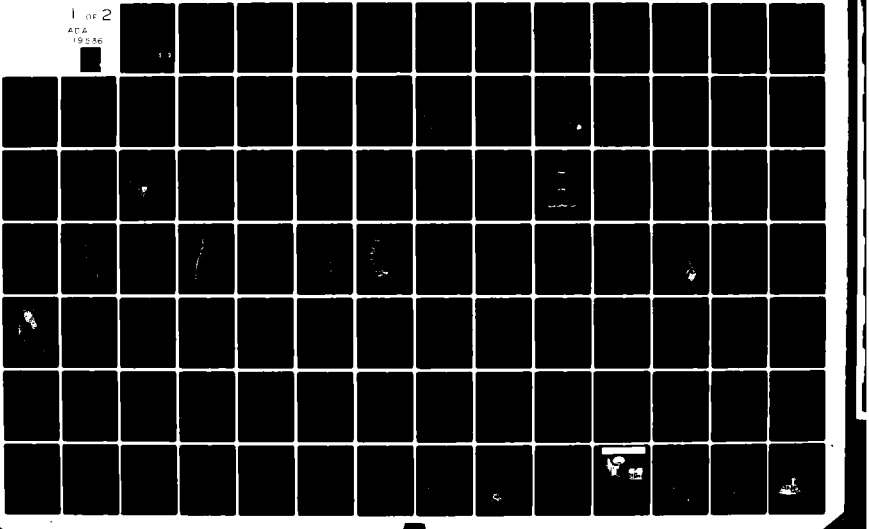

DAAH01-81-C-A782 CDRLA004

FREQUENCY SCANNING RADAR CONCEPTS FOR ARMY HIGH ENERGY LASER WEAPONS

C. Barfield, D. Epps, S. Howard
ITTGilfillan
7821 Orion Avenue
Van Nuys, California 91409

April 1982

Final Report Volume I

U. S. ARMY MISSILE COMMAND
DRSMI-RHS
Redstone Arsenal, Alabama

DAAH01-81-C-A782 CDRLA004

FREQUENCY SCANNING RADAR CONCEPTS FOR ARMY HIGH ENERGY LASER WEAPONS

DISTRIBUTION UNLIMITED

C. Barfield, D. Epps, S. Howard
ITTGilfillan
7821 Orion Avenue
Van Nuys, California 91409

April 1982

Final Report Volume I

U. S. ARMY MISSILE COMMAND
DRSMI-RHS
Redstone Arsenal, Alabama

CONTENTS

VOLUME 1

HELVADS/FALW/FALW-D

LIST OF FIGURES

LIST OF TABLES

1.0 INTRODUCTION

The data presented in this volume consists of concepts, design approaches, configurations and analyses with recommendations for frequency scanning radars compatible with the target acquisition subsystem requirements of the HELVADS, FALW and FALW-D weapon systems. In arriving at recommendations for the three subsystem requirements, a number of candidates were examined and reported on in the monthly progress reports. These candidate configurations for FSR's, with brief descriptions indicating the more important advantages, disadvantages and reasons for recommendation or non-recommendation have been included. In those instances where an overall acquisition subsystem group is shown as opposed to strictly FSR configurations, brief descriptive data for those elements other than FSR data was included, however, time and scope of effort limited data to the level necessary only to provide an understanding of the integrated group concept.

1.1 Scope of the Study

This report presents the findings of the FALW/HELVADS Frequency Scanning Radar study conducted by ITTG over the period April 1981 and February 1982. During this period eight monthly reports were submitted and this is the final and summarizing report.

The study was limited to a top level conceptual review and analysis of radar postulate systems for both HELVADS and FALW. Recommendations are made for HELVADS, FALW and FALW-D. Cost estimates and life cycle costs for representative system quantities are provided.

2.0 Study Requirements

The study requirements are as defined in the Technical Requirement 1-81 FALW/HELWS FREQ SCANNING RADARS 21 August 1980. Attachment 1 to DAAH01-81-C-A782. In summary they are:

1) Establish the baseline requirements for separate frequency scanning radars to meet the needs of HELWS (now HELVADS) and FALW.

2) Develop at least two configurations for both HELVADS and FALW.

3) Recommend a single configuration for both HELVADS and FALW.

4) Recommend a radar approach to a demonstration program for FALW (named FALW-D).

5) Develop cost and life cycle costs for the frequency scanning radars for HELVADS and for FALW.

2.1 HELVADS and Study Overview

Analysis of the mission data for the HELVADS and FALW systems resulted in the conclusion that the two systems require similar hardware. Although the threat target list appears to be skewed in favor of shorter ranges, and ground target scenarios appear to predominate for the FALW system, manned and unmanned airborne targets and ground targets are included in the missions for both systems.

The performance parameters most difficult to achieve were apparent early in the analysis; volumetric coverage from an acquisition subsystem colocated on the weapon vehicle, angular accuracy, and the extraction of reliable elevation positional data from ground targets. The small radar cross section of specific air targets presented a problem in detection with an aperture compatible with the size and weight limitations imposed by general mobility requirements and the FVS configuration. Volumetric coverage with colocated acquisition and weapon elements is difficult because of masking and beam interference. It becomes readily obvious that without multiple SAS antennae, avoidance of interference/masking is feasible only with coaxial or quasi coaxial weapon and SAS radiators/apertures. A coaxial configuration was considered and is described briefly in this report. The two major disadvantages are readily seen in the drawings, the height of the coelostat and radar tends to exceed the highway travel maximum height limit and requires a complex annular rotary r.f. coupler, in addition to complicating the slip ring components for signal interface. The overall height problem with coaxial weapon/radar configuration could be solved by a telescoping or extendable/retractable coelostat/radar mast mechanism, however the additional complexity introduced into both the laser optical train and the radar head interface with the remainder of the system is significant. If the coaxial configuration is not adopted, the coverage requirement necessitates multiple antennas located on the sides and ends of the vehicle to avoid masking by the laser, assuming central mounting of the coelostat assembly. Both configurations are described in the report. Achievement of the coverage requirements with multiple antennas while limiting the vehicle space budget for the SAS alone constituted another problem. Two recommended candidates for the HELVADS/FALW requirements are described; one is a conventional two array (back-to-back) radially rotated radar head

mounted coaxially with the coelostat, whereas the second is a unique antenna design generated to avoid the space requirement of conventional radially rotated arrays while providing the required coverage. The antenna defined for the second candidate is an axially rotated planar array. Four arrays are required for coverage and are mounted in the corners of the vehicle enclosure behind the cab. A similar configuration was examined in which the forward array was placed in front of the vehicle with mechanical mounts to fold the arrays down and to the center of the vehicle to avoid masking the operators vision, and to avoid protrusion beyond the sides of the vehicle during travel. This configuration was not recommended, however, because of the potential for mechanical interference because of the vehicle hood fold-over design and because of the potential for damage in transit. The arrays in all configurations are covered by radomes. In the axially rotated design, the radome is a disc/cylinder with approximately two inches of clearance between the inner surfaces of the radome and the antenna proper. The antenna assembly is removable from the rear of the radome and the radome front cover is removable to permit inspection of the array surfaces.

An early tracking analysis (Ref. Monthly Report: Technical Report for HELVADS/FALW/FALW-D, Conceptual Analysis & Design (For Period 06 July through 15 August 1981 Contract DAAHOI-81-C-A-782; CDRLA002) indicated the magnitude of the problem in achieving the required accuracy of 1.0 milliradian total positional uncertainty with the radar for the conditions and targets examined. In view of the unavoidable additional degradation in accuracy which would occur in transferral of the position data to the FCS sensor, a determination was made to include a small millimeter wave tracker directly linked to the first FCSS sensor (FLIR). In operation the FSR will provide volumetric coverage in accordance with mission requirements, handing over air targets selected for engagement or rapidly approaching the predetermined engagement criteria, to the millimeter wave tracker, which after track initiation "hands" the target over to the first FCSS sensor. Depending on the air situation (pressure of additional threat targets approaching engagement criteria), the millimeter tracker would continue to track the target through engagement to provide damage or kill assessment. An effort was made to identify an existing millimeter wave tracker compatible with the requirements. The latter effort was only partially successful although time constraints did not permit an exhaustive search. Two millimeter wave trackers were located which are parts of complete foreign made acquisition systems, the Marconi Blindfire radar and Hollandse Signaall LIRD-8 system. These systems include radar heads

which are significantly higher in power output than the requirement and both have larger apertures than required for the range of concern. Although the radar head portions of these systems would greatly exceed the performance requirements for the millimeter wave tracker, both are unsatisfactory from size, weight, input power and general mechanical aspects for mechanically coupled (to FCSS sensor) on-vehicle application. The feasibility of adopting selected elements from either system may warrant consideration later. The search for an existing millimeter wave tracker was weighted toward ground systems developers, however, one interesting development project intended for missile seeker application was found and is included in the appendices. The latter concerns a 35 GHz active aperture developed at Motorola, Inc. This development was done under the auspices of the Ballistic Missile Defense Agency, Redstone Arsenal for the Endo Atmospheric non-nuclear Kill (ENNK) Fuse Program. The device described in the referenced paper was based on a 5.5 inch aperture with relatively low total radiated peak power. It is reasonable to assume that a larger slotted aperture with a higher power source could be developed. In the virtual image concept described, power from four Impatt sources (injection locked) is fed to 32 image radiating elements and power from the radiating elements is combined in space. The result according to the report is a compact and efficient transmitter avoiding the r.f. losses normally associated with feed transmission lines. The frequency (35 GHz) is compatible with range requirements for this application from the standpoint of propagation, however, a different frequency may be necessary for entirely hardware related limitations. (Ref. Appendix Model for resonant transmittance in the millimeter wave region: Paper by J. H. Piercuissi, K. Torriyama, D. Fowler of the Univ. of Texas and R. Gomez of Atmospheric Sciences Lab, White Sands Missile Range, New Mexico).

The requirement in all configurations for accurate target elevation data (equal in accuracy to the azimuth position data) presents a severe problem insofar as ground targets are concerned because of multipath effects on elevation data accuracy. In consideration of extensive experience, and data collected over an extended period with narrow and wide beam radars illuminating low angle targets, the conclusion was reached early in the analysis that a narrow beam optical system is required for ground target elevation data in all system configurations.

Several imaging optical approaches were considered, however, all suffered from the difficulty in automating the target detection, verification and processing function. Mission operational requirements; high speed multiple threat targets in day and night attack scenarios necessitate a fully automatic system with operator intervention/control capability, but reaction time will

not permit operator manual detection/evaluation and system positioning. As visualized in this analysis, operator override would be limited to final firing decision and selection for engagement between targets of equal threat value.

The optical adjunct recommended in this analysis consists of a narrow beam coherent laser scanning radar (CLSR). The CLSR is directed to the target by the r.f. radar and is capable of defeating the multipath problem inherent in r.f. radar systems by virtue of an extremely narrow beamwidth. Large volume coverage with the CLSR would be prohibitive because of time requirements for scanning a hemisphere with a narrow beam, however, in the concept recommended, volume coverage is provided by the FSR and the CLSR is primarily used to obtain elevation data on ground targets. The CLSR does, however, have the capability to track air targets selected for engagement and could provide a valuable data contribution in multiple air target scenarios. The necessarily narrow beamwidth obviously limits coverage in terms of contribution to the total volumetric coverage (hemispheric-plus), however, in the absence of ground target threats the CLSR can provide useful data in the situation in which multiple airborne targets are approaching engagement range in relatively close sequence. In the latter situation the CLSR could increase the data rate providing equal or greater position data accuracy than the millimeter tracking radar linked to a FLIR subsystem.

In the FALW-D requirement a number of approaches were examined and several approaches were considered to be equally feasible. Again, in order to achieve the angular accuracy requirement in elevation, a technique immune to multipath effects is required. In view of the application, i.e. demonstration, of the FALW-D, the feasibility of using a manually initiated optical sight which would be initially pointed by the radar to the target area (ground targets), then aligned on the ground target by the operator, was considered. This low cost approach, while feasible with single target scenarios, was found to be marginal with simultaneous double and triple target scenarios. As a consequence, the CLSR was also specified in the FALW-D configuration to cope with the ground target requirement.

The approaches recommended for the mission compatible systems (HELVADS/FALW) would obviously meet (and surpass) the FALW-D demonstration requirements. In view of the far less demanding requirements for the latter, for cost and time to develop factors the recommended approach for FALW-D is based on the use of existing r.f. radars (with modification), integration circuitry and the CLSR as indicated above. The active portions of these subsystem elements would be mounted on a flat bed general purpose vehicle and operator controls/recording equipment and displays are installed in an S-280 or similar type shelter.

2.1.1 Configurations Examined

A series of FSR configurations were examined before selection of the two configurations presented herein as recommendations. The FSR approaches examined included the following: (Note 1)

a) Single planar radially rotated arrays fore and aft on vehicle cargo area.

b) Single planar radially rotated array on aft cargo area and a single planar radially rotated array mounted with a retracting deployment mechanism in front of the vehicle.

c) Two separate planar arrays rotated around the laser vertical column. (Note 2.)

d) A single pair of back-to-back planar arrays located over and coaxially to the coelostat vertical support/housing.

e) Two back-to-back pairs of planar arrays mounted on offset supports over and to each side of the coelostat horizontal housing.

f) Four non-rotating planar arrays mounted at the base of the laser vertical support, each array providing 90 degrees coverage in azimuth. (Note 2.)

g) Four axially rotated planar arrays mounted fore and aft and on each side of the vehicle cargo area. (Note 3.)

h) A variation on g) above in which an axially rotated planar array is mounted on each side of the cargo area, and rear end of the vehicle, but the forward array is mounted on an extendable/retractable mechanism in front of the cab.

NOTE 1: This description relates to the frequency scanning radar portion only; for purposes of simplicity the millimeter wave tracker and coherent laser radar included in the final recommendations have been omitted.

NOTE 2: These configurations were considered prior to receipt of information relative to the selection of the FVS Carrier as the system vehicle, and prior to receipt of information indicating the high probability that a coelostat laser configuration would be adopted.

NOTE 3: Recommended configurations.

2.1.3 Rationale for Selection of Recommended Configurations

The two configurations recommended as a result of the analyses were selected on the basis of several parameters including performance, vehicle and contiguous subsystem compatibility, space limitation, development risk, and cost. These parameters are addressed individually in the following subparagraphs.

2.1.3.1 Performance

All of the individual radar configurations examined were capable of meeting the requirements for detection range, coverage (without consideration for masking by other system elements, or masking contiguous subsystems by the radar or interference with the vehicle operation). System and subsystem physical compatibility was a prime problem in all configurations.

2.1.3.1.1 Frequency

The frequency chosen was selected for a combination of reasons; to avoid the very serious interference (overcrowding) to be expected in the X-band portion of the spectrum, to achieve the beam dimensions desired with apertures of acceptable size, the availability of power sources compatible with the duty cycles required, and the availability of solid-state low noise preamplifier devices with acceptable noise figures. The aperture size selected (approximately 40 inches overall) appears to be acceptable, in that the required combination of coverage and range can be achieved without masking other subsystems. By axially rotating the planar array, the coverage is obtained without the vehicle space dedication necessary with a conventional radially rotated antenna.

2.1.3.1.2 Antenna Configuration and Scan Coverage

The axially rotated planar array using ferrite phase shifters in each slotted waveguide radiator element was selected to provide the wide coverage (required from each radar head) with the smallest space allocation. This configuration is unique, however the alternative to achieve the necessary coverage without masking is an array or pair of arrays over the coelostat in a coaxial or quasi coaxial relationship to the coelostat vertical support. The coaxial approach is also unique in that an annular r.f. coupler and annular slip ring assembly is required in configurations in which the radar is located coaxially with

the laser radiator support assembly. ITT-Gilfillan has done a significant amount of work with annular coupler designs at S-band, including fabrication/testing of an S-band coupler (reduced size), however, additional design/analysis is required to test the S-band coupler design concept at the higher frequency selected for the HELVADS/FALW candidates. It is readily obvious that the overall coelostat assembly would be rendered more complex by the inclusion of an r.f. coupler and signal/power slip ring assemblies.

The axially rotated planar array is housed in a radome, however the latter is relatively "thin" as compared to the overall envelope dimensions for a conventional tilted-back array rotated radially. The selected approach provides a low compact envelope in which a portion of the assembly is within the vehicle cargo area housing while a portion of the array radome extends above the shelter top line.

2.1.3.1.3 Transmitter

The requirements for frequency agility, bandwidth, variable p.r.f., and cost left little or no choice in selecting the power source. A grid modulated traveling wave tube final amplifier in a fully coherent master oscillator power amplifier (MOPA) chain was selected. The transmitter or transceiver shares a digitally controlled frequency synthesizer in which the prime frequencies are provided by high stability crystal oscillators. The selected oscillators are mixed to generate the output frequencies selected via the control processor. The output of the synthesizer is then up-converted in the transmitter to drive the output TWT stage, and/or to serve as the local oscillator input to mixers in the receiver portion of the transceiver. The up-converted synthesizer output is amplified to the level necessary to drive the final amplifier by a solid state frequency multiplier and amplifier.

2.1.3.1.4 Receiver

As indicated in the foregoing paragraph, the digitally controlled synthesizer provides the local oscillator (LO) for the receiver. A low noise pre-amplifier "front end" design employing a GaAs FET amplifier was selected as the first amplifier in the receiver chain. Currently devices are available with noise figures between 5 to 6 dB over the frequency range selected providing 20 to 25 dB of amplification.

2.1.3.1.5 Adjunct Subsystems

The recommended FSR based surveillance/acquisition subsystem (SAS) includes two subsystems which are listed in the recommendation, but which are not addressed in detail to this analysis. Those subsystems include a small millimeter wave monopulse tracking radar (MWTR) and a coherent laser scanning radar (CLSR).

The wide range of threat targets encompassed in the HELVADS and FALW system mission and the target position accuracy which must be provided to the FCS improve formidible requirements on the surveillance/acquisition radar. Based on the analyses performed, the ground target threat presents a problem which would be extremely difficult, if possible at all, in a wide coverage radar without the limitation of a mobile system. The limitation, as discussed in the monthly progress reports, is largely in the degradation to be expected from multipath effect on elevation data accuracy. An additional problem concerns the ability to provide the angle accuracy required by the FSC with a wide coverage radar meeting the other surveillance and acquisition subsystem requirements on the airborne targets at the velocities required and under the target maneuvers specified in the threat summary guidance provided for the analyses. The tracking analysis completed early in the project has been included in the Appendix (Appendix A). In addition to the basic accuracy attainable by the radar, additional degradation is inevitable in the transmission of that data to the FCS. Accordingly, a small millimeter wave tracker is recommended as a part of the surveillance and acquisition subsystem which would be physically mounted with the FCS sensor directed by the FSR data. The millimeter wave tracking radar (MWTR) configuration recommended would consist of a 14 to 16 inch array located in close proximity to the first FCS sensor (FLIR) on the weapon assembly.

To cope with the latter problem, two subsystems were included in the overall HELVADS and FALW system configurations; a coherent laser scanning radar (CLSR) to obtain ground target elevation data using beamwidths a fraction the size of the FSR with the capability to extract doppler data additionally from moving targets, and a small millimeter wave tracker. In operation plot/position data of the hostile target determined to be approaching, the criteria for engagement, is transmitted to the FCS along with appropriate priority data based on completed asset impact prediction data for use by the Battle Manager. The position data slews the MWTR to the target position at which time

(after initiation of tracking) the MWTR supplies target data to the FLIR with the required accuracy, and the FSR continues to track the remaining targets if any, and performs its normal surveillance function.

Millimeter Tracker: A preliminary survey of millimeter tracking equipment elicited the fact that a developed system to suit the requirements for HELVADS/FALW was not available. However, for the purposes of this study, the preliminary radar parameters for a suitable system were considered and a calculation (1) was performed. The details are given in the parameter list Table 1 and the range calculation work sheet Table 2. A simplified block diagram of the system is given in Fig.1.

In order to achieve the sensitivity with respect to noise in the receiver/detection channel, a staggered pulse recurrent frequency (prf) of 18 kHz average was selected. The waveform would consist of a pulse packet at 4 different frequencies which has the effect of improving the target statistics almost to the point of being a non-fluctuating target. A 64 point FFT signal filter and a 2/4 N out of M detector allows a signal which is 11.1 dB below noise (on a single pulse basis) to be detected. Such a system would provide a maximum range of 8.1 km on a 0.05 sq meter target.

The antenna is a reflector/monopulse horn arrangement approximately 18 inches in diameter. It is mounted directly to the coelostat, moves with it and has a radar field of view of 4 degrees with a tracking capability of about 1 milliradian. The antenna beamwidth is 1.75 degrees.

---

1. The calculation was made in conformity with the standard procedures given by L.V. Blake in "A Guide to Pulse Radar Maximum Range Calculation" AD 701 321

TABLE 1

MILLIMETER RADAR PARAMETER LIST

• Operating Frequency	35 GHz
• Antenna Type	Reflector, Monopulse horn
• Antenna Diameter	18 inch
• Antenna Beamwidth	1.75 degrees
• Antenna Gain	39.5 dB
• Peak Power	5 kw
• PRF	18 kHz staggered
• Frequency Diversity	4 frequencies
• Signal Processing	64 point FFT

Radar antenna height: h = ft. . Target elevation angle: α = °. (See Fig. 13.)

A. Computation of T_s: $T_s = T_a + T_r + L_r T_e$	B. Range Factors		C. Decibel Values	Plus (+)	Minus (-)
(a) Compute T_a. For $T_{tg} = T_{to} = 290$ and $T_g = 36$ use Eq. (37a). Read T_a' from Fig. 11. $L_{a(dB)}$:_____ L_a:_____ $T_a = (0.876\,T_a' - 254)/L_a + 290$ T_a = °K	$P_{t(kW)}$	5	10 log $P_{t(kW)}$	4·77	.
	$\tau_{\mu sec}$	0.5	10 log $\tau_{\mu sec}$	.	3.00
	G_t	39.5	$G_{t(dB)}$	39·5	.
	G_r	39.5	$G_{r(dB)}$	39·5	.
	$\sigma_{(sq\ m)}$	0.05	10 log σ	.	13.00
	f_{MHz}	35,000	-20 log f_{MHz}	.	90·88
	T_s (°K)	2,500	-10 log T_s	.	34.00
	V_0		$-V_{0(dB)}$	11.10	.
	C_β		$-C_{\beta(dB)}$		.
	L_t		$-L_{t(dB)}$		2·50
	L_p		$-L_{p(dB)}$		3·20
	L_s Processing Loss		$-L_{s(dB)}$		6.00
(b) Compute T_r using Eq. (40). For $T_{tr} = 290$ use Table 1. $L_{r(dB)}$:_____ T_r = °K	Range-equation constant (40 log 1.292)			4.45	
	4. Obtain the column totals →			99·32	152·58
	5. Enter the smaller total below the larger →			.	.
	6. Subtract to obtain the net decibels (dB) →			+ .	-53.26
(c) Compute T_e using Eq. (41) or using Table 1. $F_{n(dB)}$:_____ T_e:_____ °K L_r:_____ $L_r T_e$ = °K	7. In Table 2 find the range ratio corresponding to this net decibel (dB) value, taking its sign (±) into account. Multiply this ratio by 100. This is R_1 →				4 67
	8. Multiply R_1 by the pattern-propagation factor F = (see Eqs. (42) through (65) and Figs. 12 through 19): $R_0 = F \times R'$ →				
Add. T_s = °K					

9. On the appropriate curve of Figs. 21 and 22 determine the atmospheric-absorption loss factor, $L_{a(dB)}$, corresponding to R'. This is $L_{a(dB)(1)}$. → 1.0

10. Find the range factor δ_1 corresponding to $-L_{a(dB)(1)}$ from the formula δ = antilog $(-L_{a(dB)}/40)$ or by using Table 2. → .94

11. Multiply R' by δ_1. This is a first approximation of the range R_1. → 4.39nm

8.1 km

TABLE 2

MILLIMETER RADAR RANGE CALCULATION

MM WAVE TRACKER

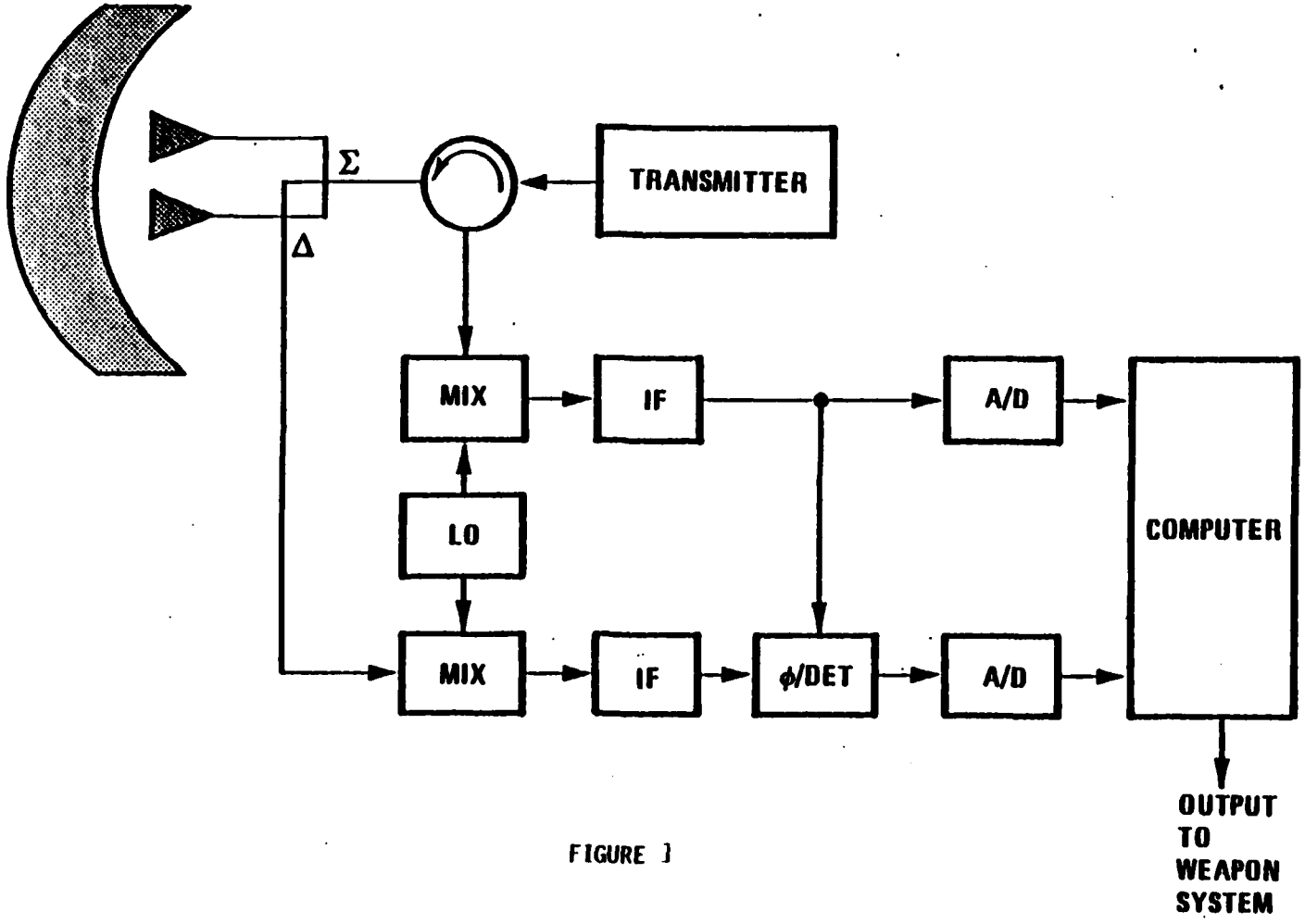

FIGURE 1

1067-43

ITT GILFILLAN

2.1.4 Performance

2.1.4.1 Configuration H-1

Phase/Frequency/Mechanical Scanning Radar System

Background

This study examines phase/frequency scanning radars to determine their applicability to the HELVADS/FALW system. The radar provides an alternative to the excessive cost of phase phase scanning systems. Relative costs are shown in Figure 2.

Phase/frequency scanning has several features that provide needed benefits for the system. The features with the derived benefits are as follows:

Feature	Benefits
• Multiple Beams (wide angle coverage at high gain)	• Higher data rate • Lower power transmitter • Higher accuracy
• Switchable beams (multiple to single) to concentrate all power in one beam	• ECCM burn-thru mode (longer range during jamming)
• Wide bandwidths up to 30%	• Improved ECM performance
• Scan-Back	• Improved accuracy • Improved ECM • Improved track quality
• Beam zooming	• Faster coverage in search
• Broader beam in search	

ANTENNA TYPE	DESCRIPTION	FEATURES	ANTENNA COSTS (Relative)
PHASE/PHASE 4 FIXED ARRAYS 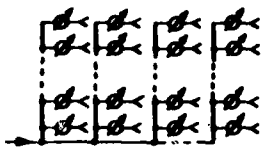	PHASE SHIFTERS K_U - BAND -6400/ARRAY -75,8000/SYSTEM C-BAND -800/ARRAY -3200/SYSTEM	BEAMWIDTH 1.5° x 1.5° • POOR RAIN PERFORMANCE BEAMWIDTH 4.5° x 4.5° • LESS ACCURACY • POOR LOW ANGLE PERFORMANCE • EASIER TO JAM (NARROWBAND)	30x 6x
PHASE/FREQ. 4 FIXED ARRAYS 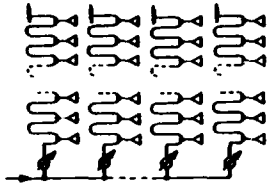	PHASE SHIFTERS -360 90/ARRAY SERPENTINES 360 SYSTEM	• LOWER COST THAN PHASE/PHASE • HIGHER ANTENNA LOSSES • SET FREQUENCY WITH SCAN ECM	2x
PHASE/FREQ. MECHANICAL BACK-TO-BACK *TOP MOUNTED* 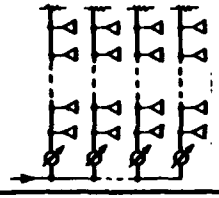	PHASE SHIFTERS 180 SYSTEM SLOTTED WAVEGUIDES 180 SYSTEM	• LOWEST COST • DATA RATE LIMITED • *MOUNTING ON TOP DIFFICULT*	0.3x
SAME CAB MOUNTED	SAME	• LOWEST COST COVERAGE IS MASKED • LASER BEAM IS OBSTRUCTED BY RADAR	0.3x
SAME TWO RADARS CAB MOUNTED	PHASE SHIFTERS 360 SLOTTED WAVEGUIDES 360	• FULL RADAR COVERAGE • SOME BLOCKING AT LASER BEAM	0.6x
PHASE/FREQ SPINNING DISH 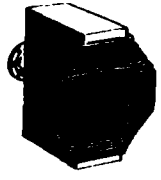	PHASE SHIFTERS 90/ARRAY 360 SYSTEM	• ARRAYS CAN BE PLACED TO PREVENT MASKING • HIGHER DATA RATE CAN BE OBTAINED	0.75x

1057-48

ITT GILFILLAN

FIGURE 2
COMPARISON OF ANTENNA CONFIGURATIONS

To illustrate the operation of these features and to understand the concepts discussed in this study, each of the features will be explained in greater detail.

Figure 3 shows the basic schematic diagram for the phase/frequency/mechanical antenna.

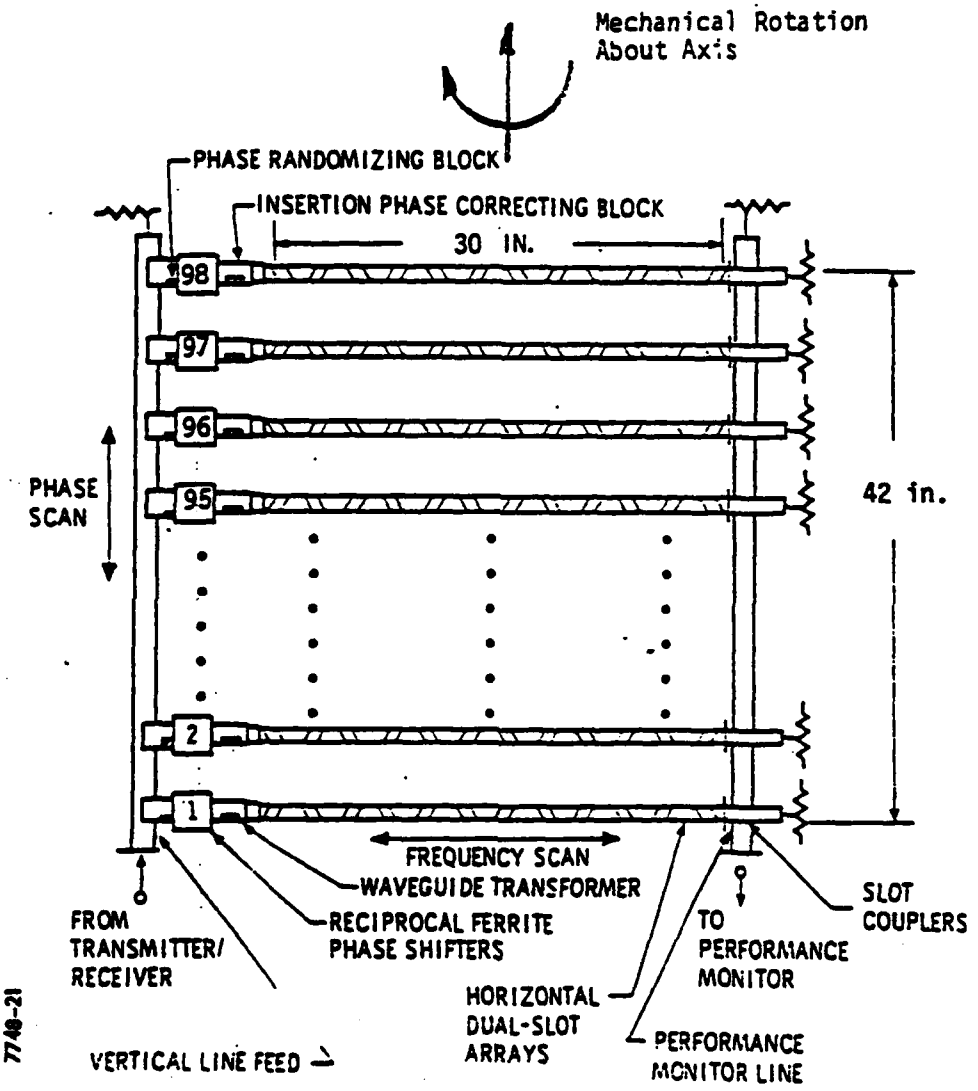

FIG. 3

Schematic representation of the basic antenna. The vertical line feed distributes the RF energy to the horizontal arrays through 4-bit ferrite phase shifters.

This antenna is made up from closely spaced edge slot waveguide radiators group to form a planar array. Each waveguide array is frequency sensitive, a characteristic which is used to provide a frequency scan back capability in azimuth as the antenna rotates. In turn each waveguide array is end fed through a phase shifter to provide phase scanning in elevation. A linear waveguide feed connects the phase shifters to the transmitter output waveguide.

Vertical Series Line Feed - The vertical line feed distributes power to the array elements with the desired amplitude relationships. This distribution is accomplished by edge-slot couplers located serially along the feed waveguide. Output ports of the coupler contain small dielectric blocks that serve to randomize the output phase and prevent quantization sidelobes.

Four-bit Ferrite Phase Shifters - The ferrite phase shifters for the array are of the reciprocal latching type with a driver attached as an integral part of each unit. These units provide the phase control to steer the beam in elevation and to obtain special elevation beam shapes. A short length of waveguide containing another dielectric block is permanently attached to the phase shifter to trim the insertion phase to permit interchangeability of devices.

Horizontal Dual-Slot Array Elements - Horizontal array elements contain edge-slot radiators located serially along the waveguide. These slots couple power from the waveguide in the correct amount to provide the desired amplitude function in azimuth. Frequency scanning of the array in azimuth results from the phase relationship between the energy traveling through the aperture waveguide and the slot positions/configuration. Each radiator consists of a pair of edge slots that provide improved radiation characteristics in comparison with single slot apertures. The input to each array element contains a transformer section for matching to the slightly different width waveguide used in the array radiating elements.

The Performance Monitor Line - The performance monitor line couples a small amount of the residual power at the end of the array elements and combines it at the output to the performance monitor. The function of this line is very similar to that of the vertical line feed, and physically it is similar. The couplers are a 4-port slot type however, with an extra terminated port to minimize reflection effects.

Conventional Rotating Phase/Frequency Planar (back-to-back)

The antennas for the candidates H-1, H-2 and H-3 are phase-frequency scanned planar arrays. The antenna mount is designed to hold two antennas mounted back-to-back and to provide 60 rpm rotation in azimuth during operation of the system. One antenna is tilted back 30 degrees from the vertical to optimize performance over the elevation sector of -15 to 41 degrees. The other antenna is tilted back 45 degrees to optimize performance from 41 to 90 degrees. The size and frequency have been selected to emphasize the tracking accuracy. Frequencies from 14 to 18 gHz have been used.

Multiple beams are formed by transmitting a single pulse and the frequency is switched within the pulse as shown in Fig. 4. In this case each of three frequencies are radiated at a different angle forming three beams. The same figure shows the capability of zooming the beam for broadening with a two beam pulse.

To place greater energy on target, three beams can be collapsed into a single beam, shown in Fig. 5. This is accomplished by transmitting a single frequency for the entire pulse. This same illustration shows 15^{o} of scan back which can also increase the dwell on target. The system could be designed for scan backs of up to 30^{o}.

To obtain the required scan coverage for search, an elevation scan program was designed. To obtain complete hemisphere coverage three frequencies are transmitted with each pulse forming a three-beam elevation group. Each of the three beams are zoomed to 3.5^{o}, providing for a coverage of about 11^{o}. This elevation scan program is shown in Figure 6. Four azimuth scans are used to obtain the coverage from -15^{o} to $+90^{o}$. After each azimuth scan, the three beams are scanned in elevation. The search scan azimuth elevation beam pattern Figure 7 illustrates this scanning from an elevation vs azimuth view. This forms the total hemisphere coverage shown in Figure 8.

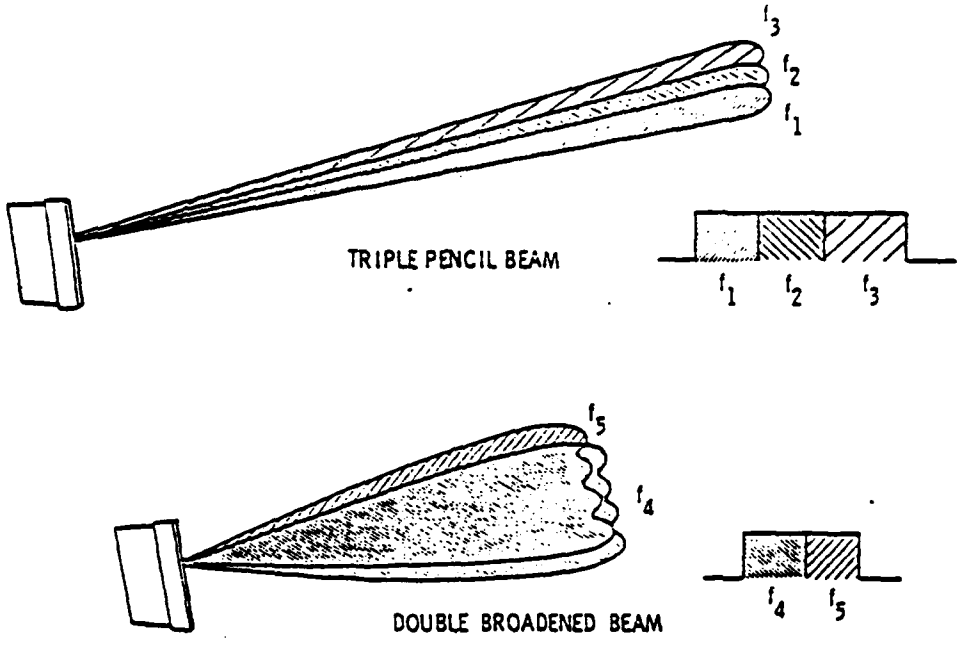

FIGURE 4 *Elevation beamshape selection*

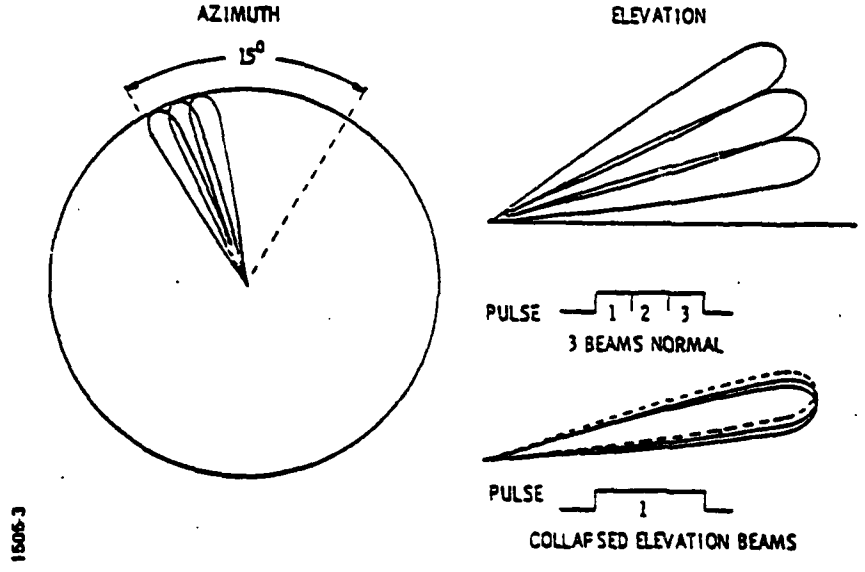

FIGURE 5 *Burn-thru mode*

ELEVATION SCAN PROGRAM

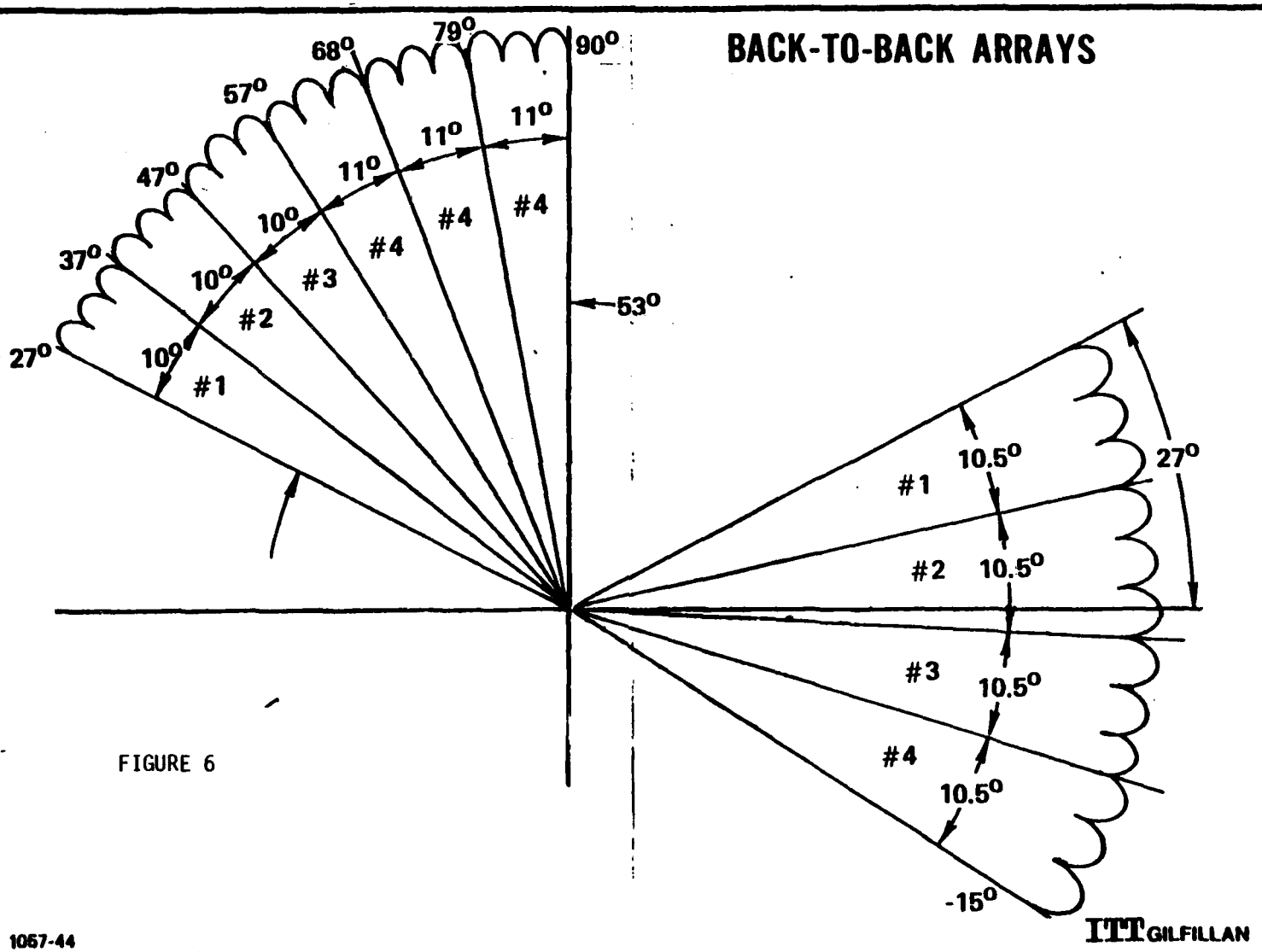

FIGURE 6

1067-44

ITT GILFILLAN

SEARCH SCAN AZIMUTH-ELEVATION BEAM PATTERN

FIGURE 7

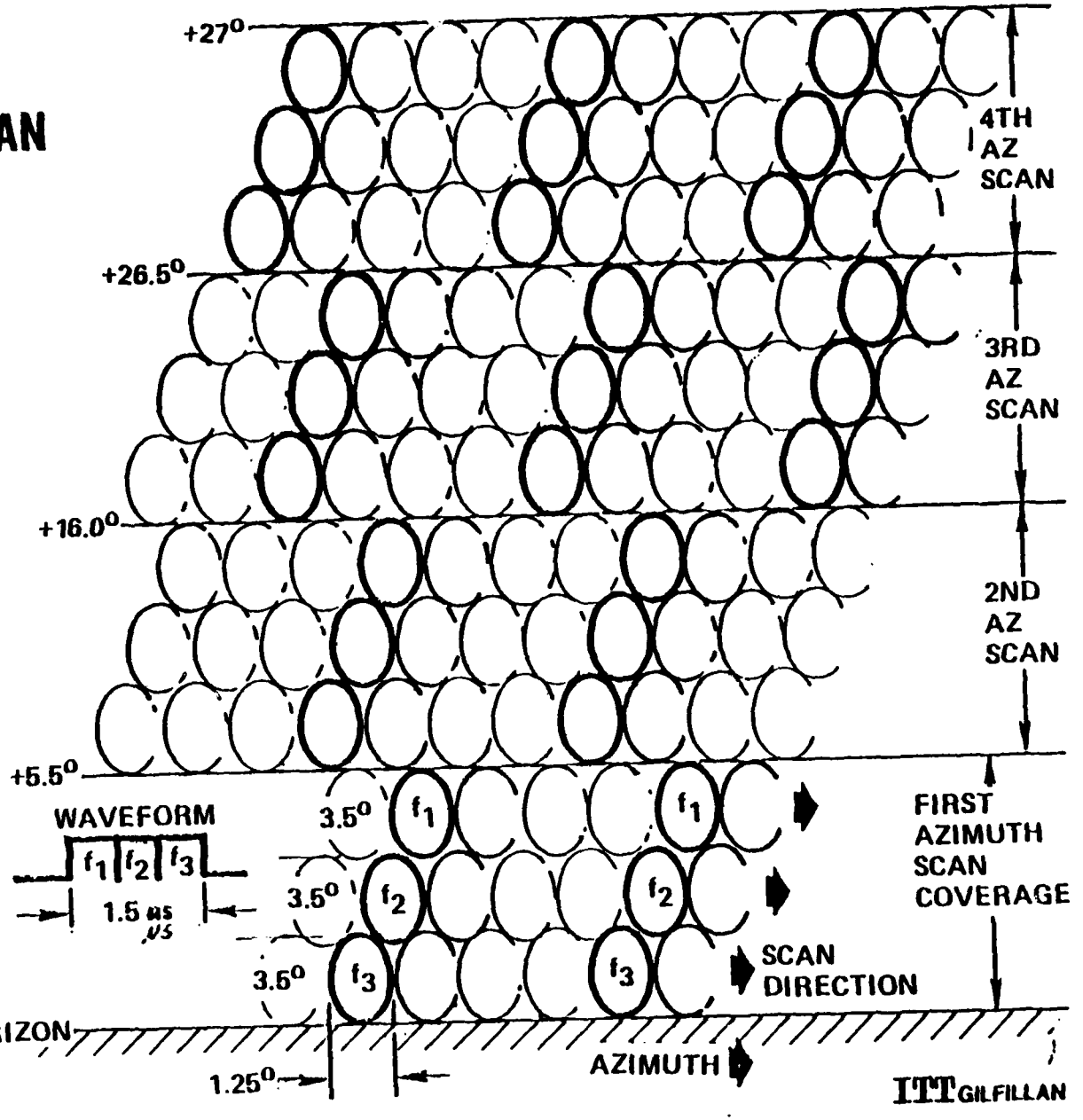

1057-45

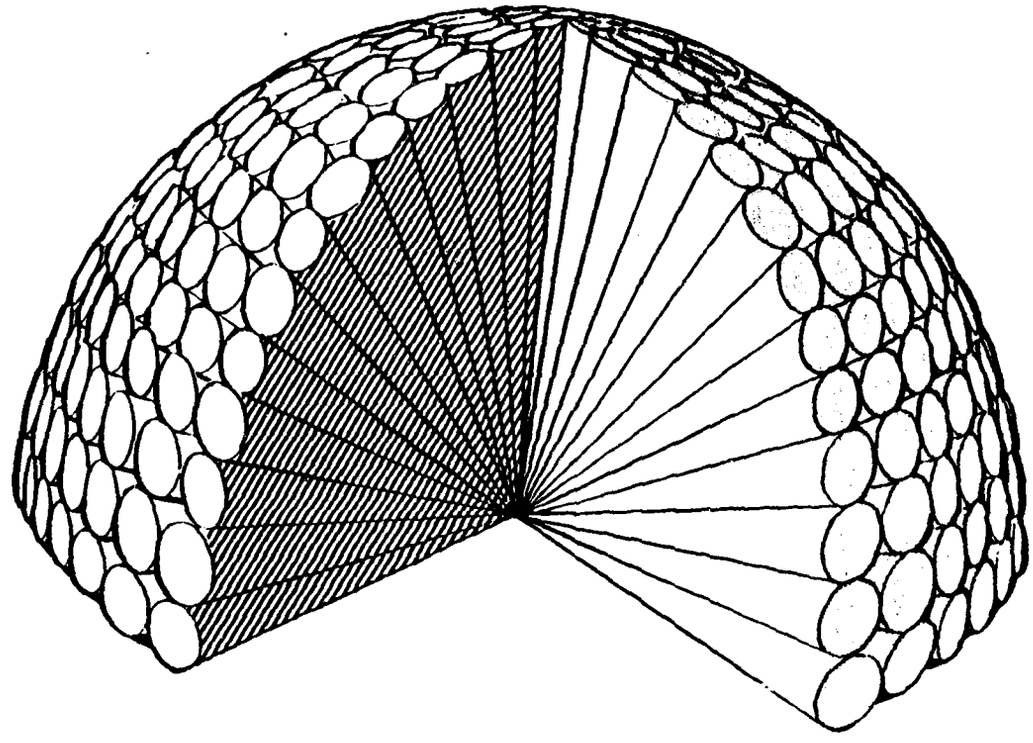

HEMISPHERICAL COVERAGE

FIGURE 8

PULSE-RADAR RANGE-CALCULATION WORK SHEET

Based on Eq. (13)

1. Compute the system input noise temperature T_s, following the outline in section A below.
2. Enter range factors known in other than decibel form in section B below, for reference.
3. Enter logarithmic and decibel values in section C below, positive values in the plus column and negative values in the minus column. For example, if $V_{0(dB)}$ as given by Figs. 4 through 9 is negative, then $-V_{0(dB)}$ is positive and goes in the plus column. For C_B, see Figs. 1 through 3. For definitions of the range factors, see Eq. (13).

Radar antenna height: h = ft. Target elevation angle: θ = 2 °. (See Fig. 13.)

A. Computation of T_s:

$T_s \quad T_a + T_r + L_r T_e$

(a) Compute T_a.
For $T_{fA} \cdot T_{fa} = 290$ and $T_B = 36$ use Eq. (37a).
Read T_a' from Fig. 11.
$L_{a(dB)}$: 1.2 L_a: 1.3
$T_a = (0.876\,T_a' - 254)/L_a + 290$
T_a = 190 °K

(b) Compute T_r using Eq. (40).
For $T_{rr} = 290$ use Table 1.
$L_{r(dB)}$: 3.9 T_r = 422 °K

(c) Compute T_e using Eq. (41) or using Table 1.
$\ell_{n(dB)}$: 6 T_0: 864 °K
L_r: 2.45 $L_r T_r$ = 212 °K

Add. T_s = 2733 °K

B. Range Factors		C. Decibel Values	Plus (+)	Minus (-)
$P_{t(kW)}$	30	10 log $P_{t(kW)}$	14.77	·
$\tau_{\mu sec}$	0.5	10 log $\tau_{\mu sec}$	·	3.00
G_t	38.2 dB	$G_{t(dB)}$	38.20	·
G_r	38.2 dB	$G_{r(dB)}$	38.20	·
$\sigma_{(sq\ m)}$	.05	10 log σ	·	13.00
f_{MHz}	16,000	-20 log f_{MHz}	·	84.10
T_0 (°K)	27	-10 log T_0	·	34.3
V_0	83 dB	$-V_{0(dB)}$	·	0.80
C_B	1	$-C_{B(dB)}$		0.00
L_t	1.5	$-L_{t(dB)}$		2.90
L_p	2.09	$-L_{p(dB)}$		3.20
L_x	Proc.	$-L_{x(dB)}$		6.00
Range-equation constant (40 log 1.292)			4.45	
4. Obtain the column totals →			95.62	147.38
5. Enter the smaller total below the larger →			·	·
6. Subtract to obtain the net decibels (dB) →			+ ·	-51.75

7. In Table 2 find the range ratio corresponding to this net decibel (dB) value, taking its sign (±) into account. Multiply this ratio by 100. This is R_0 → 5.08nm

8. Multiply R_0 by the pattern-propagation factor F = (see Eqs. (42) through (65) and Figs. 12 through 19):
$R_0 \times F = R'$ → 5.08nm

9. On the appropriate curve of Figs. 21 and 22 determine the atmospheric-absorption loss factor, $L_{a(dB)}$, corresponding to R'. This is $L_{a(dB)(1)}$ → 0.3dB

10. Find the range factor A_1 corresponding to $-L_{a(dB)(1)}$ from the formula A = antilog $(-L_{a(dB)}/40)$ or by using Table 2. → .983

11. Multiply R' by A_1. This is a first approximation of the range R_1. → 4.99 9.25km

12. If R_1 differs appreciably from R', on the appropriate curve of Figs. 21 and 22, find the new value of $L_{a(dB)}$ corresponding to R_1. This is $L_{a(dB)(2)}$. →

13. Find the range-increase factor (Table 2) corresponding to the difference between $L_{a(dB)(1)}$ and $L_{a(dB)(2)}$. This is A_2. →

14. Multiply R_1 by A_2. This is the radar range in nautical miles, R. →

Note: If the difference between $L_{a(dB)(1)}$ and $L_{a(dB)(2)}$ is less than 0.1 dB, R_1 may be taken as the final range value, and steps 12 through 14 may be omitted. If $L_{a(dB)(1)}$ is less than 0.1 dB, R' may be taken as the final range value, and steps 9 through 14 may be omitted. (For radar frequencies up to 10,000 megahertz, correction of the atmospheric attenuation beyond the $L_{a(dB)(2)}$ value would amount to less than 0.1 dB.)

GPO 889-804

RADAR RANGE CALCULATION

FIG. 9

2.1.4.1.b. Radar Range

Examination of the systems range performance shows that the most difficult requirement to meet would be the 0.05 M^2 target at 7.5 km. Once the radar meets this requirement, the other targets require less energy on target and would also be detected. It is recommended that a single radar configuration be designed to perform all tasks and used with either HELVADS or FALW. Modification of software being the only change that would be made when the radar is adapted for different weapon systems or varying threats.

A Blake Chart Figure 9 is used to determine the detection range. The target type is Swerling I, 0.05 M^2, 90% probability of detection and a probability of false alarm of 10^{-6} (Pfa) (1).

The losses in the r.f. and antenna systems are as follows:

Transmit Losses (L_t)

Waveguide	0.6 dB
Rotary Joint	0.3 dB
Transmit/Receive Cell	0.8 dB
Antenna System (Phase Shifter, Feed)	1.2 dB
Total Transmit Losses	2.9 dB

Receiver Losses (L_r)

Waveguide	0.6 dB
Rotary Joint	0.3 dB
Transmit Receive Cell	0.8 dB
Limiter	1.0 dB
Antenna System (Phase Shifter, Feed)	1.2 dB
Total Receiver Losses	3.9 dB
Receiver N.F.	6.0 dB

1) The probability of false alarm (Pfa) is as conventionally used (Ref: L.V. Blake, "A Guide to Basic Pulse-Radar Maximum Range Calculation" AD 701321.

Antenna gain of 38.2 dB is used in Blake Chart. The 1.2 dB loss shown in the Figure 9 is taken out of antenna gain and added to L_r and L_t to accommodate the Blake Chart.

The signal processing losses (L_X) are summarized in the Table below:

Summary Of Signal Processing Losses (L_X)	dB
Doppler Weighting and straddle losses	2.0
Quantization Loss	.3
$\|L\| + \alpha\|S\|$ Detection Loss	.1
Filter Collapsing Loss	.5
Range Straddle loss	1.8
CFAR (Cell Averaging) loss	1.3
Total	6.0

The magnitude of a signal is obtained by taking the square root of quadrature channels I and Q. An alternate method with hardware advantages is to add the largest of the I and Q signals to some fraction, α, of the smallest. α is usually given the value of 1/2. The loss associated with this alternative shown in the table as $|L| + \alpha|S|$ is 0.1 dB. Straddle losses accounts for loss in signal-to-noise ratio for targets not at the center of the filter in a multiple filter bank or not at the center of the range gate.

The computation of the visibility factor, Vo, is as follows:

Consider the M/N detector as illustrated below:

The standard Bernoulli trials problem involves determining the probability of M events out of N <u>independent</u> trails. This can be expressed as

$$(1) \quad P(M/N) = \sum_{i=M}^{N} \binom{N}{i} p^i (1-p)^{N-i}$$

where $\emptyset$ is the probability of a single event. For the 2/4 problem this can be expanded and rearranged to give

$$(2) \quad P(2/4) = 3p^4 - 8p^3 = 6p^2$$

In this case we are given the desired output probabilities, $P_D = 0.9$ and $P_{FA} = 10^{-6}$ and we want to find the corresponding input

probabilities P_{D_i}, P_{FA_i} for the individual events. In particular we must solve the two equations below for P_{D_i} and P_{FA_i}

(3) $$3P^4_{D_i} - 8P^3_{D_i} + 6P^2D_i = .9$$

(4) $$3P^4FA_i - 8P^3FA_i + 6P^2FA_i = 10^{-6}$$

These are easily solved, using an iterative search, to give

(5) $$P_{D_i} = .6795$$
$$P_{FA_i} = .4084 \times 10^{-3}$$

It should be mentioned that (3) and (5) are not correct if the target model is Swerling I over the four pulse-groups. Under the Swerling I assumption the trials are not independent from group-to-group and the binomial equation cannot be used to give the M/N probability. For this system, however, frequency agility between pulse groups is used. This has the effect of decorrelating the target returns from group-to-group, thereby justifying, the above approach.

Now using

$$P_{FA_i} = e^{-\lambda T}$$

and

$$P_{D_i} = e^{-\lambda T/1+(S/N)_i}$$

Where T is the detector threshold level.

We find the required $(S/N)_i$ at the input to the M/N detector

$$(S/N)_i = \frac{\ell n. P_{FAi} - \ell n. P_{Di}}{\ell n P_{Di}} = 12.83 \text{ dB}$$

at the output of the Doppler filters. This includes the coherent integration gain of 16 pulses, or 12 dB. Thus the required single pulse S/N is .83 dB.

2.1.4.1c Multiple Target Tracking

The track capacity of the radar must allow for a sufficient number of tracks to prevent saturation of the radar tracking circuits. The requirements do not state a specific number, but one can determine a reasonable capacity for the radar.

To increase the number of tracks that can be maintained, it would be desirable to divide the targets into two classes. One class would be those that are about to be handed over to the weapon system millimeter tracker or those pulling a high angular acceleration. These tracks need quality track data and would be updated every 1/2 second. All remaining targets would compose the other class.

Because a system would be required to track aircraft formations, all types (missiles, helicopters as well as ground targets) the radar should have adequate and expandable track capacity.

An example is shown to demonstrate the system operation:

Number of targets per quadrant	Time to update each data point	Number of updates per sec	Total time all updates per quad.
4	3 ms	2	24 ms
16	3 ms	1/2	24 ms
20	- -	- -	48 ms/sec

- Total number of targets/system - - -80
- Total time in track/sec - - - - - - 48 ms
- % of search time in track 4.8%

If a maximum of 10% of searchtime were devoted to track, almost 200 targets could be tracked. The radar software can be provided with sufficient capability to keep several weapon systems supplied with radar data.

2.1.4.1 d) Target Feature Extraction: The capability to collect radar return data which may be processed to extract target identity information is of paramount importance in a system where efficient kill energy management constitutes the key to multiple threat negation. This capability and the capability to perform real time kill assessment (RTKA) are most essential in the case of physically similar threats with similar attack parameters in velocity and flight path, but with widely differing degrees of vulnerability to the specific kill medium, usually by virtue of radically different kill mechanisms. A combination of return extracted data can be processed to provide target identity if sufficiently detailed target and target flight path/tactics data is available, and assuming that two or more targets of radically differing kill vulnerability do not produce identical radar returns. In the event that two or more threat targets are encountered that produce identical radar returns, the RTKA capability assumes an even more essential aspect, providing the only means of gauging energy deposition time--e.g., cut-off after and only after, detection of damage/kill based on previously tested/recorded return analyses which is then translated into the system's software in the form of a kill/damage recognition subprogram. The basic data required to implement the recognition capability includes the standard parameters of velocity, attack profile and the essential ingredient of fine grain doppler data. Experience with the ARBAT radar in tracking projectiles and observing various target perturbations including fuse events and cargo (submunition) release as well as induced yaw/nutation has led to the firm conviction that the concept is feasible.

2.1.4.1 e) ECCM Performance: The radar is designed to operate in hostile ECM environment. The design takes advantage of recent advances in ECCM technology and selection of radar parameters that are considered vital to ECCM performance, such as:

- Transmitter Power
- Operational Bandwidth
- Antenna Gain
- Antenna sidelobes
- Operational Frequency

How each of the above parameters effect the ECCM performances of radar systems is discussed.

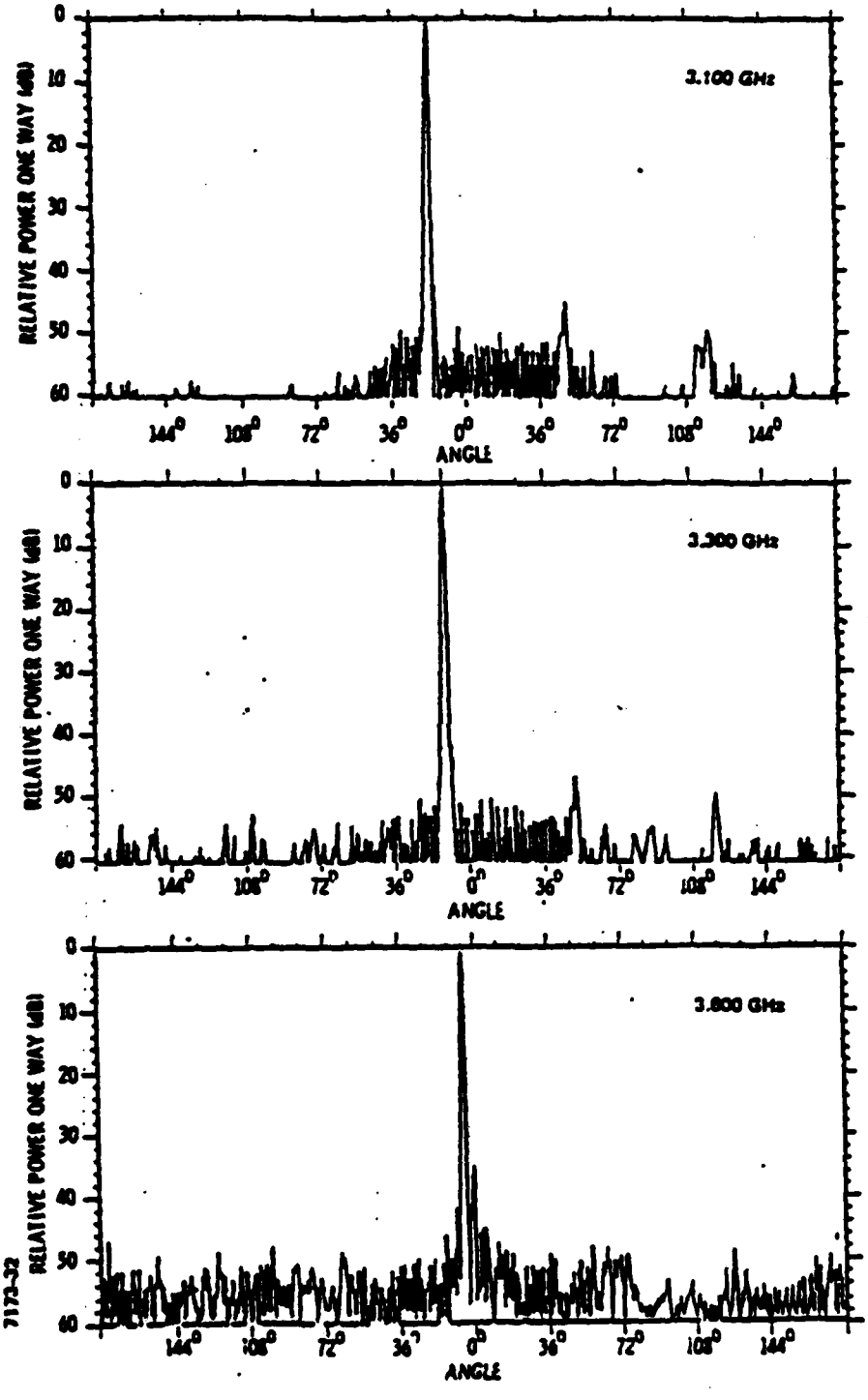

ANTENNA PATTERNS

FIG. 10

Transmitter average power (which should be as large as possible) normally varies from 300 watts to 1500 watts for tactical field radars. This design is about 3000 watts providing a power level that is as high as practicable for mobile radars. The radar signature of a frequency scanning radar is difficult to detect and characterize, particularly so if designed with frequency agility by, for example, using the phase shifters to set the frequency scanning band randomly within the much wider overall system bandwidth. The situation is further improved by the use of narrow beams, very low sidelobes and varying pulse recurrence frequencies.

ITT Gilfillan has developed planar array antennas that have 25% to 35% bandwidths as well as ultra-low sidelobes. Examples of antenna patterns are shown in Fig. 10. Sidelobes of -55 dB rms are obtained.

This means that with an operational frequency of 16 Ghz the bandwidth could be 4 Ghz. The bandwidth would be 10 to 20 times that of most field radars, providing a significant ECCM advantage.

The antenna would be built to have sidelobes of -55 dB rms. At this frequency the standoff jammer problem would be small.

The operational frequency of 16 Ghz has several inherent advantages. Jammers at these frequencies generate less power than at lower frequencies and the same percentage bandwidth provides a higher bandwidth. Also distant standoff jammers suffer atmospheric attenuation.

An examination of the absorption loss curves [1] for clear weather show that two way atmospheric losses for frequencies between 15 and 20 Ghz is between 10 and 35 dB. A jammer at 250 miles could therefore lose 10 dB in clear weather and, using data from Nathanson [2], heavy cumulus cloud introduces a further 0.7 dB per mile one way where as rain of 4 mm per hour (moderate rain) will add up to 1.2 dB per mile one way. The jammer, therefore, could lose significant amounts of power at these frequencies from clouds and precipitation depending, of course, on the amount along the path.

---

(1) L.V. Blake "A Guide to Basic Pulse Radar Maximum-Range Culculation" AD701321 Figs. 21 and 22.

(2) F.E. Nathanson "Radar Design Principles" McGraw-Hill 1969 Pages 197 and 199.

2.1.4.1 f) Clutter Performance: The radar will be operating in a strong ground clutter environment, a consequence of seeking ground and low flying airborne targets. The clutter will have two effects; it will, if not treated, obscure some targets and make the elevation data of those targets affected by multi-path meaningless.

The first effect can be counteracted by selection of a small radar cell, i.e., narrow antenna beam widths and a short pulse length coupled with the use of modern high performance doppler filters, FFT processing and PRF stagger.

FFT processing provides narrow band doppler filters which may be adaptively excised to suit the spectrum of the clutter. This is accomplished by constant false alarm rate (CFAR) action in a proportional manner. Both ground and weather clutter can thus be treated simultaneously by automatic notch selection.

Antenna beamwidths are a function of the aperture size and the wave length of the radiation. To a second degree the aperture distribution, manipulated in the design to control sidelobes, affects the beamwidth. For a given aperture the beam broadens typically by 30 percent in a low beamwidth design. The parameters given in Table I of Section 2.1.4.2, and which are discussed more fully in that section, reflect the compromises and technical trade-offs in frequency, pulsewidth, antenna size and performance.

2.1.4.1 g) Real Time Kill Assessment (RTKA): The ability to ascertain damage, or that a kill has been effected, on a tracked target could be essential for weapon energy management. This is particularly so in the case of targets where it is difficult to determine by radar return whether or not they are susceptible to sensor damage. Unless the capability for RTKA is achieved, the wide differences in required energy deposition times can significantly limit the number of targets engaged if all must be assumed to be "worst case targets" requiring maximum deposition time. In the case of unmanned airborne targets, the capability to detect and interpret doppler variation automatically resulting from relatively subtle perturbations in target body motion offers a means of achieving RTKA. The ARBAT radar developed by ITTG for USAARADCOM for testing ballistic ammunition is capable of detecting and recording doppler returns from projectiles, and has been tested with rounds from 50 mm caliber to 9 inch rounds, including rocket assisted projectiles (RAP rounds). In the course of testing at Yuma Proving Ground, Yuma, Az., (YPG) a large amount of data has been collected in which projectile body motion doppler is recorded. In a few instances the testing has included rounds equipped with Yaw-Sonde devices to permit the telemetry of projectile body

motion to a ground station for recording and analysis. Yaw-Sonde determines the projectile position change in relation to the sun and formats the sensor output for transmission to the ground receiver via an L-band link. The received data can be compared with the ARBAT radar data to correlate the optically sensed position information with the fine grain doppler data detected by the radar. The Yaw-Sonde test shots were conducted for special projects that were not a part of the normal YPG testing programs, and the detailed data has not been compared and analyzed with the ARBAT doppler data. Eight figures, Figures 11 through 18, from the ARBAT hard copy graphics printer show the readily observable effects of body motion. In consideration of the essentiality of RTKA implementation in the subject systems, the initiation of studies to address the comparison of radar doppler spectral data specifically with target body motion data collected by optical means is recommended. Further, studies to examine the task of automating the interpretation of radar doppler spectral data to enable near real time analysis of sufficient quality for energy management purposes is essential. The capabilities of the ARBAT system in tracking small projectiles and in the extraction of subtle doppler data is unique, and could provide the basis for the latter study and analysis assuming that the necessary coordination between cognizant U.S. Army agencies could be arranged.

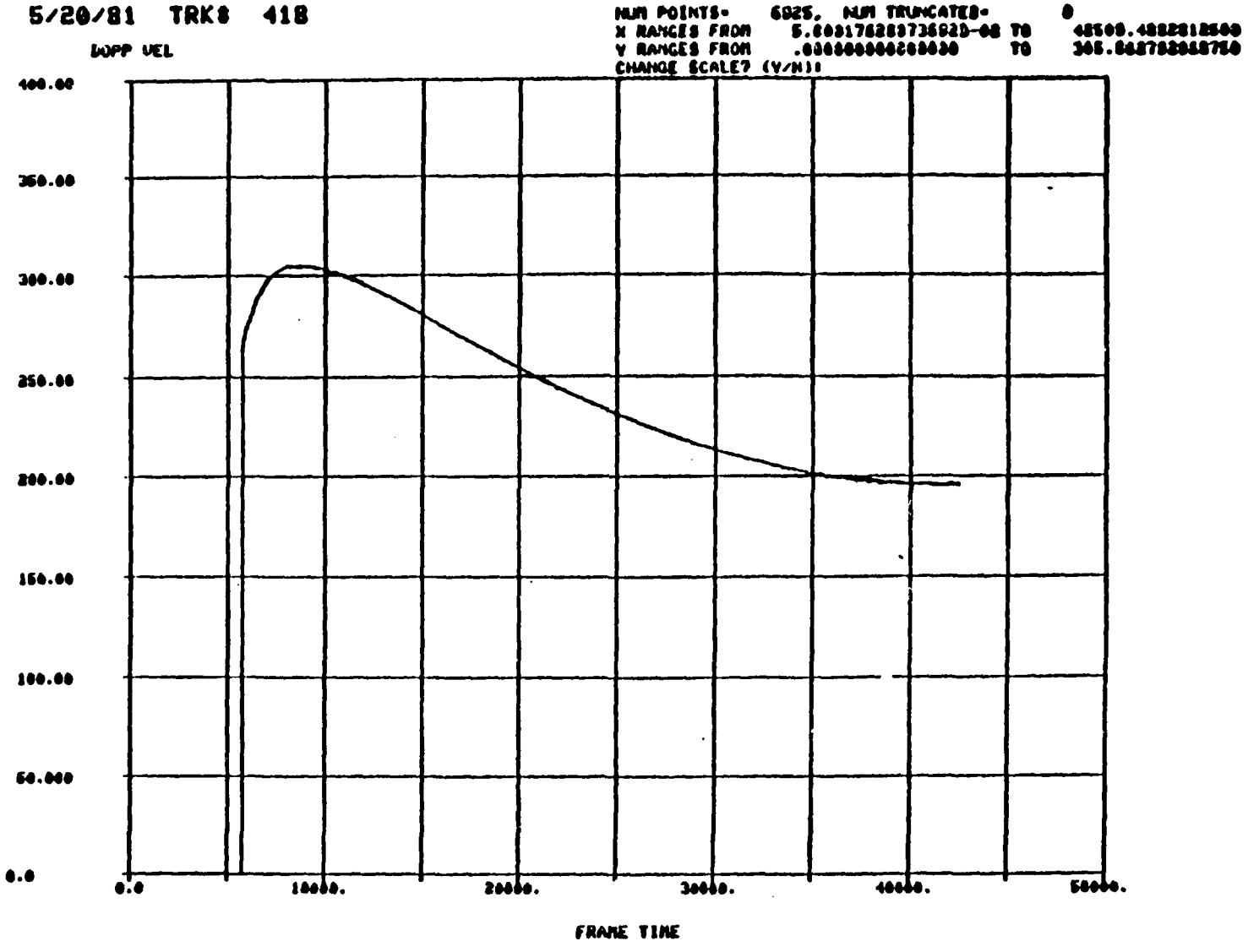

NOTE: Doppler Velocity of normal projectile (without induced yaw/nutation)

FIG. 11

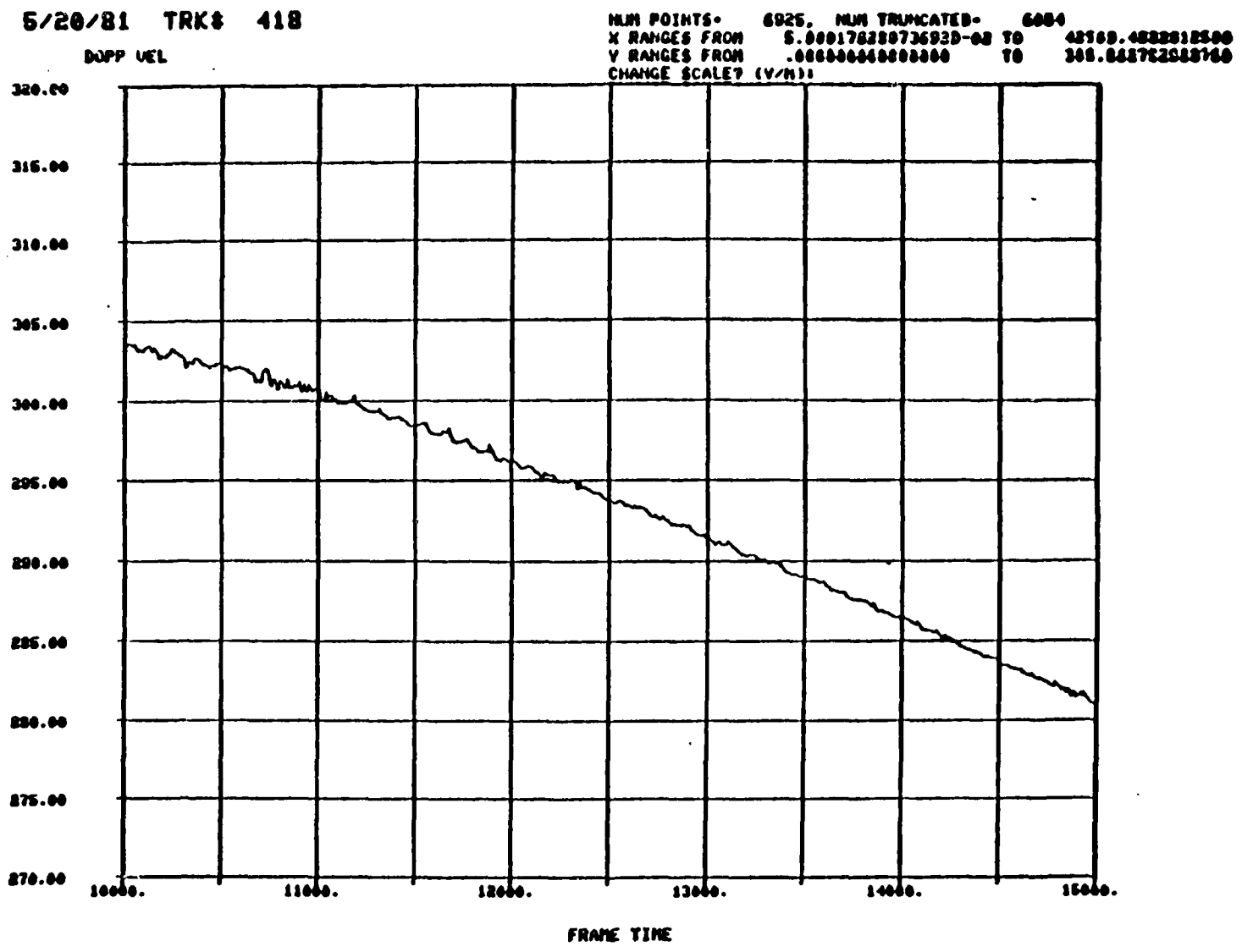

NOTE: Doppler velocity (expanded)of normal projectile (without induced yaw/nutation).

FIG. 12

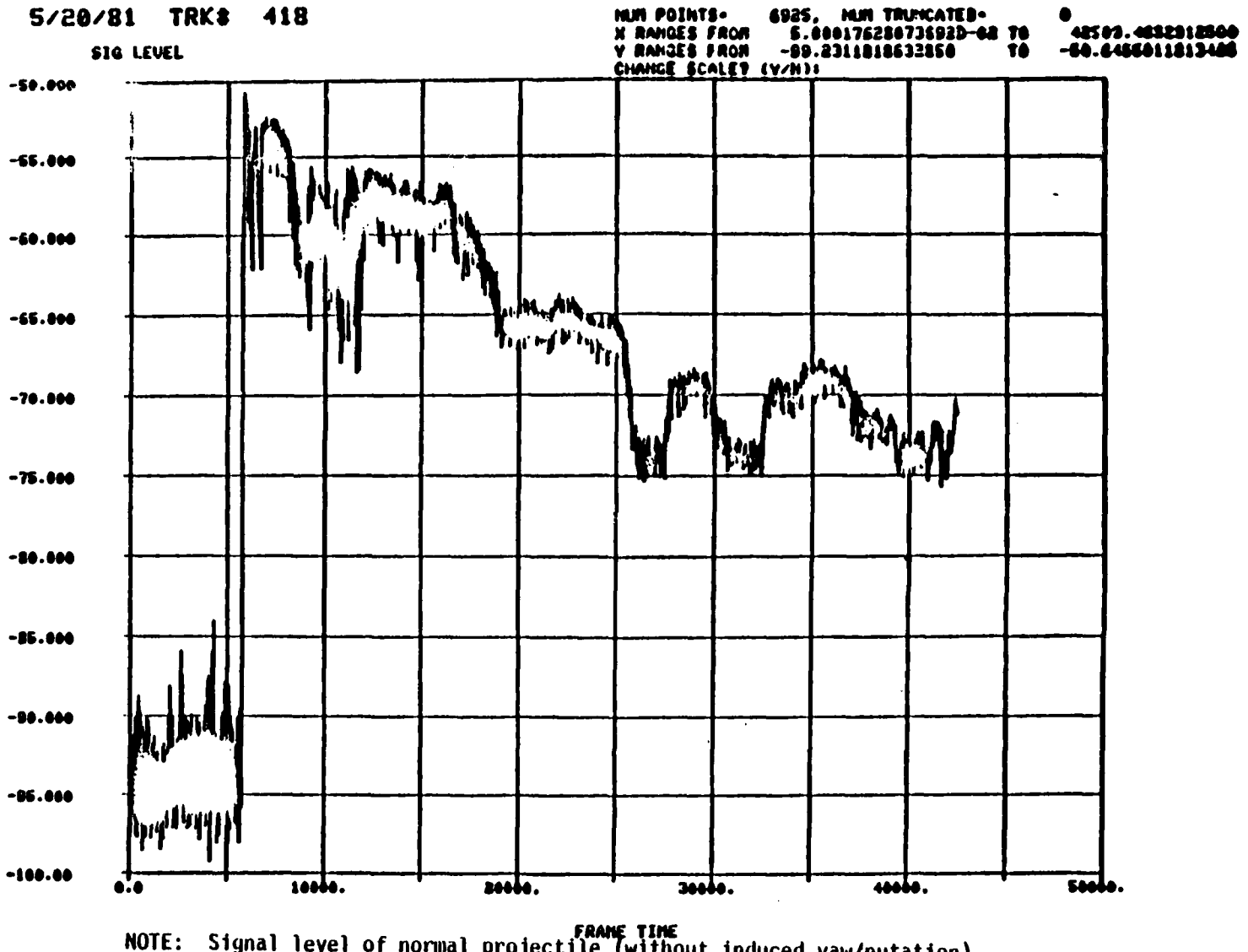

NOTE: Signal level of normal projectile (without induced yaw/nutation).

FIG. 13

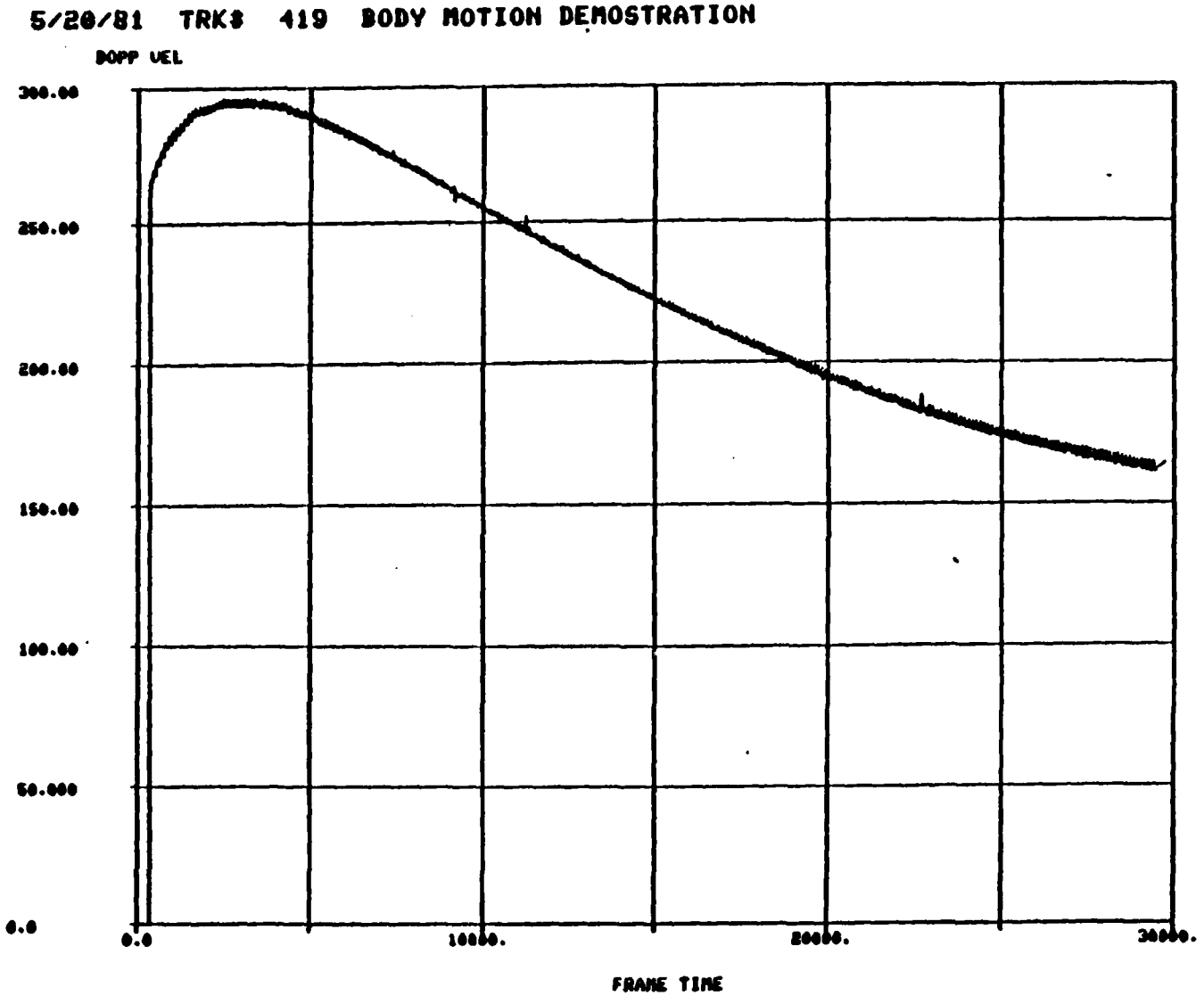

NOTE: Doppler Velocity of projectile with induced yawing/nutation.

FIG. 14

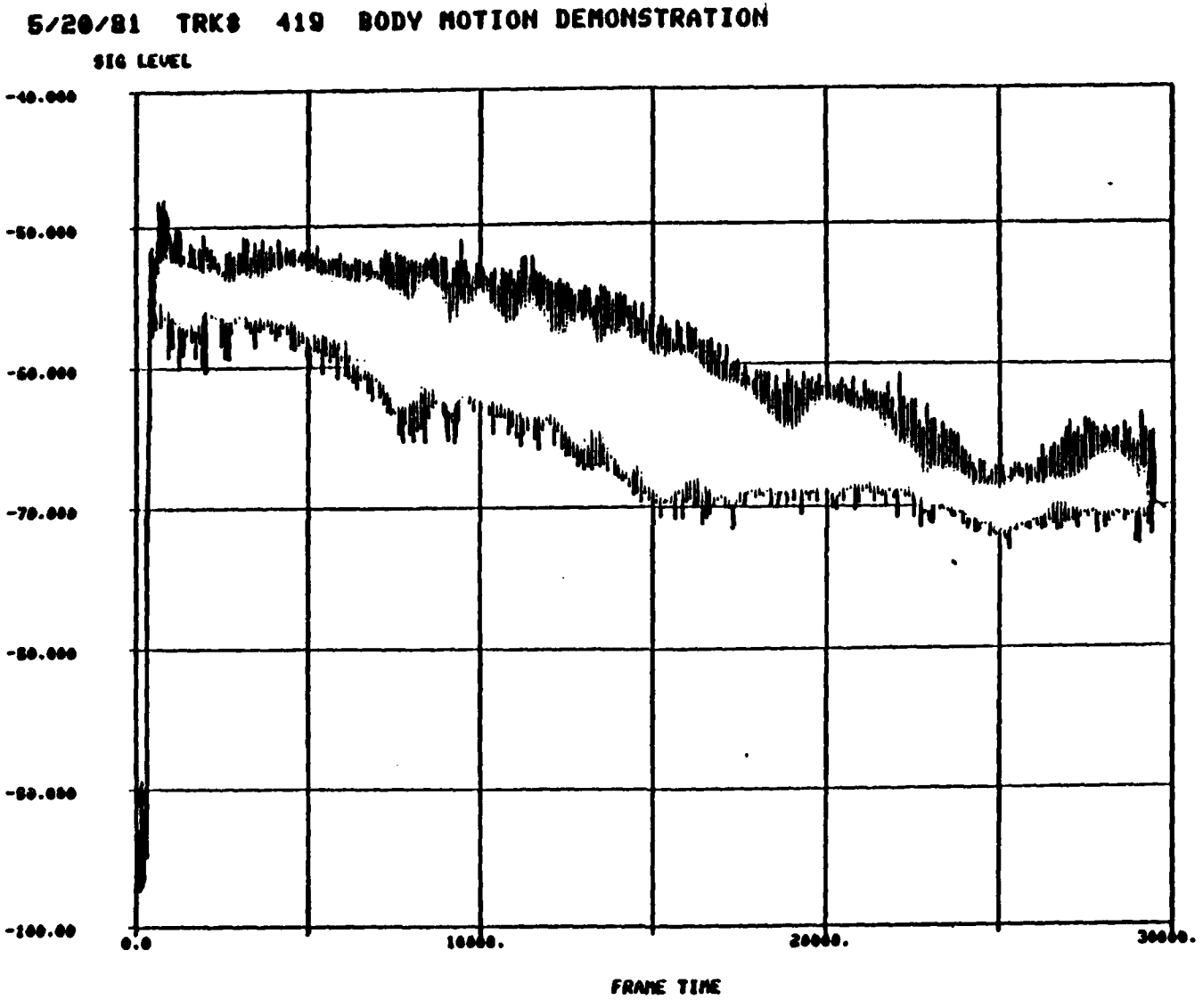

NOTE: Signal level of projectile with induced yaw/nutation

FIG. 15

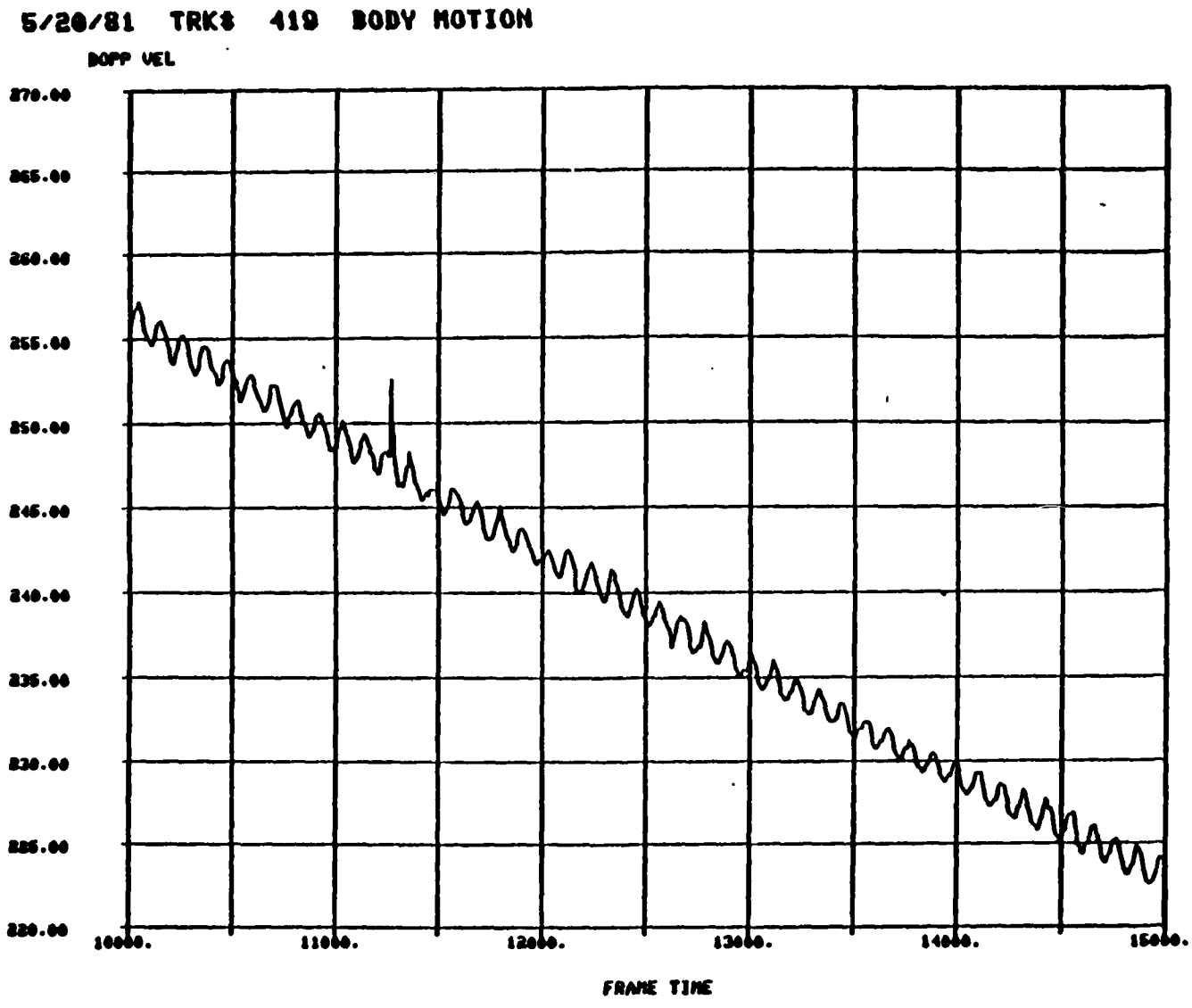

NOTE: Doppler velocity (expanded) of projectile with induced yaw/nutation.

FIG. 16

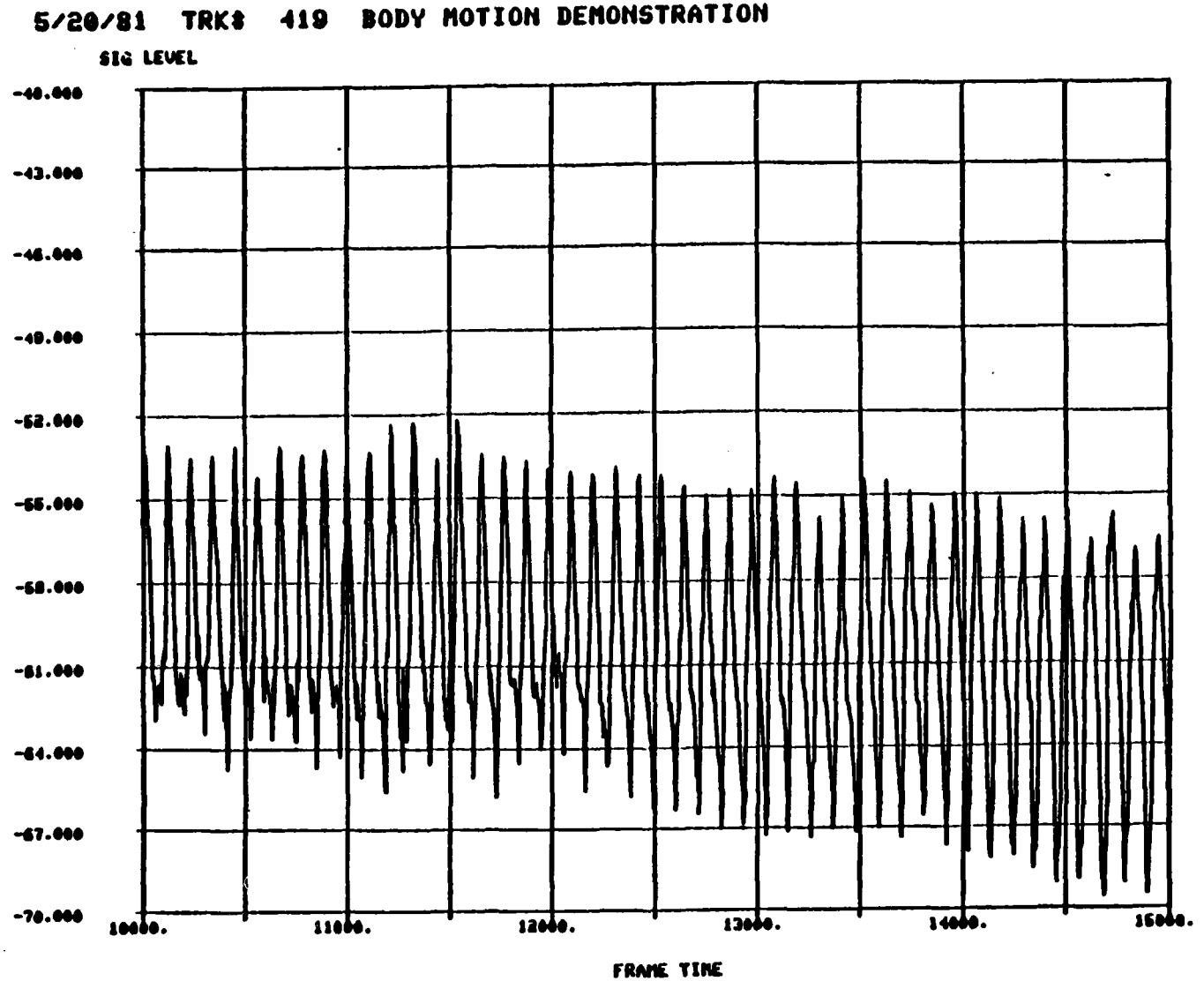

NOTE: Signal level (expanded) of projectile with induced yaw/nutation.

FIG. 17

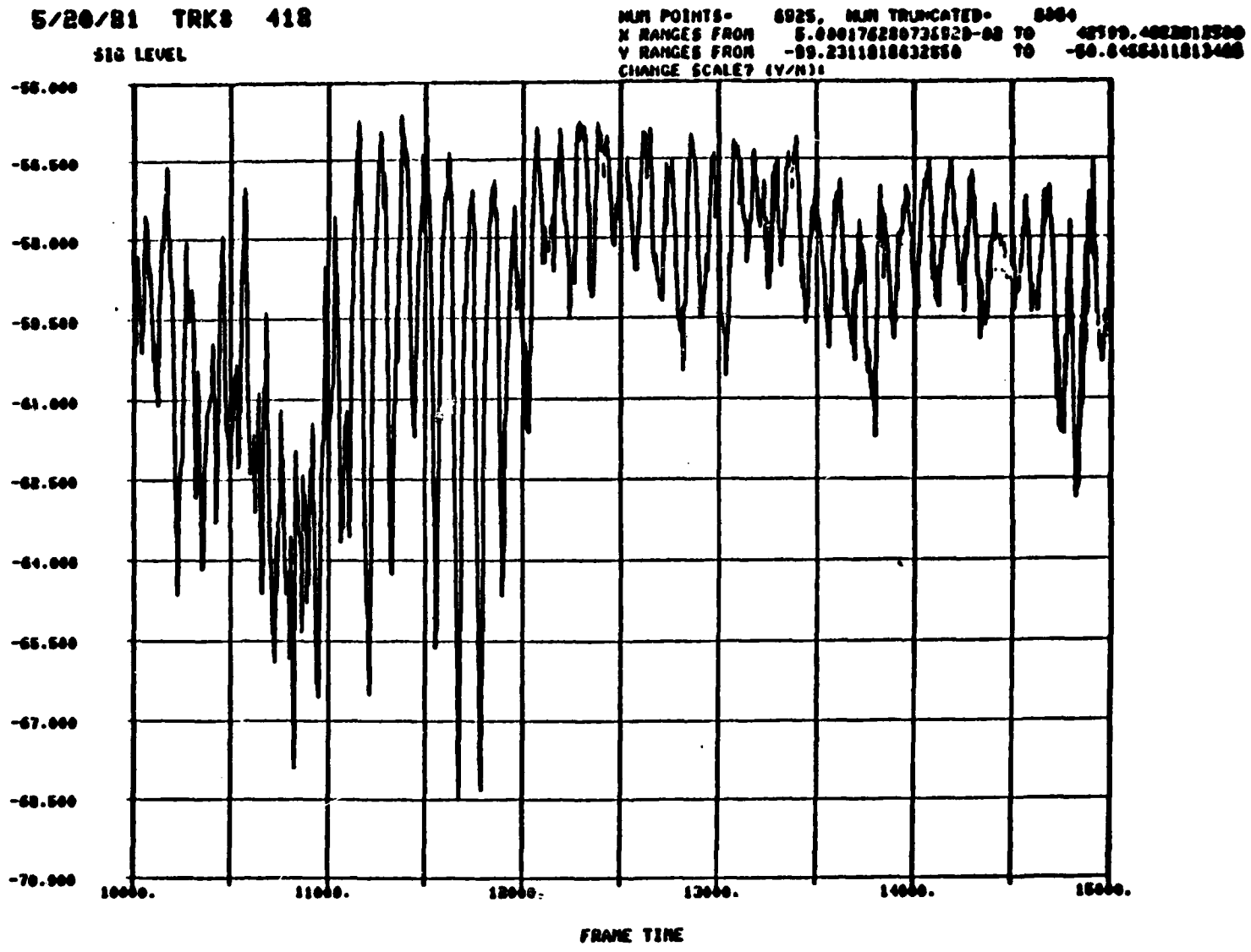

NOTE: Signal level (expanded) of normal projectile (without induced yaw/nutation.)

FIG. 18

2.1.4.1 h) False Alarm Rate: A high degree of automatic filtering by targets seen by FSR is essential to prevent system saturation and to leave for the Battle Manager highest priority decisions only. False targets are generated by fixed and fluctuating ground clutter, rain, dust, birds, insects, and a number of anamolous atmospheric conditions. An attentive operator can do much to classify these returns and behave as a highly efficient filter. Such an operator is not available to HELVADS/FALW and the false target rate must be kept to acceptable levels by automatic processing.

Dramatic improvements have been made by sequential filtering in which groups of filters form tests during detection, during tracking, and during flight path categorization. Adaptive threshold settings for accept/reject criteria and the high resolution of FFT processing are other important features to be considered in an automatic target filtering system. In extended R and D programs at ITT Gilfillan the application of such parametrics and techniques have been shown to reduce false target rates from 1440 per day to 4 a day in comparable air defense systems. However, it is clear that automatic filtering must be analyzed on a total system basis, i.e., a system analysis must be performed which includes the complete fire control chain of frequency scanning radar, tracking radar and the optical supplementary systems.

2.1.4.1 i) Polarization: The application and system requirements do not present a marked advantage for one polarization over another. It is well known that circular polarization can provide a substantial (5-15 dB) improvement in detecting targets in rain and that ground clutter, sea clutter and some classes or aircraft/missiles show greater returns at some polarizations. Polarization diversity offers some promise in target identification and protection against both passive and active jamming. The implementation of such technique is costly and results in compromises of other system features, i.e., bandwidth, power, weight and tactical capability.

In the candidate system, the radially rotating antennas will be horizontally polarized whereas in the axially rotating system the polarization, fixed of course in the array, will rotate with the array. The latter system has the advantage of compelling the use of dual polarization jammers for ECM, if the jammer is to provide complete polarization coverage without an average 3 dB loss.

2.1.4.2 Planar (Normal-Axis) Spinner

An alternate concept that permits avoidance of the masking problems at much lower cost than would be incurred by application of phase/phase array panels on each side and each end of the FVS carrier vehicle is proposed. In the ITTG

axially rotating phase/frequency radar, a circular array (approximately 3 feet in diameter) is rotated axially within a disc shaped radome at a rate of 60 rpm with a 1/4 H.P. motor. This rotation rate provides a half second position data update which is the tentative requirement, however, the small size of the array (36"dia. X 10" deep) would permit a faster rotation rate if analysis indicates the requirement for more frequent data update. Each array is mounted on the vehicle within radomes and the array assembly is tilted back 30^{0}.

The coverage volume is scanned by programming phase changes as the array rotates to cause the beam to follow a rectangular path around the coverage volume. The scan pattern to cover a rectangular area is shown in Fig. 19. In the example shown, the volume is covered by four successive revolutions in four seconds. Frequency scanning is used to produce multiple beams and to provide scan-back capability during tracking. Track data points are updated twice per array rotation (0.5 second). An additional inherent advantage in this technique is that beam dwell time increases as the beam is scanned toward the axis of rotation. Dwell time will average twice as long with this axially rotated technique as with a conventional radially rotated array radar. The longer dwell time is particularly advantageous in the detection of moving ground targets. The advantages of the axially rotated phase/frequency array are:

- Significantly lower cost than equal coverage with phase/phase arrays.
- Avoids masking (laser or radar) without the complexity and height disadvantage inherent in mounting the radar over the coelostat.
- Ground target detection is an integral function, accomplished simultaneously with detection of air targets as opposed to operation with dedicated air and ground target radars.

The basic radar system characteristics of the axially rotated planar array radar are tabulated in Table 1. Several configurations with different antenna placements were reviewed against the requirements for full unobstructed radar coverage combined with a relatively low profile. Arranging the antennas at the corners of the equipment enclosure provided a convenience solution which avoids retracting mechanisms and masking compromises. Each antenna provides the quandrant coverage shown in Figure 20.

TABLE 3

Radar Characteristics

• Operating Frequency	14 to 17 GHz
• Range - $1M^2$ Target (Ambig Range) SWI	15 km
$.05M^2$ Target SWI	8 km
• Elevation Coverage	-15^o+ to $+90^o$
• Data Rate Track	1/2 sec.
Search	4 sec
• Antenna Rotation Rate	60 RPM
• Beamwidth	
Azimuth	1.25^o
Elevation	1.75^o Normal
zoom to	3.5^o
• Array (Phase, frequency) axial spinner	36" diameter
• Array (phase frequency) azimuth rotation	42" X 30"
• Gain (includes phase shifter loss)	37 dB
• P.R.F. Stagger; Nominal/range	16 kHz to 20 kHz
• Peak Power/Antenna	30 kw
• Power Ave/Antenna	800 w
• Pulses/Dwell (16 pt. FFT)	16
• Dwells/Beamwidth	4.

AXIALLY ROTATED FLAT ARRAY SCAN PROGRAM

(PRELIMINARY EXAMPLE)

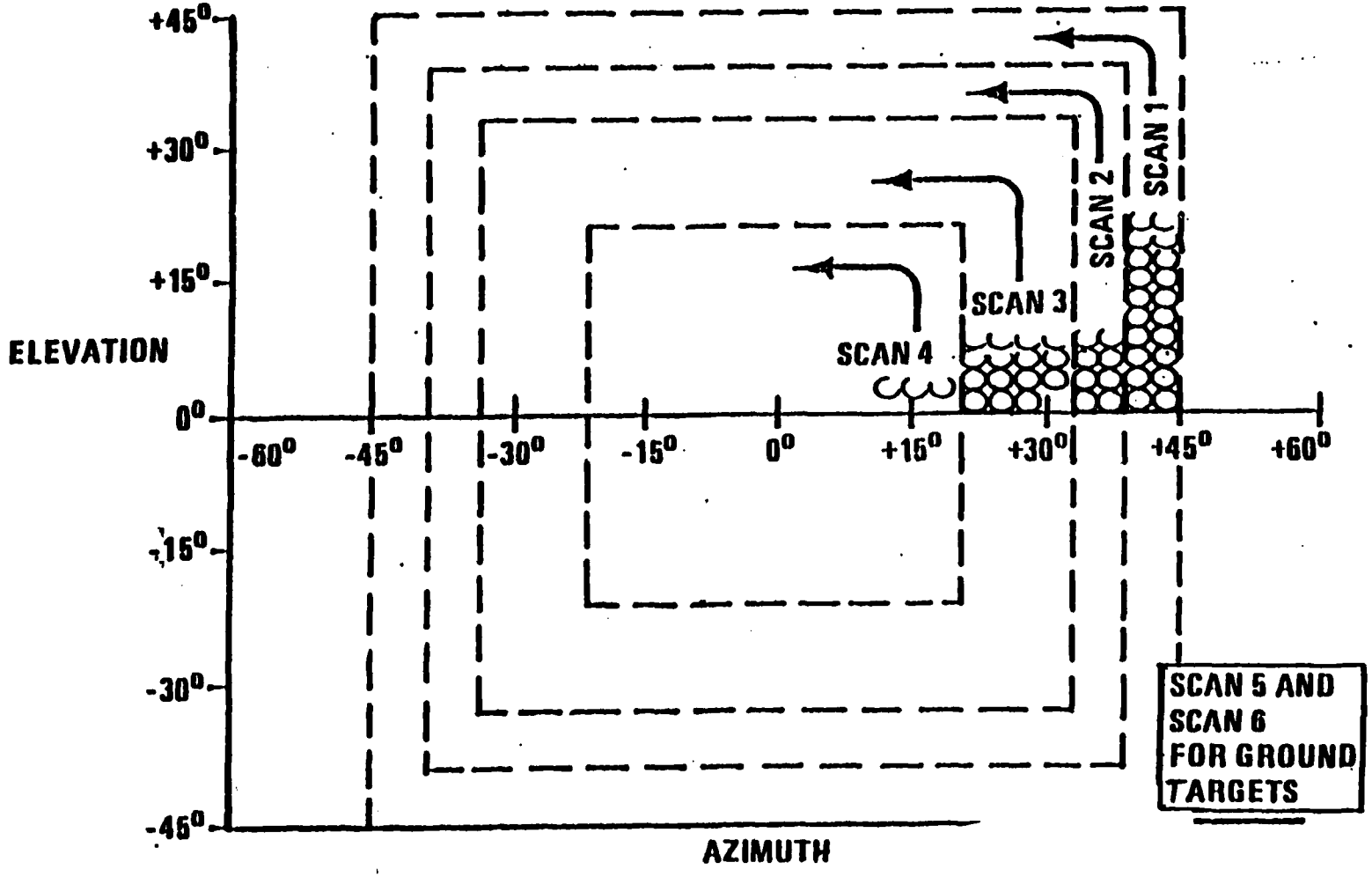

1057-30

FIGURE 19

GILFILLAN

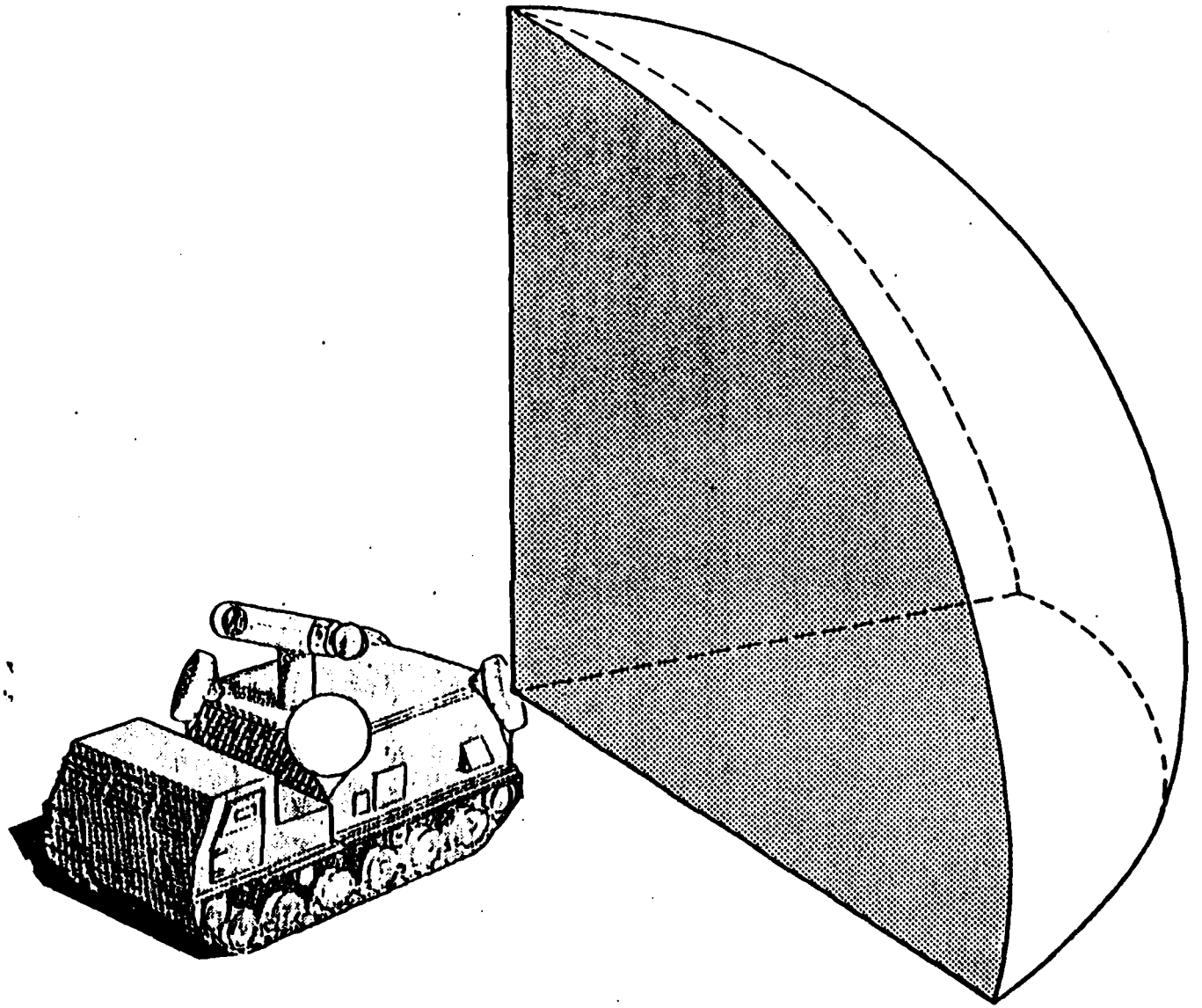

FIGURE 20

Single Quadrant of Coverage

HELVADS/FALW ANTENNA

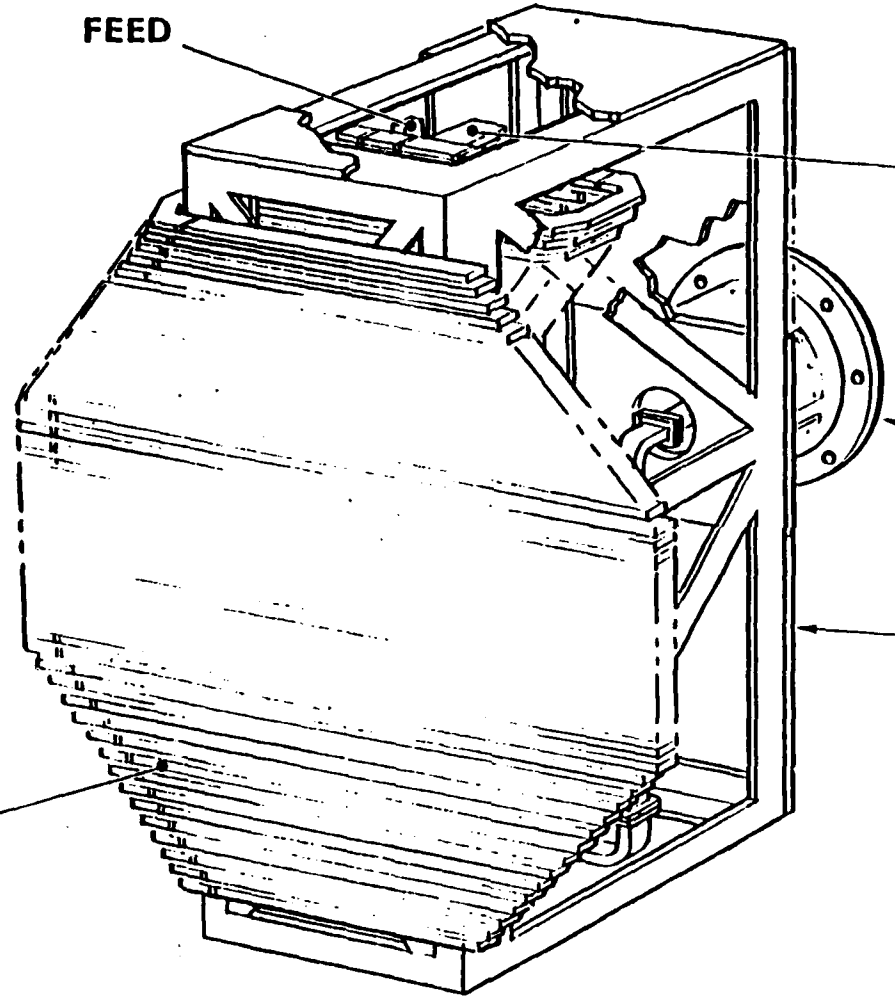

FRONT VIEW

RADOME
NOT
SHOWN

1057-36

FIGURE 21

ITT GILFILLAN

HELVADS/FALW ANTENNA

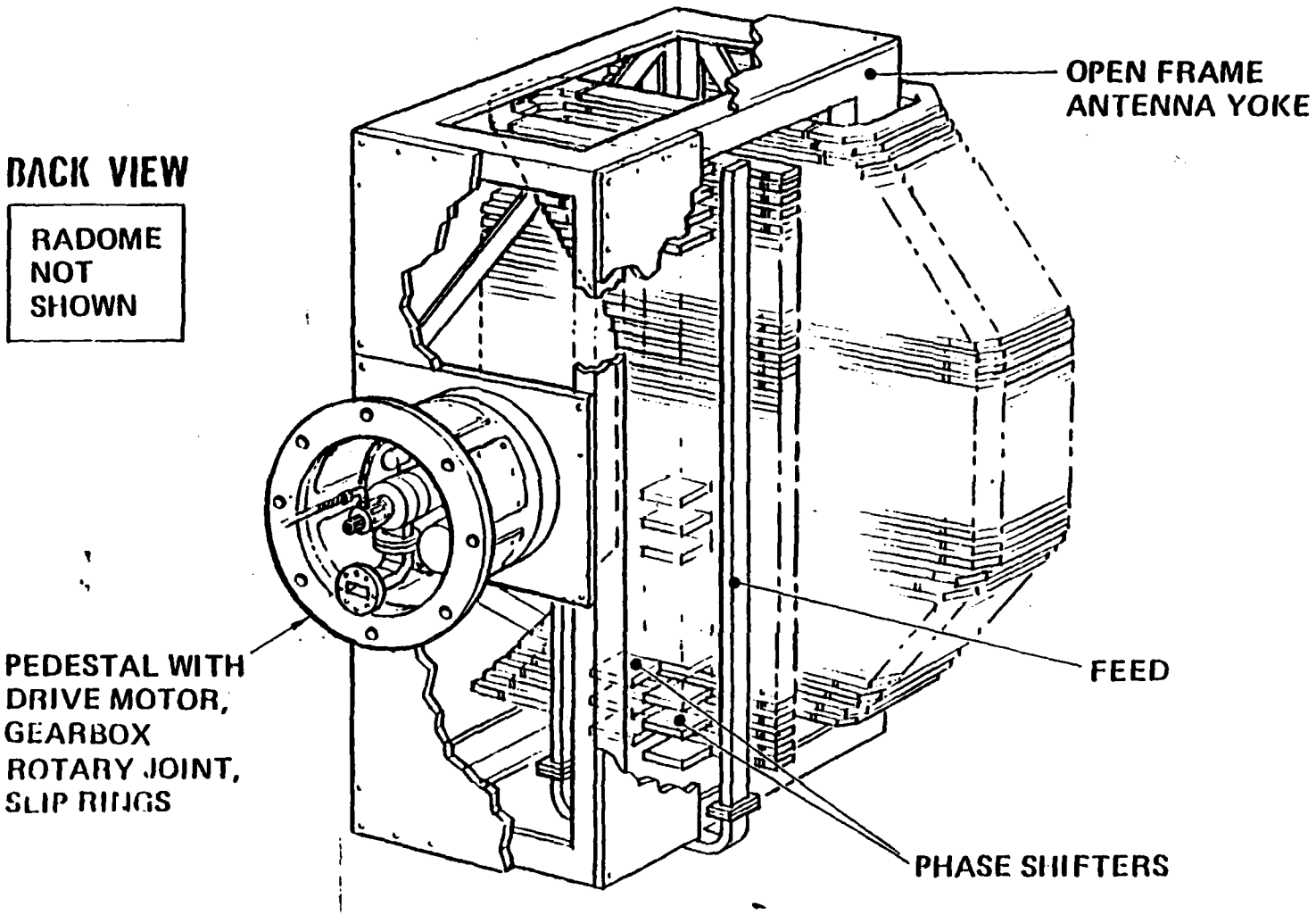

1057-35

FIGURE 22

ITT GILFILLAN

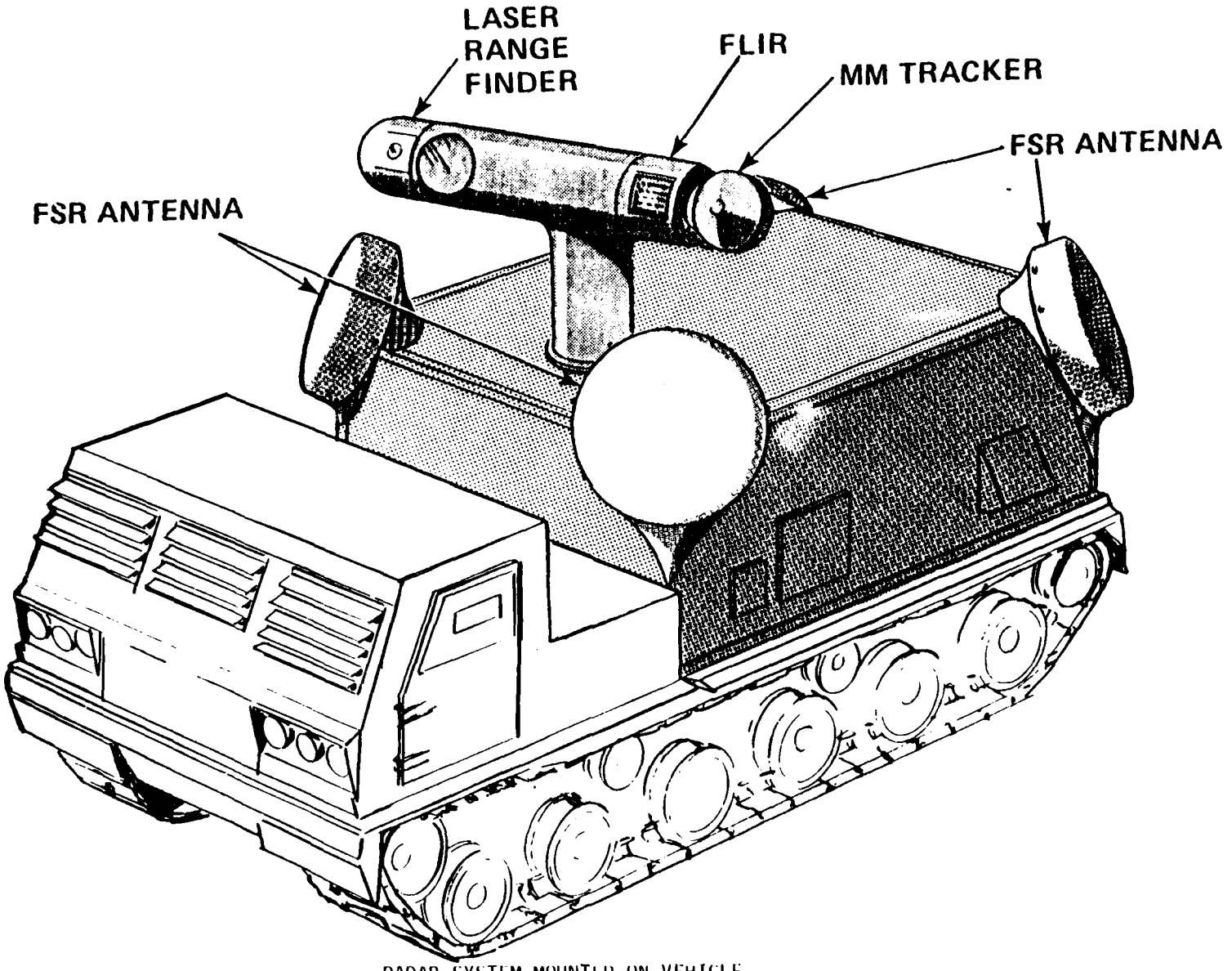

RADAR SYSTEM MOUNTED ON VEHICLE

FIGURE 23

BLOCK DIAGRAM

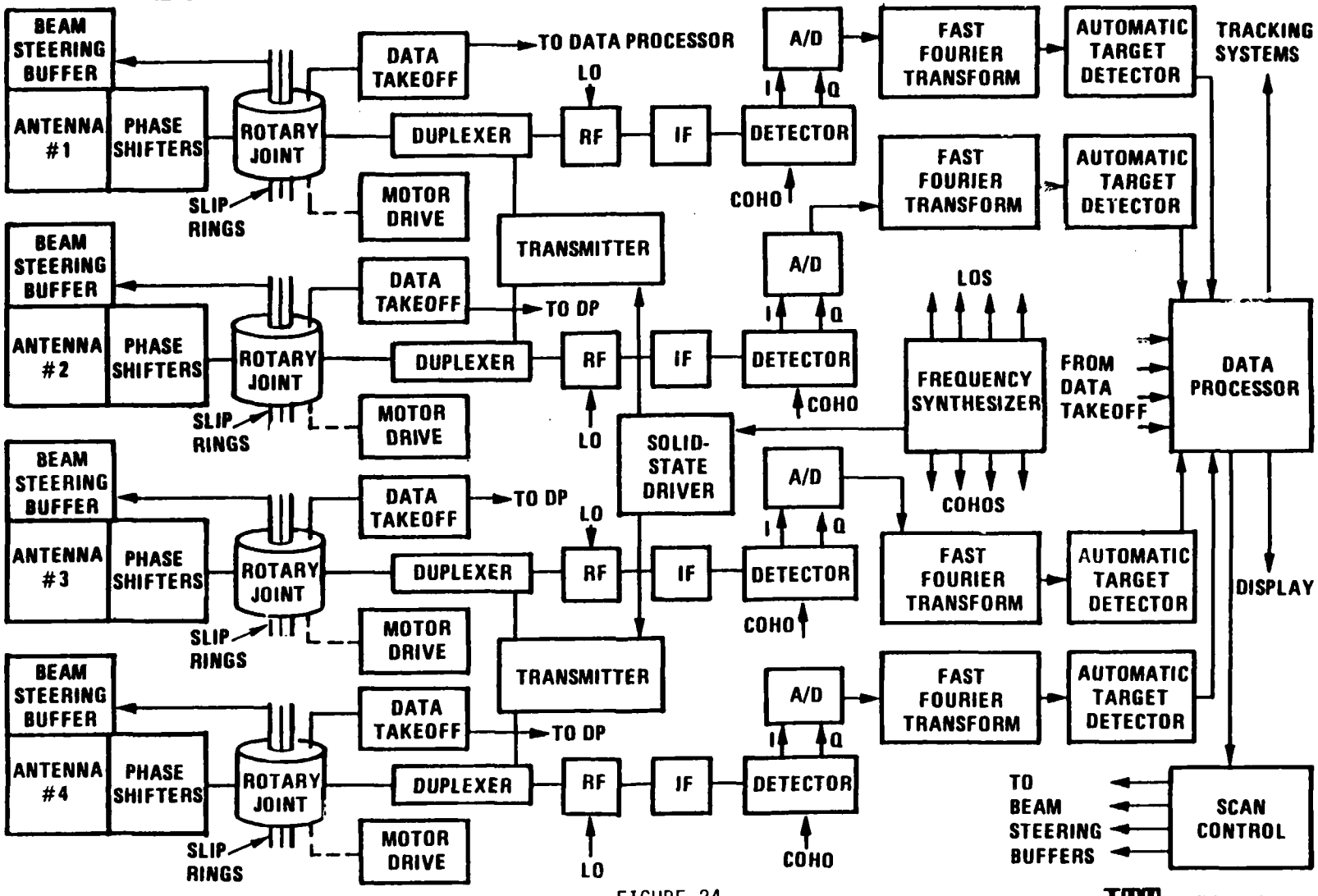

1057-40

FIGURE 24

RADAR SYSTEM BLOCK DIAGRAM

ITT GILFILLAN

PARAMETER COMPARED	HELVADS-1 H-1	HELVADS-2 H-2	FALW-1 F-1	FALW-2 F-1
Antenna Configuration	One pair back to back radially rotated planar arrays	Four Single axially rotated planar arrays	Same as H-1	Same as H-2
Data Rate	1X (Meets Req $\frac{t}{}$)	2 X (Exceeds Req $\frac{t}{}$)	1X	2X
Vehicle Space Requirement	1X	5X	1X	5X
Prime Power Requirement	1X	3X	1X	3X
Survivability	1X	3X	1X	3X
Reliability	1X	2X	1X	2X
Development Risk	1X	2X	2X	2X
Development Cost	1X	3X	2X	3X
Production Cost	1X	3X	1X	3X

TABLE 4

RELATIVE MERITS OF H-1/F-1 AND H-2/F-2 SYSTEMS

The design of the antenna was developed sufficiently, particularly in mechanical detail, to establish weight, drive power and cost data. Figures 21 and 22 are three dimensional views of the antenna showing the linear elements with the frequency sensitive feed and phase shifters folded behind the radiating surface. A full complement of four antennas are shown together with associated equipment mounted on a vehicle in Figure 23. The antennas are mounted at the upper corner of the equipment enclosure to give an unobscured coverage of more than a hemisphere.

Operational, cost and development risk parameters for the two antenna (and system) configurations are compared using broad factors. The trade-offs to be borne for the advanrages of the H-2/F-2 System can be seen in Table 4.

A block diagram of the four antenna system is shown in Figure 24. It will be seen that four separate receiver systems are required, two transmitter tubes service the four antennas and the frequency synthesizer, signal and data processing subsystems are common to all four. This block diagram will be used in Section 3 as one basis for developing the production and life cycle costs.

2.3 FALW-D Recommendations

It is recommended that, program considerations permitting, a single antenna version of the recommended HELVADS FSR be developed and be deployed in conjunction with supplementary optical equipment for FALW-D.

In the event that a decision is made in favor of using modifications of existing systems, it is recommended that either of the two following configurations be used. The decision on which of the two would rest on the overall test requirements of FALW-D. System A is simply a detection system which will "see" the required targets. System B adds the capability of target damage assessment.

System A

(1) Air Traffic Control Radar AN/TPN-18A with MTI

(1) RASIT type 72A Ground Surveillance Radar

(1) Single Head Laser Radar

System B

(1) Ballistic Ammunition Testing Instrumentation Radar (ARBAT)

(1) RASIT Type 72A Radar

(1) Single Head Laser Radar

These two systems are discussed in the next section and further details are provided in the appendices.

2.3.1 Rationale for the FALW-D Radar Selection

In reviewing possible candidates for the "fall back" systems in which the potential of ready availability is a prime consideration, equipments already in the U.S. Army have a clear advantage assuming that cross-agency usage is possible. The AN/TPN-18A is a good candidate if used with the M.T.I. addition for the detection of low flying targets. The parameters of this system with M.T.I. are given in the characteristics summary, Table 5. Figure 25 is a block diagram of the system. In configuration it is used on a field tripod but may be deployed on a small trailer. This latter arrangement may be more convenient for FALW-D. The display and control equipment is suitable for truck or trailer mounting. To illustrate the equipment configuration, a descriptive brochure is provided in Appendix D.

AN/TPN-18A WITH MTI CHARACTERISTICS SUMMARY

System	
Principle	Dual scanning beam az/el data
Configuration	Dual transportable shelters
Scan coverage	Azimuth: 30° or 60° Elevation: 11° or 36°
Data rate	1 second PAR mode 4 seconds ASR mode
Azimuth Antenna	
Gain (Minimum)	36.5 dB
Beamwidths	Horizontal plane 1.1° max Vertical plane 3.5° max
Sidelobe level	-23 dB (Horizontal Plane) -23 dB (Vertical Plane)
Polarization	Linear/Circular
Scan Coverage (PAR)	30° or a 60° selectable sector
(ASR)	360°
Elevation Antenna	
Gain (Minimum)	35 dB *minimum*
Beamwidths	Vertical plane 1.1° max Horizontal plane 3.2° max
Sidelobe level	-18 dB (Vertical Plane) -14.5 dB (Horizontal Plane)
Polarization	Linear/Circular
Scan Angle, (Selectable)	-1° to +10° -1° to +35°
Transmitter	
Frequency	9000-9200 MHz
Peak output power	200 kW nominal
Pulse length	0.34 μsec
prf	1440 pps fixed or 7, 8, 9 staggered
Receiver	
Type	Dual conversion
MDS	-106 dBm (GaAs FET)
Normal	Linear, log/FTC
MTI	Linear limiting
Video bandwidth	3.5 MHz
MTI	
Type	Pulse Coherent
Filter	Digital single or double canceller
Sample rate	4.36 MHz
IMP factor	31.4 dB (Search Mode)
(ground clutter)	31.9 dB (PAR Mode)
A/D converter	8-bit
Displays	
Type	Beta Scan
Tube size	10-inch
Cursors	Glideslope, courseline
No. of preset cursors	2 sets
Display range	5 nmi
(Selectable)	10 nmi
	20 nmi
	40 nmi
Power Requirements	
Voltage	120/208 Vac, ±10%, 3-phase
Frequency	400 Hz ±5%

TABLE 5

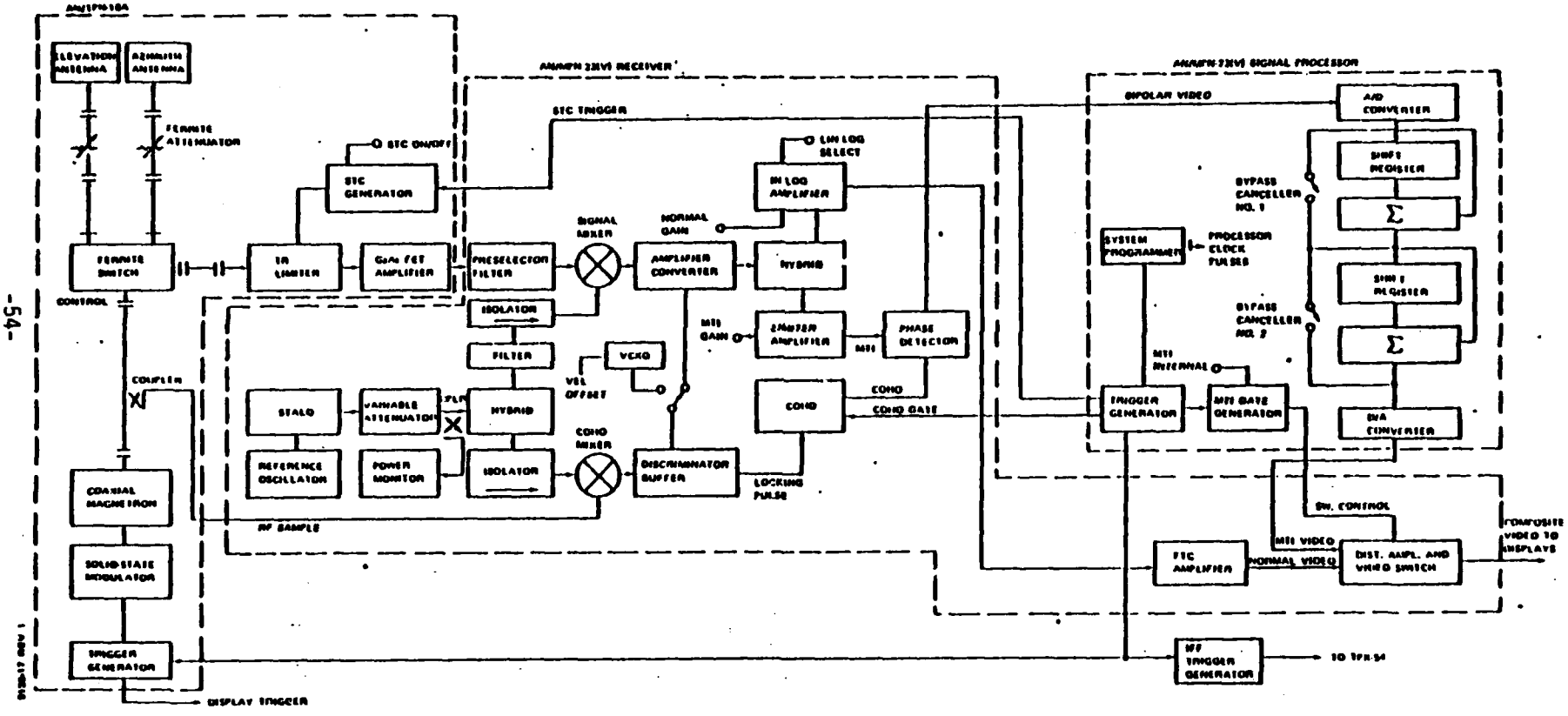

MODIFIED TPN-18A BLOCK DIAGRAM

FIGURE 25

The possibility of the additional capability of ARBAT is attractive in that the ARBAT radar could provide tracking of fast airborne targets including missiles and an RTKA function by body data collection, extraction, analysis and result output.

A number of ground surveillance equipments are in use in the U.S. Army e.g., AN/PPS-5, AN/PPS-15, AN/TPS-25 and the AN/TPS-58, each with its own specialized operational characteristics. However, none of these, with the possible exception of the PPS-15, which it is understood has been modified for recent netting experiments, and the TPS-58, have the performance capability, coupled with a flexible digital interface, for consideration in FALW-D. As noted above, the TPS-58, although more recent than the TPS-25, has been in service many years and is becoming difficult to support. The RASIT radar was therefore considered.

This radar, described in Appendix F, is in service in the French and German Armies. It is used for the detection of ground targets and low flying light fixed wing aircraft and helicopters and is a derivative of the AN/TPS-58 Target Acquisition radar which has been in the army inventory since 1970. It is a more modern system than the TPS-58 making full use of digital integrated circuitry and has a convenient serial digital interface for system integration. Systems have previously been made available by the French authorities for U.S. Army tests and it is assumed that this may still hold.

Laser radars whose purpose is to provide elevation data on ground targets were briefly reviewed to the extent outlined in Appendix G and no recommendations are made as to specific systems since this was considered to be outside the scope of this study.

2.3.2 FALW-D Radar Performance

For a FALW-D system which consists of a truncated version of the recommended HELVADS/FALW radars, the performance analysis given in Section 2.1.4.2 holds good since the truncation only applies to the volumetric coverage, not the detection performance.

In the case of System A, the range performance of the TPN-18A on a small (0.05 square meter) target has been calculated as almost 14 km. This calculation and the associated list of input parameters is given in Table 5. The target and noise statistics used are typical of those used in the assessment of air traffic control radars, a Swerling I target with a 90 percent probability of detection on one scan and a probability of false alarm of 10^{-6}. This latter probability is used as is customarily defined, it represents the probability that a false

RANGE CALCULATION TABLE

RANGE FACTORS	+dB	-dB
P_t = 150 kW	21.8	
τ = 0.34 μsec		4.7
G_t = 37.2 dB	37.2	
G_r = 37.2 dB	37.2	
σ = 0.05 sq. m.		13.0
F = 9080 MHz		79.2
T_s = 1100°K		30.4
V_o = Required SNR		12.0
L_t = Transmit Loss		0.2
L_p = Pattern Loss		1.6
L_x = System Loss		4.6
CONST FOR Km	15.2	
R^4 (100Km Units)		
		-34.3 dB
		= 13.9 Km

Target Statistics: Swerling I 90% probability of detection and 10^{-6} probability of false alarm.

Scanning rate, beamwidth and p.r.f. give 17 hits per scan.

Table 6

alarm is obtained each time there is an opportunity. By good approximation a noise pulse has a duration equal to the inverse of the receiver bandwidth, usually the IF bandwidth, and therefore the probability of false alarm is the probability that such a noise pulse will cross the detector threshold during an interval of time also approximately equal to the reciprocal of the bandwidth.

For ground clutter conditions preliminary calculations using representative radar range cells (0.25 microsecond pulsewidth 5-10 km range and antenna beamwidths of 1 to 2 degrees) show that a ground clutter return varies from 25 sq. meters to 100 sq. meters or 27 to 33 dB greater than a 0.05 sq. meter target and 14 to 20 dB greater than a 1 square meter target. A reflectivity coefficient of -20 dB was assumed. This value encompasses the 84 percentile of all forms of measured ground clutter except city clutter and encompasses the 50 percentile of city clutter. The improvement factor of the TPN-18 is 32 dB which is adequate for ground clutter rejection except in the case of strong clutter and the smallest 0.05 square meter target. Further consideration will be necessary i.e., the use of FFT modification to gain more rejection in this extreme case.

The ARBAT system which is suitable for tracking projectiles for ranges exceeding the FALW-D requirement, is described in Appendix E. The performance of the RASIT ground surveillance system is as follows:-

Range (for a detection probability of 90 percent)

For pedestrian	12 to 14 km
For jeep	18 to 20 km

Accuracy

In range	$\pm$10m
In bearing	$\pm$10mils

Discrimination between close targets

In range	40m
In bearing	45mils

Sectors surveyed

Adjustable from $\pm$200 to $\pm$1100 mils about the sector center-line, the latter being positioned anywhere in a 360^{o} circle by a control on the console.

Elevation angle

Adjustable from -200 to +400 mils by a control on the console.

Distance between the operator's console and the antenna

Maximum 50m

Further details of the RASIT System are given in Appendix F.

2.3.3 FALW-D Cost

The estimated cost of a radar system for FALW-D may be obtained, for the truncated version of the HELVADS/FALW System, from the development costs summarized as a part of the production costs in Section 3. To this must be added the manufacturing costs of an appropriate fraction of one of the development models. These estimates must be treated with caution. They are developed by means of the parametric estimating procedure PRICE suited for production estimation. An estimate of the cost of manufacturing a stand alone truncated system would be developed differently and only after a much deeper design analysis than possible in this study.

The cost of System A and B similarly requires more detailed definition but for different reasons. The loan of service equipment or the lease of company prototype equipment in the case of existing radars may be possible for the period of the demonstration.

The auxiliary equipment, particularly for computer and data processing, is changing in cost and characteristics quite rapidly. Even a top level estimate at this time would be of questionable value.

3. SYSTEM COSTS & LIFE CYCLE COSTS

Methodology

For the purposes of this study ITTG chose to use the PRICE (Programmed Review of Information for Costing and Evaluation) model which the company leases from RCA. The system is well known and is in general use throughout the industry and is particularly suited to cost analyses of systemsdefined only to top level.

The price model uses parametric estimating procedures with the following fundamental data as inputs:

- Quantities of equipment to be developed and produced.
- Schedules for development procurement and production.
- Hardware geometry consisting of size; weight of electronic and structural elements.
- New design and complexity factors.
- Hardware operational environment and specification requirements.
- Manufacturing complexity.
- Manufacturing/fabrication processes.

The block diagram, Figure 24, was used as the basis for the subunit count and each subunit was defined in terms of the input parameters stated above. The inputs are necessarily subjective, arrived at by small committee, and based on and extrapolated from examples taken from current military programs.

An additional exercise was undertaken although not strictly within the task framework of the study and that was the development of a cost for a small run of six systems, a number chosen to represent a preproduction program.

The results are summarized below:

6 Systems

Development and one prototype	5,700
Production of 5 systems	7,600
Cost of each production system	1,520

Number of	Theater 1 (Cont. U.S.)	Theater 2 (Pacific)	Theater 3 (Europe)
Org. Maintenance Locations	6	1	5
Org. Supply Locations	6	1	5
Intermediate Maintenance Locations	3	1	2
Intermediate Supply Locations	3	1	2
Depot Maintenance Locations	1	0	1
Depot Supply Locations	1	0	1

TABLE 7

ESTIMATED SUPPORT LOCATIONS FOR LIFE CYCLE COST ESTIMATE

200 Systems

Development and one prototype	5,700
Poduction of 199 Systems	194,300
Cost of each production System	970

400 Systems

Development and one prototype	5,700
Production of 399 Systems	380,300
Cost of each production System	950

Units are thousands of 1983 dollars. A 25 month development program and 19 month , 60 month, and 102 month production programs were postulated for the 6, 200 and 400 systems.

A number of assumptions had to be made to extend the estimate to life cycle costs. The service life was assumed to be 20 years. The equipment would see service in the continental United States, in the Pacific and in Europe, the number of equipment at these locations being 100, 20 and 80 respectively. The three theaters were estimated to have the support locations shown in Table 7.

The life cycle costs include the cost to maintain and support the equipment for the life of the program, the cost of procuring consumable spares, cost of retaining the new item in the supply system, cost of labor at military maintenance locations, shipping costs, spares storage costs and floor space costs.

The estimate additional life cycle cost is 97,600K dollars (1982) for 200 systems or an additional 490K per system, approximate 1/3 of the total cost.

APPENDICES

A. Tracking Analysis

B. Model for resonant transmittance in the millimeter region

C. 35 GHz Active Aperture

D. AN/TPN-18A Air Traffic Control Radar

E. ARBAT Radar Description

F. Description of the Rasit 72A Ground Surveillance Radar

G. Coherent Laser Radar

APPENDIX A

TRACKING ANALYSIS

3.5 Preliminary Tracking Analysis: A preliminary tracking analysis was completed during this report period. The analysis was intended as a quick-look exercise and consequently used as a basis worst or near worst case target parameters (10g maneuvers at 2000 feet/sec). Accordingly the capability of the radar used for the analysis in terms of angular measurement accuracy was conservatively selected, 2.2 and 3.3mr (1σ). Bias errors are assumed to be calibrated out and range errors are negligible. Tracking accuracies in the range of 1 to 10 mr are desired. Target update intervals needed to obtain the desired accuracies are derived herein.

Section 3.5.1 describes the analysis approach employed; namely, a steady state analysis using an α-β tracker. Both dynamic lag errors due to target acceleration and random errors due to the noisy radar measurements are considered.

Section 3.5.2 presents tabular and graphical accuracy results as a function of target range and the target update interval (0.125 to 1.0 seconds). Section 4.0 gives conclusions of the study.

3.5.1 Analysis

A steady state tracking analysis is employed to derive tracking accuracy results as a function of target range and target update interval. The radar is assumed to make measurements at regular intervals spaced in time by T seconds. To simplify the analysis, it is assumed that a measurement is obtained on each radar look. (This should be nearly the case due to the short ranges of interest.) An α-β tracking filter with a $\beta = \alpha^2/(2-\alpha)$ and $0 < \alpha, \beta \leq 1$ is assumed.

Tracking errors due to target acceleration and noisy radar measurements are considered. The target angular position predicted one measurement interval ahead in time is the quantity for which tracking errors are evaluated.

For a constant acceleration turn, the α-β tracking filter will exhibit a predicted angular position dynamic lag error given by

$$\text{Lag} = \frac{aT^2}{\beta R} \qquad (1)$$

where a = target acceleration
T = target update interval
β = track filter parameter
R = target range

The radar measurement errors are assumed to be independent from look-to-look. The standard deviation of the predicted angular position (σ_p) is related to the single look radar measurement accuracy (σ_m) by

$$\sigma_p = \frac{2\beta + \alpha\beta + 2\alpha^2}{\alpha(4 - 2\alpha - \beta)}^{\frac{1}{2}} \sigma_m \qquad (2)$$

For $\beta = \alpha^2/(2-\alpha)$ and $0.1 \leq \alpha \leq 1.0$, which is the region of interest for this application, σ_p may be approximated as

$$\sigma_p = (0.49 + 1.7\beta)\sigma_m \qquad (3)$$

The error in doing so is at most 4%.

From equations (1) and (3), the lag plus 1σ random error is given by

$$E = \frac{aT^2}{\beta R} + (0.49 + 1.7\beta)\sigma_m \qquad (4)$$

The value of tracking filter parameter which minimizes the total error E can be determined by taking the derivative of equation (4) with respect to and equating it to zero. Doing so yields

$$\beta = T\sqrt{\frac{a}{1.7\,R\sigma_m}} \qquad (5)$$

If the optimum β is greater than unity, then β is set equal to one* and the total error is evaluated using equation (4). If β is less than unity, equation (5) for β is substituted into equation (4) giving

$$E = 2T \frac{1.7a\sigma_m}{R} + 0.49\sigma_m \quad (6)$$

The dynamic lag error with optimum $\beta(<1)$ is given by

$$\text{Lag} = T \frac{1.7a\sigma_m}{R} \quad (7)$$

The one sigma random error with optimum $\beta(<1)$ is given by

$$\sigma_p = \frac{1.7a\sigma_m}{R} + 0.49\sigma_m \quad (8)$$

.3.5.2 Results

Using the analytical expressions presented in Section 2.0, tracking accuracy results have been calculated for a 10 g maneuver, radar measurement accuracies (σ_m) of 2.2 and 3.3 mr, target update intervals (T) of 1.0, 0.5, 0.25, and 0.125 seconds, and target ranges of 2,3,4,6, and 8km. These results are summarized in Tables 1 and 2. The total error (E) as a function of target range and target update interval is plotted in Figures 1 and 2 for 2.2 and 3.3mr radar measurement accuracies, respectively.

For target update intervals of 1.0 and 0.5 seconds there is either none or very little smoothing by the tracking filter. For a 3.3mr radar measurement accuracy, which is more representative of the longer ranges

* This corresponds to simple extrapolation (no smoothing).

(6 to 8km), the total error is greater than 10mr virtually everywhere (T = 1.0 and 0.5 sec).

Shorter update intervals are needed to obtain errors less than 10mr.

Table 1 - Track Accuracy Results for a 10g Target Maneuver and 2.2mr Radar Measurement Accuracy

T = 1.0 sec

Range (km)	Lag Error (mr)	1σ Random Error (mr)	Total Error (mr)
2	49.0	4.8	53.8
3	32.7	4.8	37.5
4	24.5	4.8	29.3
6	16.3	4.8	21.1
8	12.3	4.8	17.1

T = 0.5 sec

Range (km)	Lag Error (mr)	1σ Random Error (mr)	Total Error (mr)
2	12.3	4.8	17.1
3	8.2	4.8	13.0
4	6.1	4.8	10.9
6	4.1	4.8	8.9
8	3.4	4.5	7.9

T = 0.25 sec

Range (km)	Lag Error (mr)	1σ Random Error (mr)	Total Error (mr)
2	3.4	4.5	7.9
3	2.8	3.8	6.6
4	2.4	3.5	5.9
6	2.0	3.0	5.0
8	1.7	2.8	4.5

T = 0.125 sec)

Range (km)	Lag Error (mr)	1σ Random Error (mr)	Total Error (mr)
2	1.7	2.8	4.5
3	1.4	2.5	3.9
4	1.2	2.3	3.5
6	1.0	2.1	3.1
8	0.8	1.9	2.7

Table 2 - Track Accuracy Results for a 10 g Target Maneuver and 3.3mr Radar Measurement Accuracy

T = 1.0 sec

Range (km)	Lag Error (mr)	1σ Random Error (mr)	Total Error (mr)
2	49.0	7.2	56.2
3	32.7	7.2	39.9
4	24.5	7.2	31.7
6	16.3	7.2	23.5
8	12.3	7.2	19.5

T = 0.5 sec

Range (km)	Lag Error (mr)	1σ Random Error (mr)	Total Error (mr)
2	12.3	7.2	19.5
3	8.2	7.2	15.4
4	6.1	7.2	13.3
6	4.8	6.4	11.2
8	4.1	5.7	9.8

T = 0.25 sec

Range (km)	Lag Error (mr)	1σ Random Error (mr)	Total Error (mr)
2	4.1	5.8	9.9
3	3.4	5.0	8.4
4	2.9	4.5	7.4
6	2.4	4.0	6.4
8	2.1	3.7	5.8

		T = 0.125 sec.	
Range (km)	Lag Error (mr)	1σ Random Error (mr)	Total Error (mr)
2	2.1	3.7	5.8
3	1.7	3.3	5.0
4	1.5	3.1	4.6
6	1.2	2.8	4.0
8	1.0	2.7	3.7

3.5.3 Conclusions

1. Target update intervals of approximately 0.25 sec are required to obtain a total error of less than 10mr at all target ranges for a second order (position and velocity) tracking filter.

2. Transient errors at the onset of a maneuver have not been analyzed and could possibly result in even larger errors.

3. A third order (position, velocity, and acceleration) tracking filter would eliminate the steady state dynamic lag error due to target acceleration. Longer smoothing times might be possible, depending on the duration of the target maneuver and higher order time derivatives of target motion (jerk, etc.) Further information is required to investigate this option.

3.6 Body Motion Detection: The results from the yaw-sonde data collection (155mm) were expected from Yuma Proving Ground at the end of July, however, the data has not been received as of this report date. That data will be supplied when received from the Army .

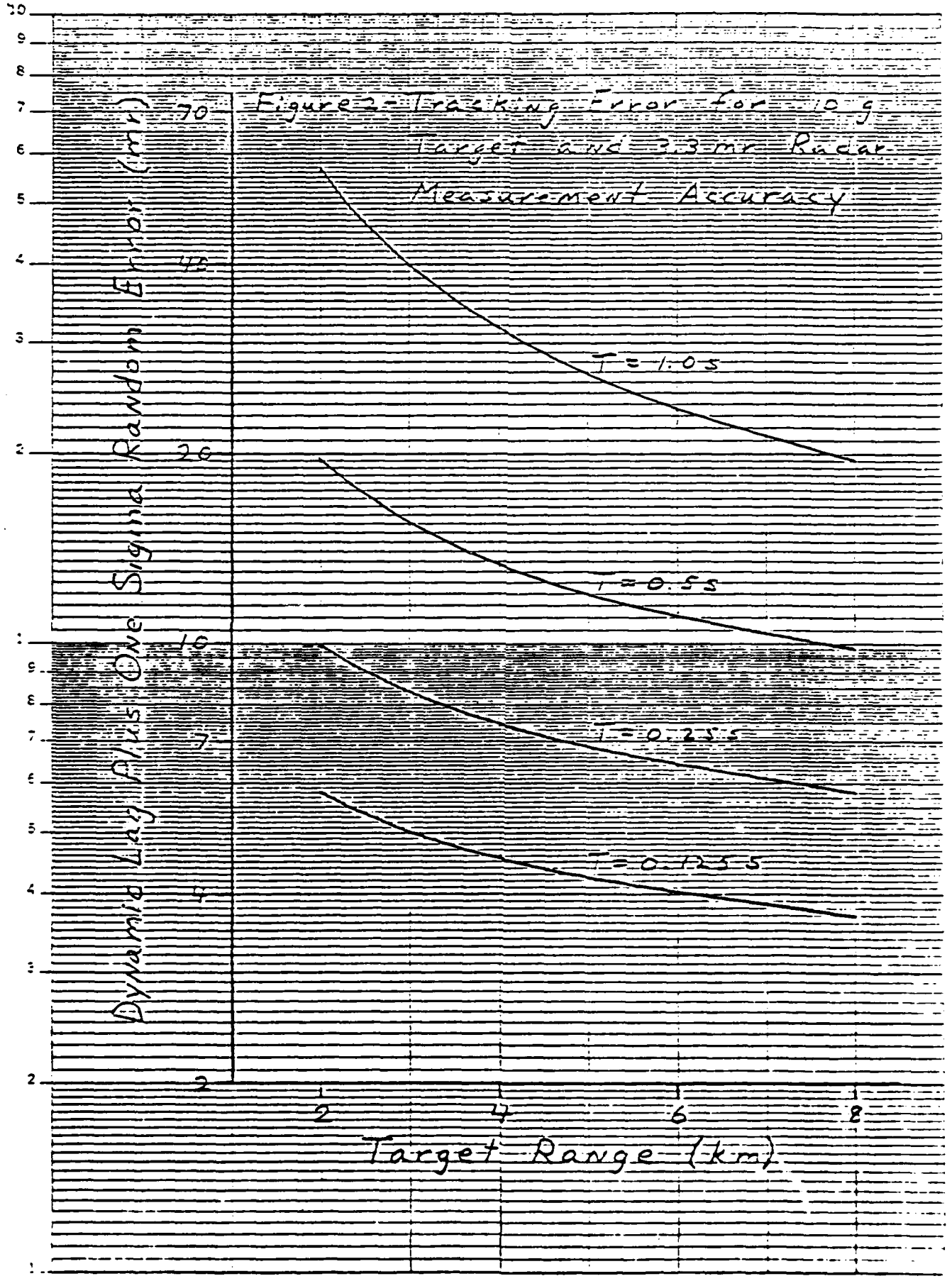
Figure 2 - Tracking Error for .10 g Target and 2.3 mr Radar Measurement Accuracy
Dynamic Lag, 1/2 One Sigma Random Error (mr)
70
40
20
10
7
4
T = 1.0 s
T = 0.5 s
T = 0.25 s
T = 0.125 s
2
4
6
8
Target Range (km)

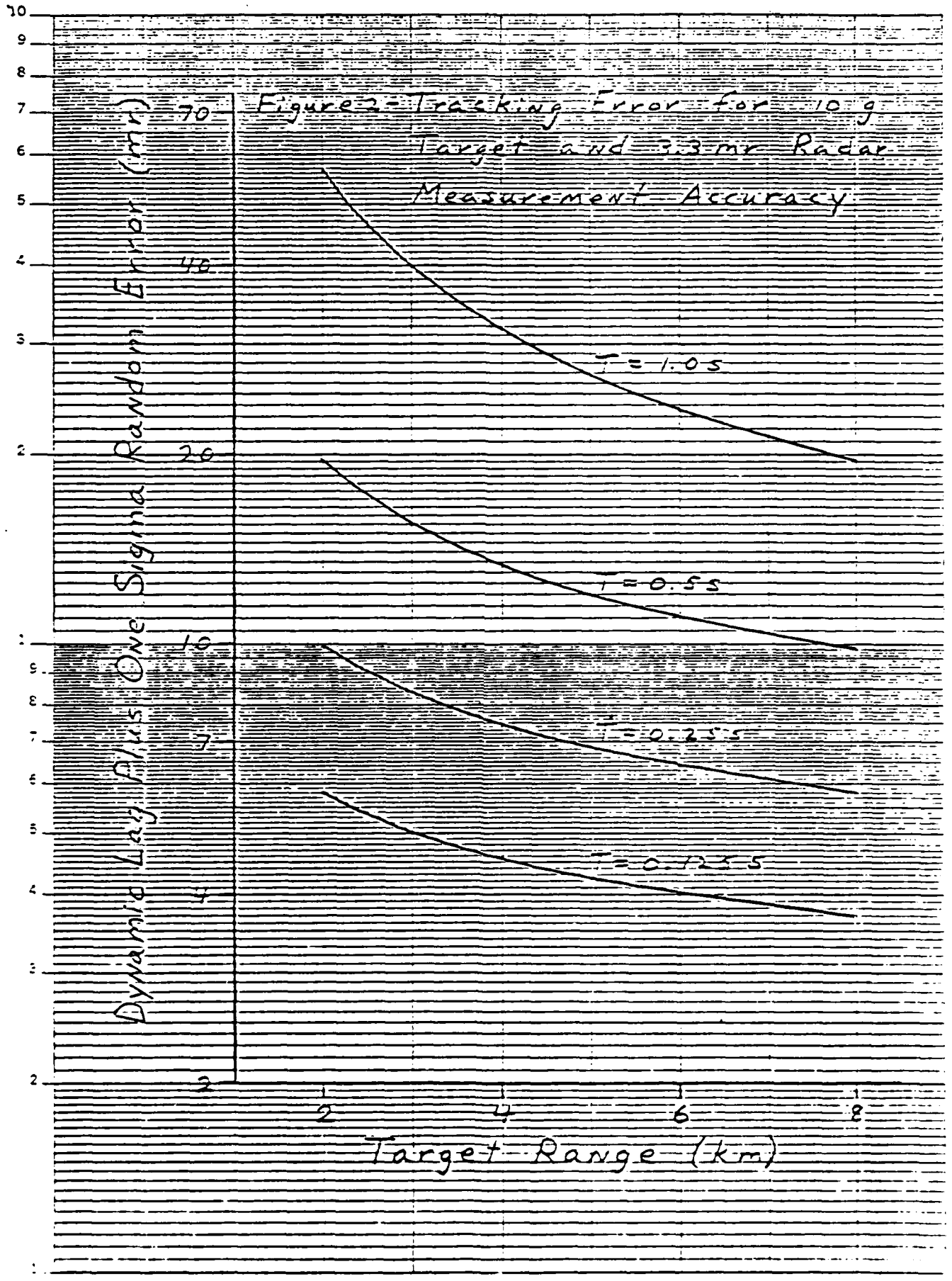
Figure 2 - Tracking Error for 10 g Target and 3.3 mr Radar Measurement Accuracy
Dynamic Lag, 1 Sigma Random Error (mr)
Target Range (km)
T = 1.0 s
T = 0.5 s
T = 0.25 s
T = 0.125 s
10
9
8
7
6
5
4
3
2
70
40
20
10
7
4
2
2
4
6
8

APPENDIX B

MODEL FOR RESONANT TRANSMITTANCE IN THE MILLIMETER REGION

Model for resonant transmittance in the millimeter wave region

Joseph H. Pierluissi, Ken Tomiyama, Doug Fowler
Department of Electrical Engineering, The University of Texas at El Paso
El Paso, Texas 79968

Richard B. Gomez
Atmospheric Sciences Laboratory, White Sands Missile Range, New Mexico 88002

Abstract

A study is made of the modeling of atmospheric resonant transmission in the millimeter wave region. The model consists of an exponential function whose argument is defined as the product of a spectral parameter, and the pressure, the temperature and the absorber amount to some powers. All the model functional parameters were determined through least-squares analysis of line-by-line data, computed with the use of the Van Vleck-Weisskopf line shape, at conditions typical of the lower 5 km of the atmosphere. The development was extended at 1 GHz intervals throughout the entire millimeter wave region (30 through 300 GHz). Individual models were developed for water vapor and oxygen, with a resulting reproducibility of 0.08 and 0.66%, respectively.

Introduction

Considerable interest has developed in recent years for the use of the millimeter wave region (30 through 300 GHz) in military and industrial applications. These waves propagate more efficiently through the atmosphere under adverse weather conditions than optical waves, and have associated radiators which are smaller than their counterparts in the microwave region. However, millimeter waves are strongly absorbed by the resonant lines of atmospheric water vapor and oxygen.

Since there are relatively fewer absorption lines as compared to the infrared region, most transmittance calculations for millimeter waves are performed using the rigorous line-by-line method. Controversy still prevails as to the most appropriate line shape to adopt, and as to the origin and extent of the continuum absorption. Neither of these questions are dealt with in this paper. Here, emphasis is placed on the methodology needed for the development of a simple analytical expression for the transmittance, which does not require a summation over all overlapping lines. Numerous occasions occur in practice where the rigorous and time-consuming line-by-line method is used, when a simpler model would have been amply justified.

For the purpose of arriving at the desired model for atmospheric transmittance the authors extend well-documented numerical algorithms from the infrared into the millimeter wave region. In contrast to the low resolution "band models" of the infrared, the narrow band widths of the instruments in the latter spectral region require the adoption of nearly monochromatic models. The technique basically consists of curve-fitting an exponential function to transmittance data in the form of curves-of-growth (i.e. transmittance versus the logarithm of the absorber amount) at given frequency intervals, assuming a power law for the meteorological variables. The model was applied to water vapor and oxygen with line-by-line data obtained through the use of the Van Vleck-Weisskopf line profile. The results indicate that the methodology is not only suitable to the millimeter wave region, but even simpler to apply than in the infrared region.

2. Proposed Model

The transmission of radiation at a frequency f through an atmospheric medium at pressure P and temperature T, containing absorbing gases, is given by Beer's Law in the form

$$\tau_f = e^{-K(f,P,T)U} , \tag{1}$$

where τ_f is the transmittance, K is the absorption coefficient, and U is the absorber amount given by the product of the absorber density ρ and the path length R. For infrared bands the quantity of interest is the weighted mean transmittance τ defined over a bandwidth Δf as

$$\tau = \int \tau_f \phi_f df \Big/ \int \phi_f df , \tag{2}$$

where ϕ_f is the frequency response of the instrument. As a result of an intensive study involving infrared absorption by water vapor, ozone, uniformly-mixed gases and trace gases [1,2] it was found that τ in [1,2] can be very well approximated by the double exponential

$$\tau = \exp\left\{-10^{a_1 + a_2 X + a_3 X^2 + \ldots}\right\} , \tag{3}$$

with

$$Y = \log_{10}\left\{C\left(\frac{P}{P_o}\right)^n\left(\frac{T_o}{T}\right)^m U\right\} \quad , \tag{4}$$

where a_1, a_2, a_3, n, and m are constants, C is a spectral parameter defined over Δf, and P_o and T_o are the standard pressure and temperature, respectively.

Since in the millimeter wave region typical bandwidths are of the order of 1 GHz, Δf in (2) may be viewed as a Dirac delta function $\delta(f-f_o)$ such that (3) may also be justified as an approximation to (2) at the bandwidth center frequency f_o. However, because of the narrowness of Δf, it should be expected that all the absorber constants will now show frequency dependence near the line centers. For numerical simplicity, and with little sacrifice in accuracy, it is convenient to linearize the exponent in (3) by retaining only the first two terms. Substituting (4) into (3) results in the equation

$$\tau = \exp\left\{-10^{a_1}\left[C\left(\frac{P}{P_o}\right)^n\left(\frac{T_o}{T}\right)^m U\right]^{a_2}\right\} \quad , \tag{5}$$

which when equated to (I) gives $a_2 = 1$. Defining $C' = 10^{a_1} C$ in (5) it gives

$$\tau = \exp\left\{-C'\left(\frac{P}{P_o}\right)^n\left(\frac{T_o}{T}\right)^m U\right\} \quad , \tag{6}$$

where now

$$X = \log_{10}\left\{C'\left(\frac{P}{P_o}\right)^n\left(\frac{T_o}{T}\right)^m U\right\},$$

which constitute the transmittance model adopted in the present work.

It is of interest that the resulting model in (6) is in close agreement with the classical "scaling approximation" proposed decades ago [3] for use as band models. This latter approximation seems to have arisen by assuming that the absorption coefficient is separable as the product of the three independent variables f, P, and T. Equation (6) is also frequently called the "power law" and is being used as an approximation for a multitude of attenuation mechanisms.

In the millimeter region it is customary to specify the amount of absorption in terms of an attenuation coefficient α, defined from (1) as

$$\alpha = K(f, P, T)\rho \quad ,$$

such that by comparison with (6) it becomes

$$\alpha = C'\left(\frac{P}{P_o}\right)^n\left(\frac{T_o}{T}\right)^m \rho \quad , \tag{7}$$

which is usually expressed in dB/Km.

Application of model to water vapor and oxygen

For the purpose of testing the validity of the model in (6) in the millimeter wave region, transmittance data were generated for water vapor and oxygen for the first five kilometers of the atmosphere. The computer code developed by Liebe and Rasich [4], with the nonresonant absorption removed, was used in connection with several atmospheric models [5] to generate an average of 23" data points for each absorber per frequency. This code uses the modified Van Vleck-Weisskopf line shape for transmittance calculations in the lower 20 Km of the atmosphere. The absorber densities in these atmospheric models were modified to correspond to conditions of 5,50 and 100% relative humidity. At each meteorological condition, the range was varied so as to generate a wide range of data between zero and unity transmittance.

Curve-fitting to the curves of growth has the advantages that the resulting model will be valid over a broad range of transmittance levels, and that its accuracy may be realistically appreciated in terms of percent transmittance deviation from the original. The data in this form have been traditionally used for the extraction of the transmittance function itself either graphically [6] or through a computer algorithm [7]. The calculations were repeated at 1 GHz interval in the range from 50 to 300 GHz for water vapor, and from 50 to 159 GHz for oxygen. Because of the strong absorption in the lower atmosphere by the 183.31 GHz line of water vapor it is useless to model oxygen beyond 159 GHz.

The numerical procedures consisted of minimizing through linear least squares the square error E_i, given by

$$E_i = \left\{ \log_{10} (-\ln \tau_i) - \log_{10} (-\ln \tau) \right\}^2 \quad , \tag{8}$$

where τ is computed from (6) at conditions P_i and T_i and the τ_is are the line-by-line transmittance values. Substituting (6) into (8) gives

$$E_i = \left\{ \log_{10} (-\ln \tau_i) - \log_{10} C' - n \log_{10}\left(\frac{p}{p_o}\right) - m \log_{10}\left(\frac{T_o}{T}\right) - \log_{10} U \right\}^2 \quad . \tag{9}$$

The total square error follows as

$$E = \sum_{i=1}^{I} E_i \quad , \tag{10}$$

in which I is the total number of data points at each spectral interval. The model parameters are then determined from the 3x3 matrix obtained from (9) by taking the partial derivatives of E with respect to $\log_{10}$ C', n, and m.

At one gigahertz interval throughout the millimeter wave region the model parameters were determined individually for water vapor and oxygen. Figures 1 and 2 depict samples of the line-by-line calculated absorption coefficients and the corresponding transmittances for one kilometer path at standard conditions. Figures 3a, b and c show graphically the numerical procedure used in obtaining the model parameters for water vapor at 67, 94 and 185 GHz, in a medium with 50% relative humidity. In the final analysis all the data for the three values of relative humidity were combined. Figure 3a shows a scatter of the curves of growth at each frequency due to the various pressure-temperature combinations. The result of plotting the same data versus the logarithm of the equivalent absorber amount, defined as

$$W = \left(\frac{p}{p_o}\right)^{n/T_o} \left(\frac{T_o}{T}\right)^m U \quad , \tag{11}$$

is depicted in Figure 3b. In (11) the optimal values for n and m obtained from the least squares analysis were used. The effect of the displacement parameter C' is illustrated in Figure 3c, where it is noted that the three transmittance curves for the three frequency intervals are slided spectrally to form a single curve. The X parameter defined in (6) was used. The same graphical development for oxygen is shown in Figures 4a, b and c.

The nearly exact overlapping of the transmittance curves obtained as a result of the model development occurs because in the millimeter wave region the functional form of the curve is known to be exponential. This is not the case in the infrared region because of the spectral averaging, and techniques analogous to these are used to extract the functional form itself. When no analytical functions are used at the offset in the analysis, the extracted transmittance function is usually called "empirical".

In all computations in this paper the absorber amount was determined with the use of the relations,

$$\begin{aligned} U_v(\mathrm{gm/cm^2}) &= 10^{-1}\, \rho_v(\mathrm{gm/m^3})\, R(\mathrm{Km}) \quad , \\ U_{O_2}(\mathrm{atm.\ cm}) &= 10^5 \frac{\rho_{O_2}}{\rho_{O_2\,(STP)}} R(\mathrm{Km}) \quad , \end{aligned} \tag{12}$$

where

$$\frac{\rho_{O_2}}{\rho_{O_2\,(STP)}} = 10^{-6} M \left(\frac{p}{p_o}\right)\left(\frac{T_o}{T}\right) \quad ,$$

and where the subscripts "v" and "O_2" stand for water vapor and oxygen, respectively, and M is the mixing ratio of oxygen in parts per million by volume. With these definitions and (7), it follows that the attenuation coefficients for water vapor and oxygen may be written, respectively, as

$$\alpha_v\,(\mathrm{dB/Km}) = 0.8686\, C'_v \left(\frac{p}{p_o}\right)^n \left(\frac{T_o}{T}\right)^m \rho_v\,(\mathrm{gm/m^3}) \quad , \tag{13}$$

$$\alpha_{O_2}\,(\mathrm{dB/Km}) = 8.686 \times 10^5\, C'_{O_2} \left(\frac{P}{P_o}\right)^n \left(\frac{T_o}{T}\right)^m \frac{\rho_{O_2}}{\rho_{O_2\,(STP)}}\,,$$

in which C'_V is in cm^2/gm and C'_{O_2} is in $(atm.\ cm)^{-1}$.

Discussion and conclusions

A numerical procedure commonly used in the infrared region has been extended to the millimeter wave region, and it has been found that in the latter case it is easier to apply still providing comparable accuracy. The transmittance function does not need to be extracted from the data, and fewer terms in the exponent are required for the numerical optimization of the model parameters. At a given frequency the model makes use of three parameters per absorber, while the line-by-line method requires the use of the four spectroscopic parameters for each one of the six lines of water vapor and the 36 lines of oxygen.

The displacement parameter C' is shown in Fig. 5 as a function of frequency for both absorbers. The individual magnitudes of this parameter are indicative of the strengths of the absorption, and are also measures of the displacement of the transmittance curve along the absorber amount axis. The relative vertical displacement between absorbers is dependent on the units adopted for the absorber amount. The behavior of the pressure exponent n across the millimeter region is illustrated in Fig. 6. The figure shows that it is nearly one for both absorbers in the window region, while it drops to negative values near the strong absorption lines. This is to be expected since at the line center the absorption coefficient is inversely proportional to the line half-width, while in the wings it is directly proportional to the line width. Hence, Fig. 6 shows that near the line centers for both absorbers n tends to negative one, while in window regions it reaches an average value of about one.

The temperature coefficient m is illustrated in Fig. 7 where it shows a behavior analogous to that of n. In the windows it ranges from about zero to 2.5, while near the strong lines it drops significantly. The former effect is to be expected since in the windows the absorption coefficient is directly proportional to both the line intensity and the half width, which in turn are proportional to T_o/T elevated to some positive power. Near the line centers the absorption coefficient is still directly proportional to the line intensity but it is then inversely proportional to the half width. The drop at these frequencies, however, is not generally as large as in the case of n because the line intensity multiplying the absorption coefficient varies more strongly with temperature than the half width.

In the infrared region these exponents are often assumed to be spectrally independent, at least within the principal absorption bands of the major absorbers. The standard deviation of the transmittance from the original line-by-line data is shown in Fig. 8, which shows that it generally remains below 0.001. The exception is oxygen, which shows an increasing deviation beyond 159 GHz. This deviation, however, is meaningless since the absorption in this region is strongly dominated by the water vapor line at 183.31 GHz and others above.

A summary of the model parameters and of the transmittance deviations for some typical window and line center frequencies in the millimeter wave region is included in Table 1 for the convenience of model users. It should be pointed out that the use of a different line shape function would have yielded somewhat different results. In such a case, the curve-fitting procedures discussed here may be easily applied by the user to the line-by-line data obtained with those line shapes. The model may be also developed with comparable accuracy for the higher regions of the atmosphere at 5 Km intervals or more. It should be recognize however, that at the higher altitudes other mechanisms become operative and that finer spectral intervals in the modeling become necessary. A complete set of the model parameters discussed in this paper may be obtained free of charge by contacting the authors.

Acknowledgements

The authors wish to express their sincere gratitude to Lupe Rodriguez and to Doug Madden for their expert assistance in the preparation of the manuscript.

References

1. J. H. Pierluissi, K. Tomiyama, and R. B. Gomez, "Analysis of the LOWTRAN transmission functions," Appl. Opts. Vol. 18, pp. 1607-1611, May 1979.
2. J. H. Pierluissi and K. Tomiyama, "Numerical Methods for the generation of empirical and analytical transmittance functions with applications to the atmospheric trace gases," Appl. Opts. Vol. 19, pp. 2298-2309, July 1980.
3. R. M. Goody, Atmospheric Radiation, Oxford Univ. Press, London (1961).
4. H. J. Lieve and R. K. Rosich, "Computer program for EHF transfer properties of clear air," Institute for Telecommunications Sciences, Boulder CO, (1979).
5. S. L. Valley, ed., Handbook of Geophysics and Space Environments, McGraw-Hill, New York (1965).
6. R. A. McClatchey et al, "Optical properties of the atmosphere," Environmental Research Paper 331, AFCRL, Hanscom AFB, MA, (1970).

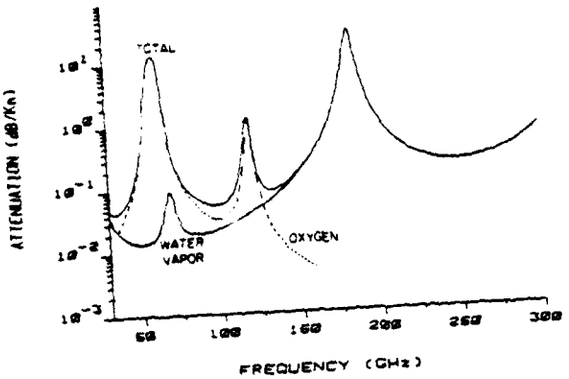

Figure 1. Absorption coefficients for water vapor and oxygen obtained from line-by-line calculations at T_o = 300 K, P_o = 101.33kPa, for a water vapor density of 7.5gm/m^3 and an oxygen mixing ratio of 2.09 x 10^{5}ppmv.

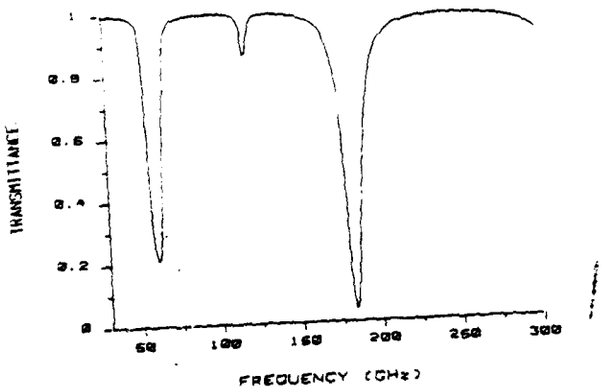

Figure 2. Total transmittance along a one-kilometer path with a combination of water vapor and oxygen at the conditions of Figure 1.

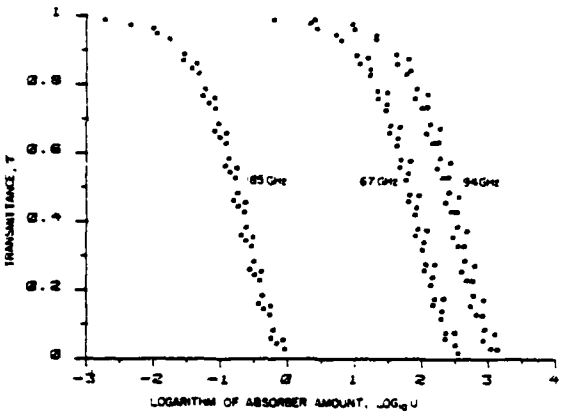

Figure 3a. Representative scatter diagram of the original water vapor transmittance data at 50% relative humidity.

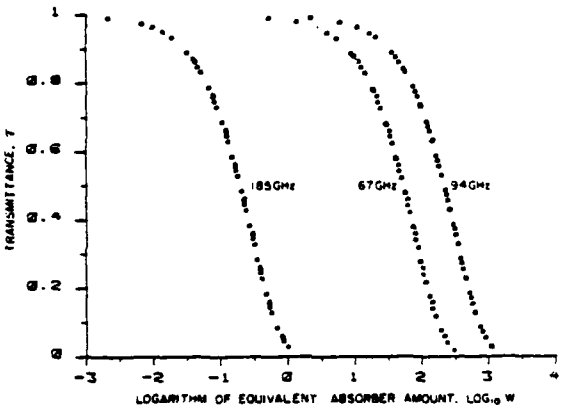

Figure 3b. The same water vapor as in Figure 3a, but smoothed out with the use of the optimal pressure and temperature parameters in the calculation of the equivalent absorber amount W.

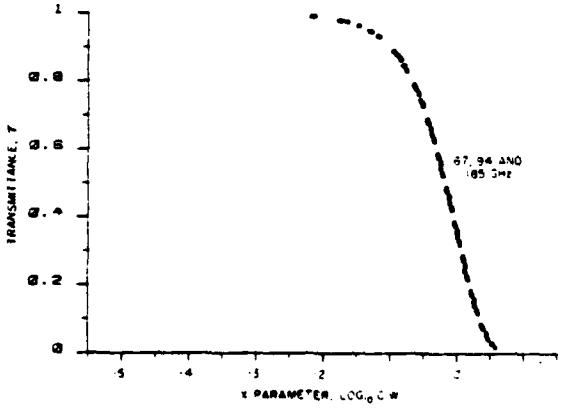

Figure 3c. The same water vapor data as in Figure 3b, but reduced to a single transmittance curve with the use of the spectral coefficient parameter C'.

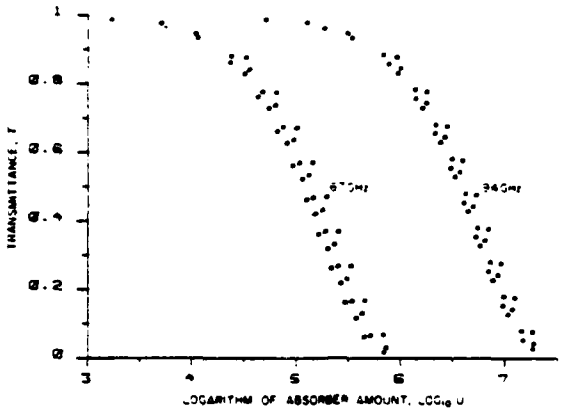

Figure 4a. Representative scattered diagram of the original oxygen transmittance data at 50% relative humidity.

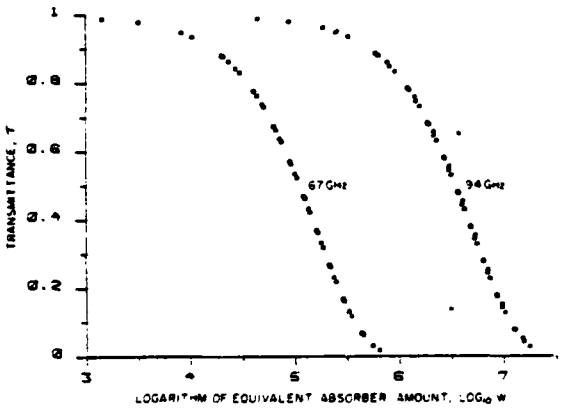

Figure 4b. The same oxygen data as in Figure 4a, but smoothed out with the use of the optimal pressure and temperature parameters in the calculation of the equivalent absorber amount W.

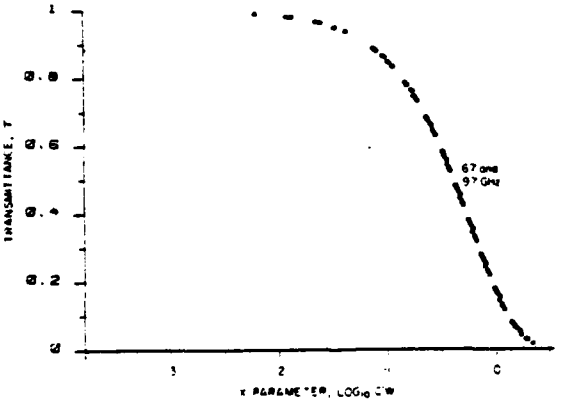

Figure 4c. The same oxygen data as in Figure 4b, but reduced to a single transmittance curve with the use of the spectral coefficient parameter C'.

APPEN C

35 GHZ ACTIVE APERTURE

35 GHz ACTIVE APERTURE

M. F. Durkin
R. J. Eckstein
M. D. Mills
M. S. Stringfellow

Motorola, Incorporated
Government Electronics Division
Scottsdale, Arizona 85252

R. A. Neidhard

Air Force Avionics Laboratory
Wright-Patterson AFB, Ohio 45433

ABSTRACT

Characteristics of a millimeter wave active array are described. Injection-locked pulsed IMPATT oscillators providing 36 watts peak transmitter power are integrated with a stripline-fed image array having a gain of 29 dBi. Performance of the transmitter, antenna and integrated active aperture are discussed.

Introduction

In recent years, considerable effort has been directed toward development of solid-state millimeter wave transmitters having sufficient power output for use in short range radars. Most of this work has concentrated on circuit techniques for combining the power from a number of solid-state sources. In many applications, however, additional benefits can be realized by integrating solid-state sources with the antenna and combining their powers in space. Such an approach eliminates most of the RF losses in connecting transmission lines. This paper describes a 35 GHz active array that spatially combines the power from pulsed IMPATT oscillators that are integrated with a printed circuit antenna.

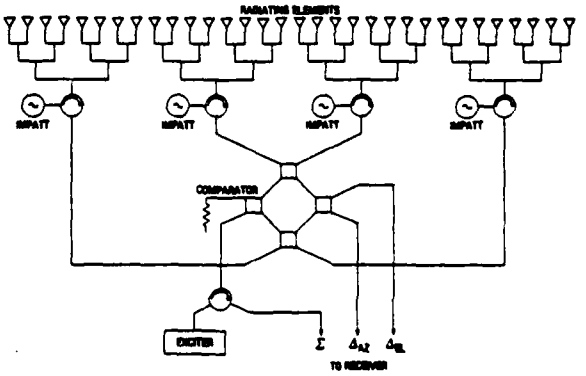

FIGURE 1: ACTIVE APERTURE BLOCK DIAGRAM

Design Concept

A block diagram of the 35 GHz active aperture is shown in Figure 1. The antenna array consists of 32 image radiating elements[1] in a 5.5-inch diameter aperture. The image array concept greatly reduces the number of radiators required and simplifies the array feed network. The array is divided into quadrants for monopulse operation, and each quadrant is fed by an injection-locked pulsed IMPATT oscillator. A two-stage exciter provides the injection locking signal that is distributed to the aperture oscillators through the monopulse comparator.

Antenna Array

The antenna array for the 35 GHz active aperture utilizes image radiating elements. The image effect is created by placing a partially reflecting planar surface above the plane of the array and parallel to it. A sheet of high dielectric constant ceramic is used in this case. Energy reflected from the ceramic surface is again reflected in the antenna ground plane. These multiple reflections form a series of images in the ground plane that are phased in accordance with the spacing between the ceramic and the ground plane. Spacing the ceramic one-half wavelength above the ground plane results in proper phasing for radiation normal to the plane of the antenna. The radiation pattern formed for each element is that of an end-fire array phased for radiation along its axis. Using this directive, high gain radiator, only 32 radiating elements are required in the 5.5-inch aperture compared to hundreds in a conventional array design of the same size. The simplified array feed network keeps losses in the 35 GHz printed circuit antenna to a minimum.

The 32 element array is implemented in balanced stripline. The circuit layout is shown in Figure 2. The image elements are excited by radiating slots in one ground plane. The modular IMPATT oscillators are integrated with the array feed circuit by means of coupling slots in the rear ground plane. Connection to the monopulse comparator terminals are also made by coupling slots.

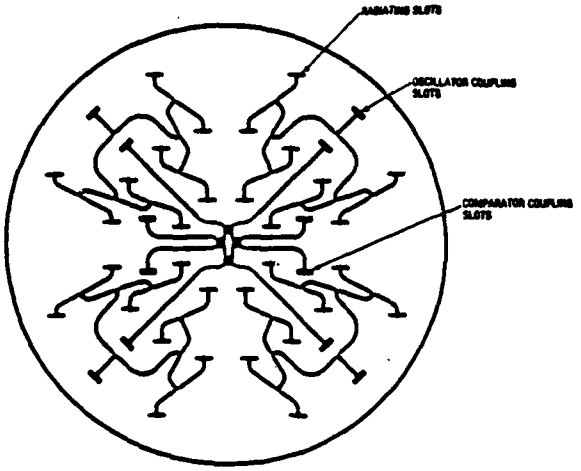

FIGURE 2: ANTENNA ARRAY CIRCUIT LAYOUT

Typical sum and difference radiation patterns of the passive antenna array are shown in Figures 3 and 4. Sum pattern sidelobes are down at least 20 dB in the E-plane and 18.5 dB in the H-plane. The beamwidth is less than 4.3 degrees. A gain of 29.13 dBi is provided for the active aperture transmitter. Difference pattern null depths are at least 28 dB below the sum peak.

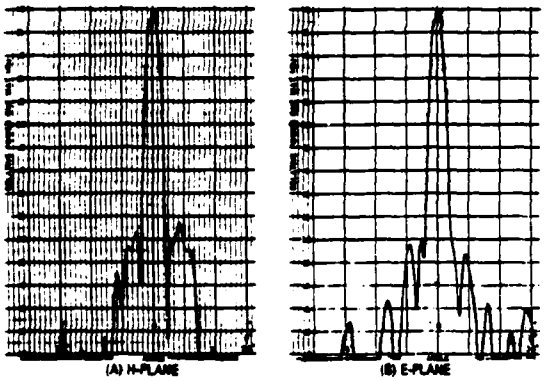

FIGURE 3: SUM CHANNEL RADIATION PATTERNS

Transmitter

The transmitter block diagram is shown in Figure 5. Four IMPATT oscillators serve as aperture power sources, one in each quadrant of the array. These are injection-locked by a two-stage exciter consisting of one Gunn oscillator and one IMPATT oscillator. The three oscillator stages of the transmitter are timed such that the pulse of each stage lies within the pulse of the preceding locking stage. Stability for the Gunn oscillator is provided by an external Q of 100 and 60 dB of load isolation.

An injection signal acts in a manner that reduces the real part of the load on a diode oscillator. Each

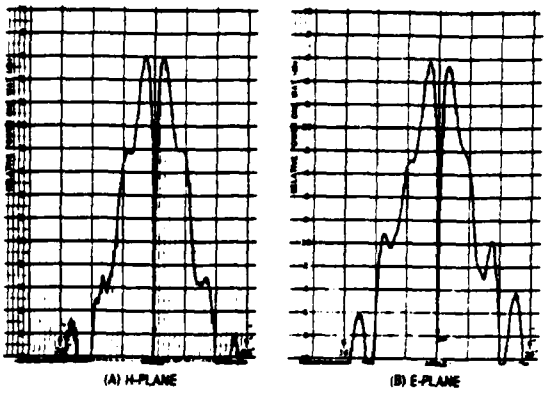

FIGURE 4: DIFFERENCE CHANNEL RADIATION PATTERNS

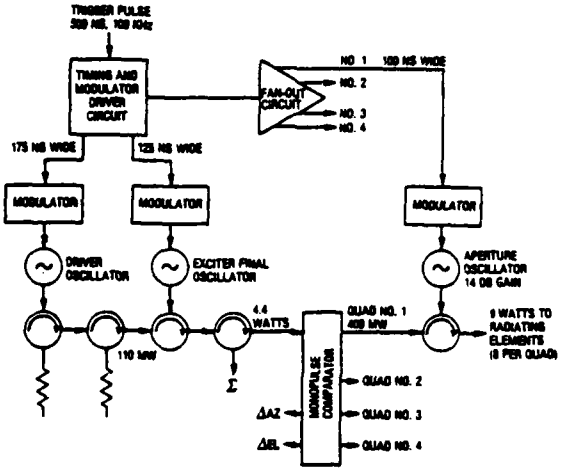

FIGURE 5: TRANSMITTER BLOCK DIAGRAM

aperture oscillator is tuned so that the addition of the locking signal loads the diode to the peak of its power curve. The output power of each oscillator and the locked gains of the IMPATT oscillators are indicated in Figure 5. Performance of the transmitter is summarized in Table I. A total of 36 watts peak transmitter power is provided by approximately 9 watts from each of the four aperture oscillators. The pulsewidth of the individual oscillators is 100 nanoseconds.

TABLE I. TRANSMITTER PERFORMANCE

EXCITER	
Power Output	4.4 watts peak
Pulse Length	125 ns
Pulse Repetition Frequency	100 kHz
Duty Factor	1.25 percent
Phase Chirp	10 degrees
APERTURE OSCILLATORS	
Power Output	9 watts peak (nominal)
Pulse Length	100 ns
Pulse Repetition Frequency	100 kHz
Duty Factor	1 percent
Phase Chirp (Absolute)	45 degrees
Phase Chirp (Relative)	20 degrees between oscillators

To obtain maximum radiated power from the active array, it is necessary that the four aperture oscillators track each other in phase during the transmit pulse. There are two sources of errors that can result in phase offsets between the aperture oscillators. The first is path length variations in passive components such as the array feed circuit, monopulse comparator and circulators. This type of error can be minimized by mechanical adjustments. The second source of phase errors results from differences in injection-locked phase offsets between the IMPATT oscillators. This type of error may be caused by differences in the free-running frequency of the oscillators or by differences in the chirp characteristics of the oscillators.

The free-running frequency of the oscillators can be adjusted by tuning. Frequency chirping during the pulse is caused by an increase in the diode temperature and can be minimized by shaping the bias current pulse. Using this technique, the transient phase error between the four aperture oscillators has been reduced to a maximum of 20 degrees.

Active Aperture Performance

Figure 6 shows the stripline antenna array and transmitter subassembly prior to integration. The antenna and transmitter were mated and tested as an integrated active array. After integration with the antenna, the changed conditions of impedance match and isolation between oscillators caused a reduction in the injection signal level. The four aperture oscillators were readjusted to obtain proper transmitter performance, and this reduced the oscillator outputs. Due to this factor, the measured radiated power was 1.6 dB below the maximum expected with a transmitter output of 36 watts. All of the IMPATT oscillators exhibited noise during the first 5 nanoseconds of the pulse. This noise effectively defocused the space combined output at the start of the pulse and reduced the transmitted pulse length to 95 nanoseconds.

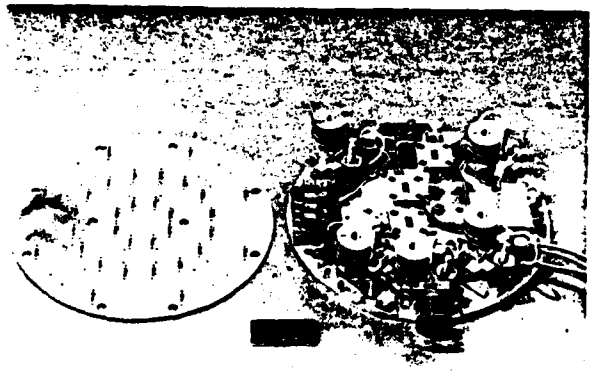

FIGURE 6: ANTENNA AND TRANSMITTER BEFORE INTEGRATION

Transmitted radiation patterns for the active aperture are shown in Figure 7. Sidelobes in the H-plane are down at least 17.5 dB. The E-plane pattern shows some asymmetry caused by uncompensated phase error, and the highest sidelobe is down 15.1 dB. However, the phase error is not large enough to have a significant effect on the combined power output. The boresight error between the monopulse null position and the transmitted sum peak is less than 0.5 degree.

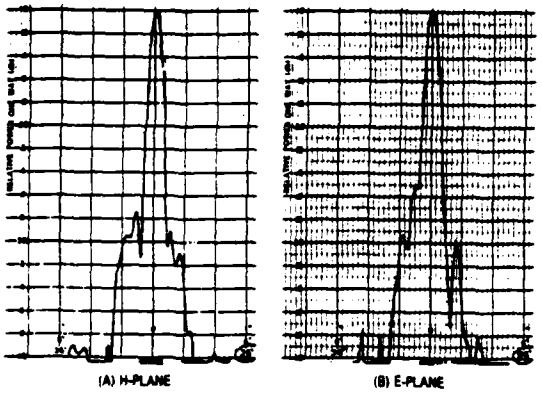

FIGURE 7: TRANSMITTED RADIATION PATTERNS

Acknowledgement

The work reported in this paper was sponsored by the Air Force Avionics Laboratory, Air Force Wright Aeronautical Laboratories, Air Force Systems Command, Wright-Patterson AFB, Ohio 45433, under Contract No. F33615-79-C-1794.

References

1. Sasser, B.H., "A Highly Thinned Array Using the Image Element," presented at the 1980 IEEE International Symposium on Antennas and Propogation, June 1980.

This paper presented at the 1981 IEEE/MTT-S, International Microwave Symposium, June 1981.

APPENDIX D

AN/TPN18A AIR TRAFFIC CONTROL RADAR

GILFILLAN

AN/TPN-18A Air Traffic Control Radar

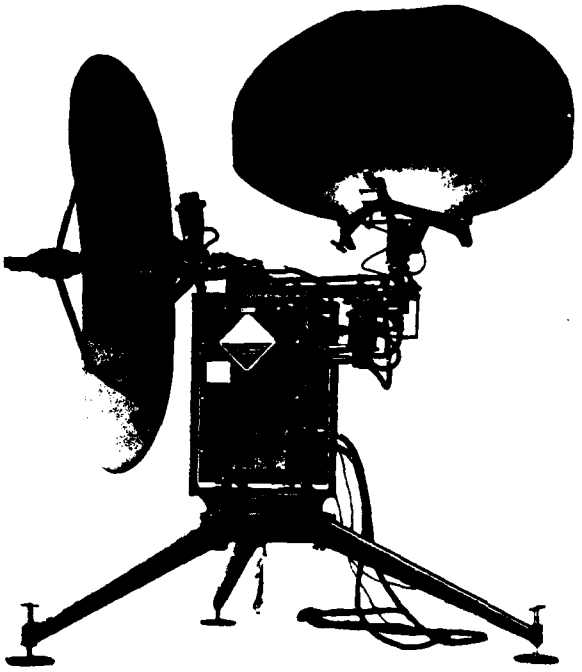

The AN/TPN-18A Ground Controlled Approach Radar System, developed for the U. S. Army, is a lightweight, tactical ground-based radar which provides precise three-function information to airport/heliport controllers. These functions consist of terminal area surveillance (ASR), precision approach for control of landings (PAR), and height finding for aircraft monitoring. This versatile system is readily transported by helicopter, cargo aircraft, or truck, and is suitable for truck/trailer mounting for full mobility in combat-related operations. The earlier TPN-8 version, designed for the Marine Corps' military all-weather tactical operations, has since been adapted by other military services.

The AN/TPN-18A radar includes a transmitter-receiver group which consists of a completely solid-state transmitter and receiver, an antenna system, an indicator group which consists of the two indicators, and a miscellaneous group consisting of remote cables and operating spares.

The AN/TPN-18A is used by controllers to guide and land aircraft in poor visibility. In addition to the search, final approach, and height-finding modes, the controller may choose the simultaneous mode for displaying surveillance data on one indicator and precision approach and height-finding data on the other. Thus two controllers can be utilized during periods of heavy traffic. Further, IFF signals can either appear with the radar surveillance data or may be displayed separately up to a range of 80 nautical miles.

Elevation coverage of the AN/TPN-18A extends to as much as a 35-degree scan angle, providing an ideal instrument for height-finding operations. The indicator display may be expanded from the -1 degree to +10 degree angle to a -1 degree to +35 degree angle. During precision approach operations, the AN/TPN-18A scans an azimuth sector as wide as 60 degrees, providing unusual equipment siting flexibility. Extra-wide 60-degree azimuth scan allows AN/TPN-18A to look at a 10-mile-wide sector at a 10-mile range or a 20-mile-wide sector at a 20-mile range. The selection of the 30- to 60-degree azimuth scan is an operational control.

The apparent beamwidth of the elevation antenna is reduced through instantaneous automatic gain control techniques which allow the operator to detect small deviations from the glidepath. The operator may also remotely select either linear or circular polarization. Circular polarization significantly reduces the clutter effect of rain or snow.

COVERAGE:
Search mode: 360 deg azimuth, 24 nmi detection range (1 sq m target, P_D = 90%, Swerling I)
40 nmi display range
80 nmi range (beacon return)
Height finder mode: 35 deg elevation; 30 deg azimuth
Precision approach mode: 11 deg elevation; 30 deg azimuth
Extended azimuth mode: 11 deg elevation; 60 deg azimuth

DATA RATES:
Search: 4 sec
Height finder: 1 sec; 1 azimuth and 1 elevation look every sec
Precision approach: 1 sec; 1 azimuth and 1 elevation look every sec
Extended azimuth: 2 sec; 1 azimuth and 1 elevation look every 2 sec
Simultaneous ASR and PAR: 4 sec azimuth, 2.5 sec elevation

ACCURACY:
Search: 2.0 deg azimuth; 500 ft or 2% range
PAR: 20 ft or 0.5 deg azimuth
20 ft or 0.5 deg elevation
60 ft or 1% range

ELEVATION ANTENNA:
Beam width: 3.2 deg horizontal, 1.1 deg vertical
Gain: 35 db vertical
Polarization: circular or linear
Size: 8 ft high by 2 ft wide

AZIMUTH ANTENNA:
Beam width: 1.1 deg horizontal; 3.5 deg vertical cosec ^{2} to 27 deg
Gain: 36.5 db
Polarization: circular or linear
Size: 6.5 ft wide by 4 ft high

TRANSMITTER:
Frequency range: 9.0 to 9.6 GHz (tunable)
Peak power: 200 kw nominal
Modulator type: line type, solid-state
Pulse width: 0.2 μsec or 0.8 μsec, selectable
PRF: 1200 pps

RECEIVER:
Type: superheterodyne double conversion
MDS: wide pulse (0.8 μsec) mode: 107 dbm min
narrow pulse (0.2 μsec) mode: 102 dbm min
Noise figure: 6.6 db max
Bandwidth: wide pulse mode: 2.0 ±0.5 MHz
narrow pulse mode: 5.0 ±1.0 MHz
STC: RF STC selectable by operator
FTC: log or linear or off selectable by operator

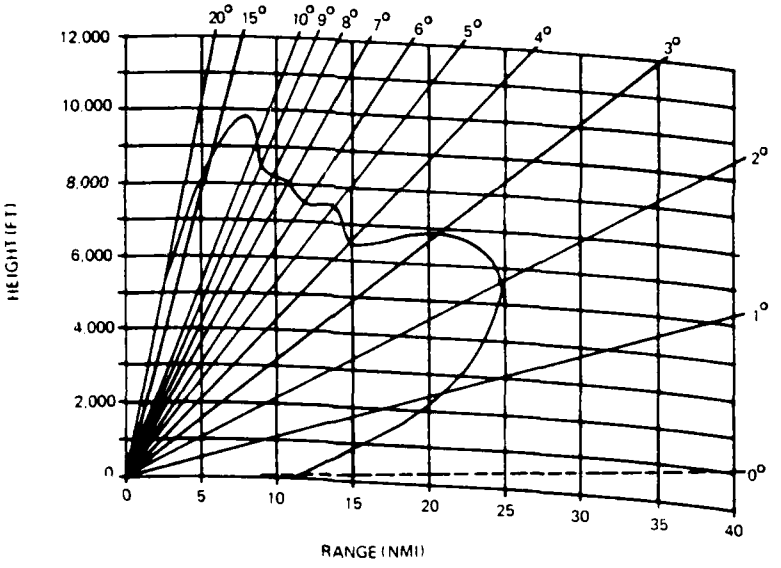

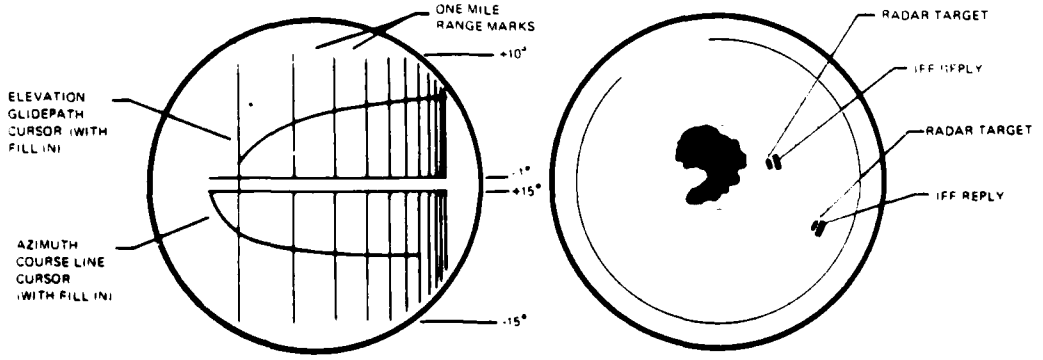

Az-el Beta Scan Display **PPI Display**

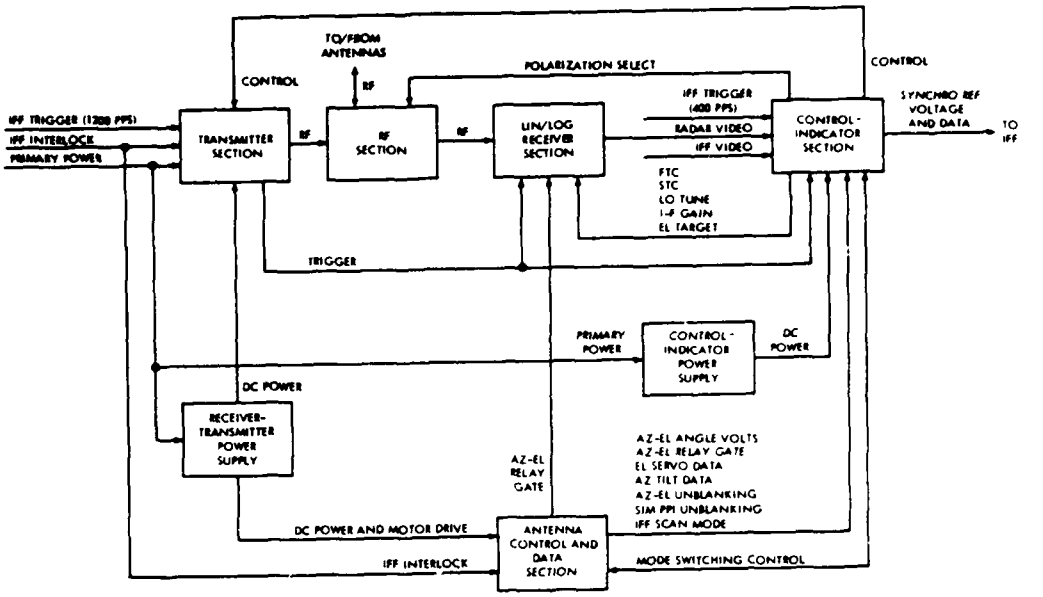

AN/TPN-18A Functional Organization

Both the elevation and azimuth antennas are horn-fed sections of a paraboloid reflector constructed from epoxy-laminate honeycomb fiberglass and supported by a back structure for rigidity.

The elevation antenna has a dual horn feed for monopulse operation. Elevation scan coverage is from -1 degree to +10 degrees or +35 degrees, and the antenna can be slewed plus or minus 15 degrees in azimuth by the operator.

The azimuth antenna has a single horn feed and has both circular and horizontal polarization. Azimuth coverage may be over a 30-degree sector, 60-degree sector or continuous revolution at 16 rpm. The antenna can be tilted vertically from 1 degree to +25 degrees.

The transmitter RF power source is a solid-state tunable magnetron oscillator operating in the X-band (9000 to 9600 MHz). Peak power out is 200 kilowatts nominal with a pulse repetition rate of 1200 pps. The trigger generator and pulse forming networks are implemented with solid-state components.

The receiver is a double conversion superheterodyne which will operate as both a single or dual channel system. When operated as a dual channel receiver, the difference channel provides instantaneous gain control for the sum channel to provide an increased angular resolution mode. A linear-logarithmic amplifier is operator selectable. RF sensitivity time control (STC) is provided.

Two identical control indicators present either PPI or az-el beta scan displays on 5-, 10-, 20-, 40-, or 80-mile ranges. When operated in the height-finder mode, the operator positions a height cursor on the elevation portion of the beta scan display and the altitude of the aircraft is read directly from a counter on the control indicator. When operated in the simultaneous mode, one of the two indicators displays ASR data while the other displays PAR data. IFF data only is presented on the 80-mile range. In the precision modes, IFF data may be displayed on one indicator in PPI while precision data is displayed on the master indicator.

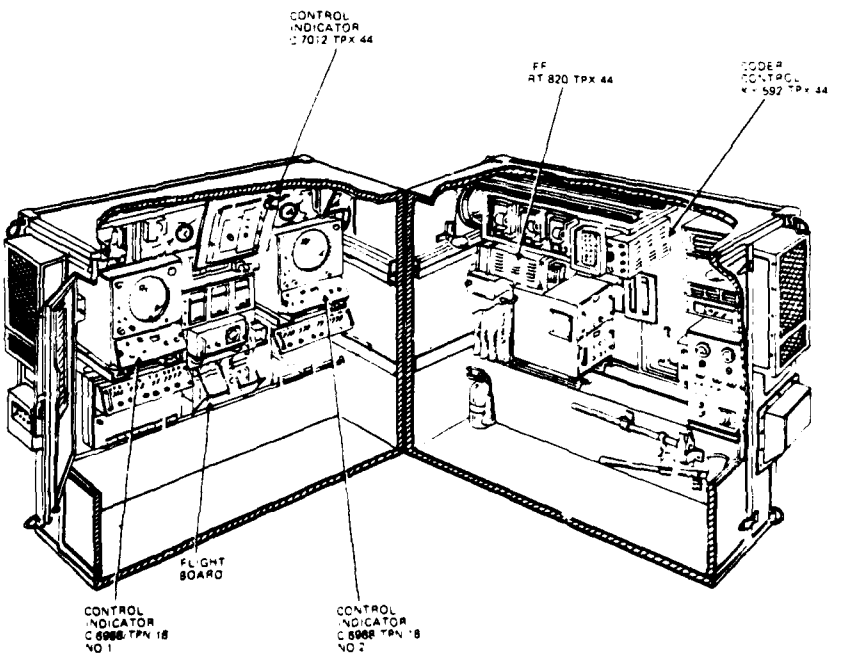

AN/TPN-18A Equipment Shelter

SUPPORT SERVICES

Your ITT Gilfillan equipment is always backed by a full range of logistics support services. We can furnish:

- Personnel to install your equipment
- Operator and maintenance personnel training
- On-site maintenance support which includes: field services engineers; off-the-shelf repair parts; complete operator, maintenance, and training documentation
- Factory overhaul services

For further information about ITT Gilfillan equipment or logistics support services, please call the nearest office in your location.

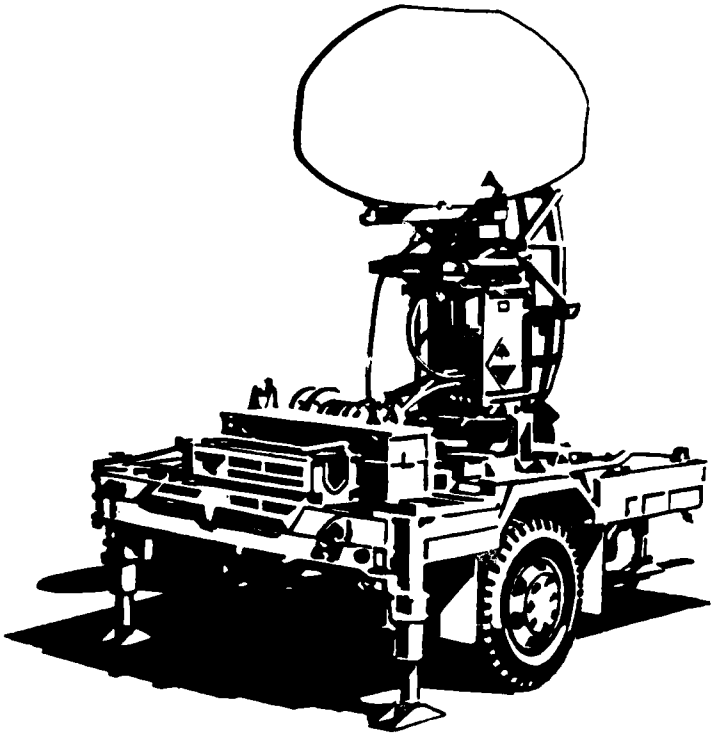

UNITED STATES (East Coast)

ITT Gilfillan
1707 L St. NW
Suite 300
Washington, D. C. 20036
Telephone: (202) 296-6000

EUROPE

ITT TE Group - NA
Avenue Louise, 480
1050 Brussels, BELGIUM
Telephone: 649 96.20

MIDDLE EAST

ITT Africa and the Middle East
P.O. Box 709
Tehran, Iran
Telephone: 830889

ITT TE Group – NA
P.O. Box 5239 Jabal Amman
Amman, JORDAN
Telephone: 42071

FAR EAST

ITT Far East & Pacific, Inc.
P.O. Box 5249 G.P.O.
Hong Kong
Telephone. H-251251

ITT Far East & Pacific, Inc.
P.O. Box 2401
Jakarta, INDONESIA
Telephone. 53411-5

SOUTH AMERICA

Intertrade Office
Standard Electrica, S.A.
Praca Aquidauana 7 Vincente Carvalho
Caixa Postal 20.049
20.000 Rio de Janeiro RJ Z C 22
BRAZIL
Telephone 230 9863

The best ideas are the ideas that help people.

AD-A119 536 ITT GILFILLAN VAN NUYS CA F/G 17/9
FREQUENCY SCANNING RADAR CONCEPTS FOR ARMY HIGH ENERGY LASER WE--ETC(U)
APR 82 C BARFIELD, D EPPS, S HOWARD DAAH01-81-C-A782
UNCLASSIFIED NL

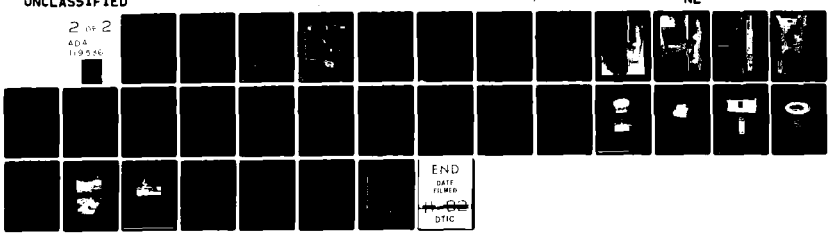

APPENDIX E

ARBAT RADAR DESCRIPTION

3.3 ARBAT Radar Description

3.3.1 General

The ARBAT (Application of Radar to Ballistic Ammunition Testing) radar was designed for ARRADCOM at Picatinny Arsenal for use in testing both production lots and experimental (R & D) rounds. The driving issues behind the development in the R & D role were the cost of handmade experimental rounds and the need for a large amount of data on each shot necessitating an automatic system capable of collecting trajectory and event data from 25 milliseconds after round exit from the tube to maximum tracking range, or to round event, if any. In the production testing role the need was a system capable of collecting a large amount of data during flight and the capability to provide selected specific data on a "quick-look" basis without the delay associated with reduction of the detailed data for the large number of rounds required in lot acceptance testing.

The ITT-G design is based on an X-band fully coherent transceiver with 700 mHz bandwidth. The transceiver operating frequency is determined by a digitally controlled synthesizer which is in turn controlled by a Data General Eclipse general purpose processor via an ITT-G special purpose processor interface. All transceiver variable operational parameters (PRF, RF gain, transmitter frequency, phase command) are controlled digitally via the central processor. The same commands may be initiated manually via thumbwheel switches for testing and calibration purposes.

The transmitter configuration is a TWT output stage using a nominally 25 kW peak power TWT driven by a 1.0 watt TWT which is in turn driven by a X36 varactor multiplier located in the transceiver (on the antenna). The X36 multiplier is driven by the synthesizer located in the operations van. A simplified block diagram of the overall system is shown in Figure 3.3a and a pictorial functional organization of the major hardware elements is shown in 3.3b.

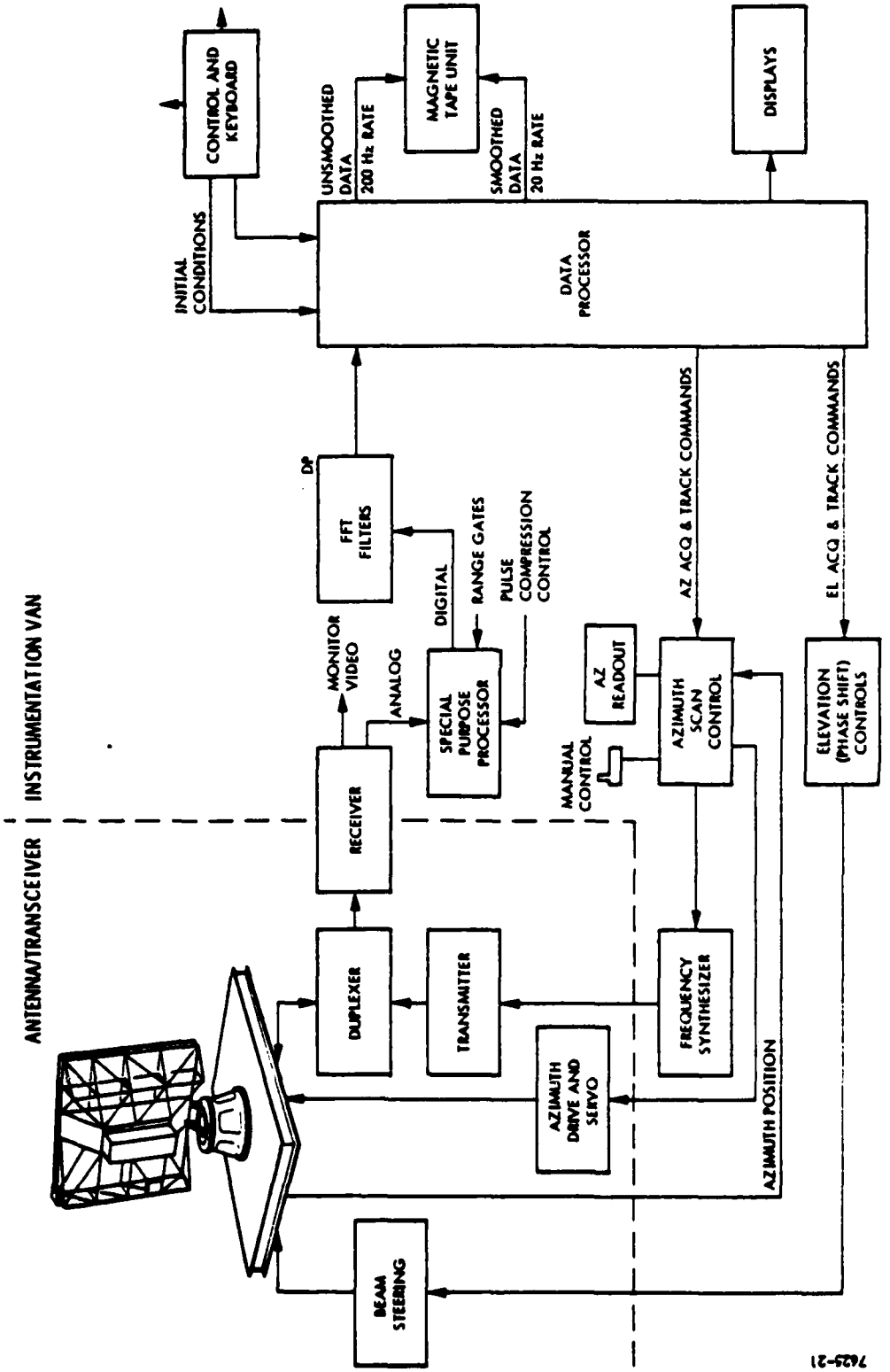

Fig. 3.3a Functional Organization of Proposed Instumentation Radar

Fig. 3.3b

FUNCTIONAL ORGANIZATION OF ARBAT

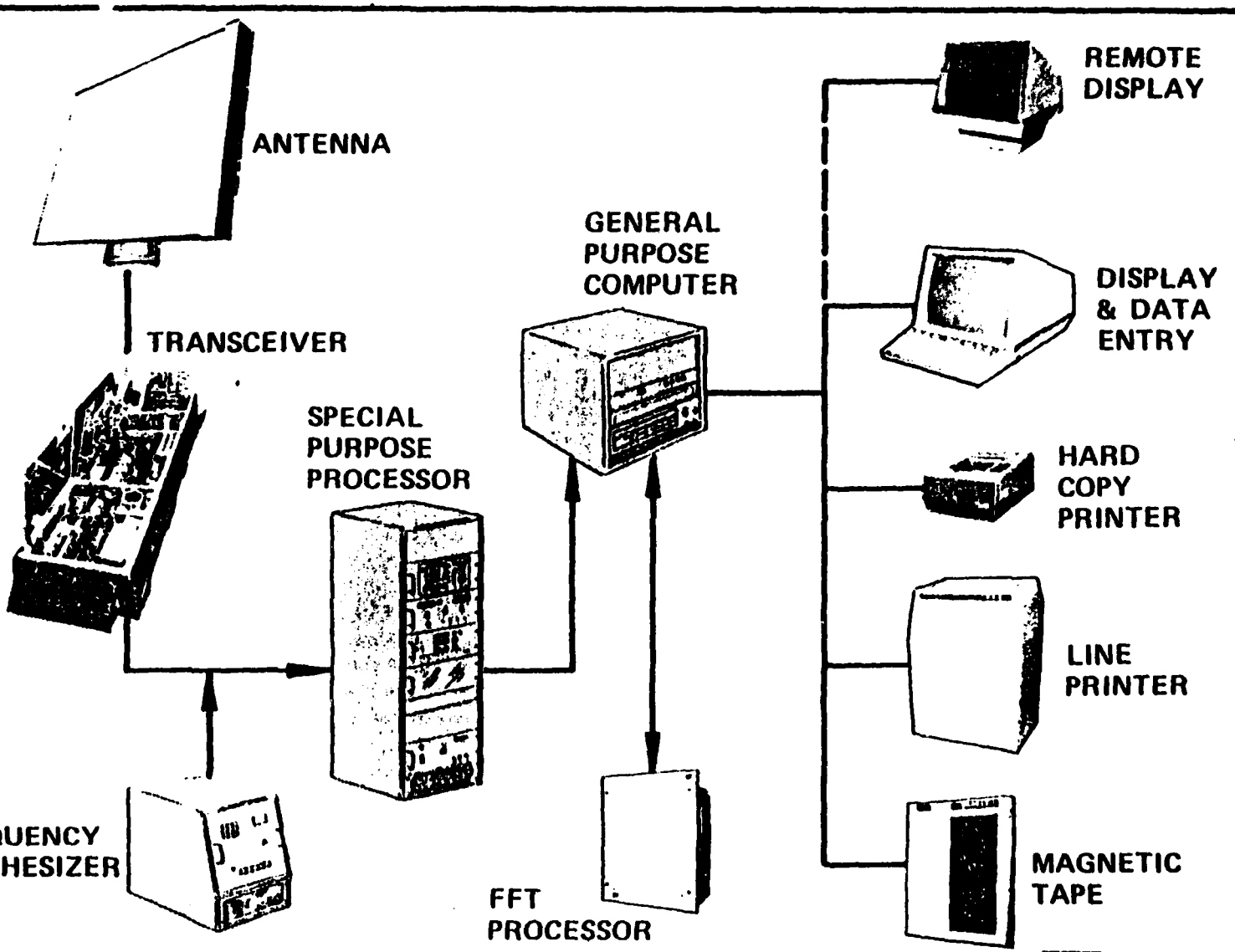

0010-23

ITT GILFILLAN

The ARBAT system antenna employes a planar array, with an aperture of 10 ft. X 12 ft., which radiates a pencil beam 0.55 degrees in azimuth by 0.66 degrees in elevation, phase scans the beam in elevation for 70^{0}, frequency scans in azimuth over 7^{0}, and mechanically scans in azimuth $\pm 170^{0}$. A combination of phase and frequency scanning steers the beam electronically over the above increments which complements the mechanical azimuthal scan. A schematic of the array is shown in Fig. 3.3c.

The beam is formed and scanned in elevation by 167 reciprocal digital diode phase shifters fed from a vertical series line feed containing 167 four-port couplers of the cross-guide type. The vertical line feed is constructed of standard X-Band waveguide. Power is fed into the waveguide transmission line at the bottom of the array and is coupled out of the primary line by crossguide couplers. To achieve the desired sidelobe performance, the crossguide coupling values have been selected to give a Taylor excitation function in the elevation plane of the array. The small amount of power (2 percent) left over at the end of the line is dissipated in a terminating load.

The phase shifters are controlled by a digital beam-steering buffer whose principal function is to generate the required incremental phase shift required to scan the beam in elevation. These phase commands provide correction for two effects that otherwise would produce inaccuracies; 1) the array beam-forming elements are frequency sensitive and, without correction, would produce an undesired elevation scan with azimuth frequency scan; 2) RF phase randomization is incorporated in the elevation beam-forming elements to reduce the phase-quantization sidelobes that would ordinarily be produced by the digital phase shifters.

Since the antenna has the ability to electronically scan 70^{0} in elevation, the plane of the array has been tilted back 25^{0}. This provides for the -10^{0} and the $+60^{0}$ elevation scan volume without mechanical tilt.

The one-sigma accuracy, including stability, of the analog-digital antenna temperature sensor is 2 degrees C. This accuracy factor corresponds to an antenna pointing angle accuracy (as a function of temperature) of 0.115 milliradians.

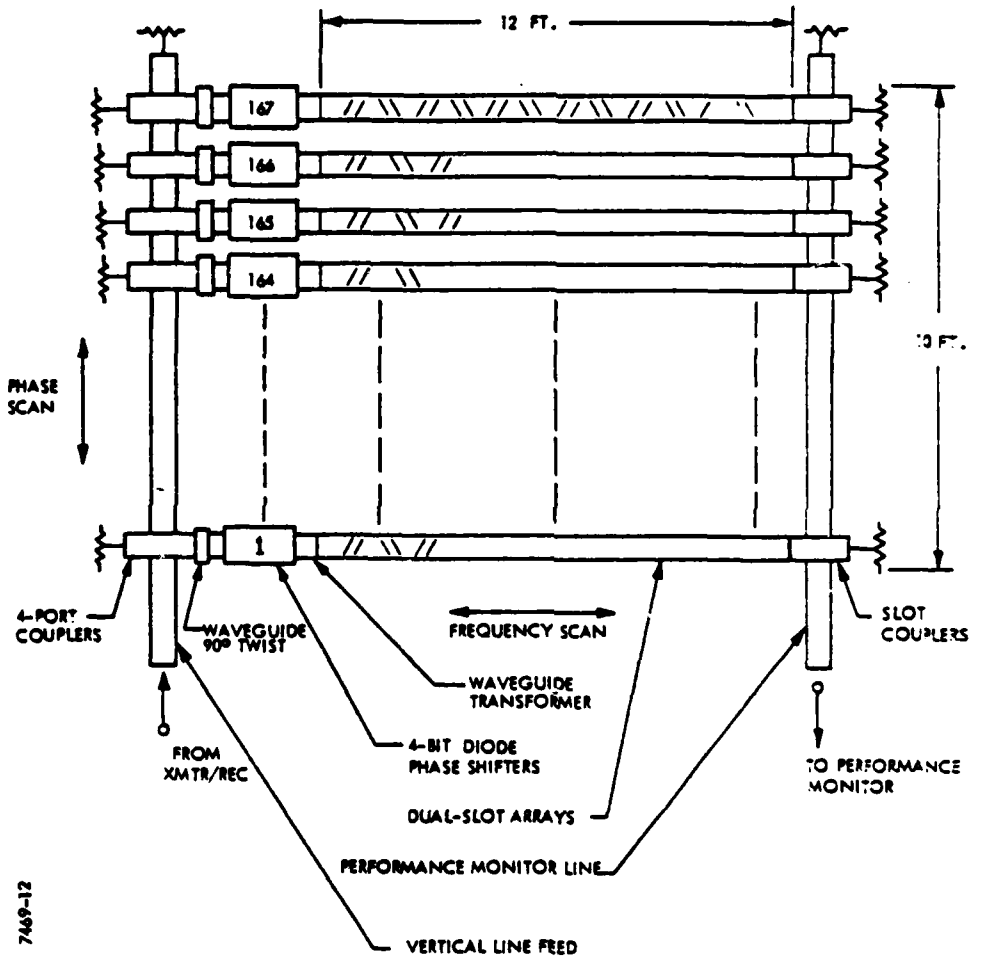

Antenna Schematic showing Arrays and Phase Shifters

FIG. 3.3c

The radar beam is steered $\pm 170^{0}$ in azimuth by mechanical rotation of the array. In addition, the beam can be positioned $\pm 3.5^{0}$ from array normal by selection of the transmitted frequency. The Data Processor determines the correct combination of frequency and mechanical steering to maintain track under conditions of maximum radial acceleration. The horizontal arrays which form and position the beam in azimuth are X-Band waveguides with 322 edge-slot radiators paired to achieve wide band performance.

A performance monitor line is connected to the horizontal arrays between the last pair of slots and the load located at the end of the arrays. Some of the power remaining at the end of the arrays is coupled into the monitor line where it combines to form a signal which is used as a dynamic check of the quality of antenna performance.

Antenna temperature is sensed at two points with a resistance thermometer. The current through the thermometer is amplified by an operational amplifier and converted to a 6-bit binary word in an A/D converter.

3.3.2 ARBAT Subsystem

The ARBAT systems is organized into two subsystems, the Antenna Subsystem and the Instrumentation Van Subsystem. The Antenna Subsystem includes the following major units/groups:

a) Transport vehicle
b) Antenna Pedestal
c) Antenna Servo Drive and Control
d) Antenna
e) Transceiver (Transmitter, modulator, H.V. power supply, X-band receiver, programmable T-R limiter, up/down conversion elements, First and Second IF amplifiers and line drivers)
f) Beam Steering Buffer
g) Antenna Waveguide Dehydrator
h) Phase Shifter Power Supplies

i) Beam Steering Buffer and Antenna Performance Monitor Circuits Power Supply.

The Instrumentation Van subsystem includes the following major units/ groups:

a) Frequency Synthesizer
b) Second IF and Video Processor
c) Radar Set Control
d) Special Purpose Processor
e) Operator Console/Keyboard
f) General Purpose CPU (Data General Eclipse)
g) Array Processor
h) Mag Tape units (2)
i) Mag Disc
j) Hard Copy Unit
k) Teletype

The following figures show the Antenna Subsystem (Figs 3.3d and 3.3e) and the Instrumentation Van Subsystem (Figs 3.3f and 3.3g).

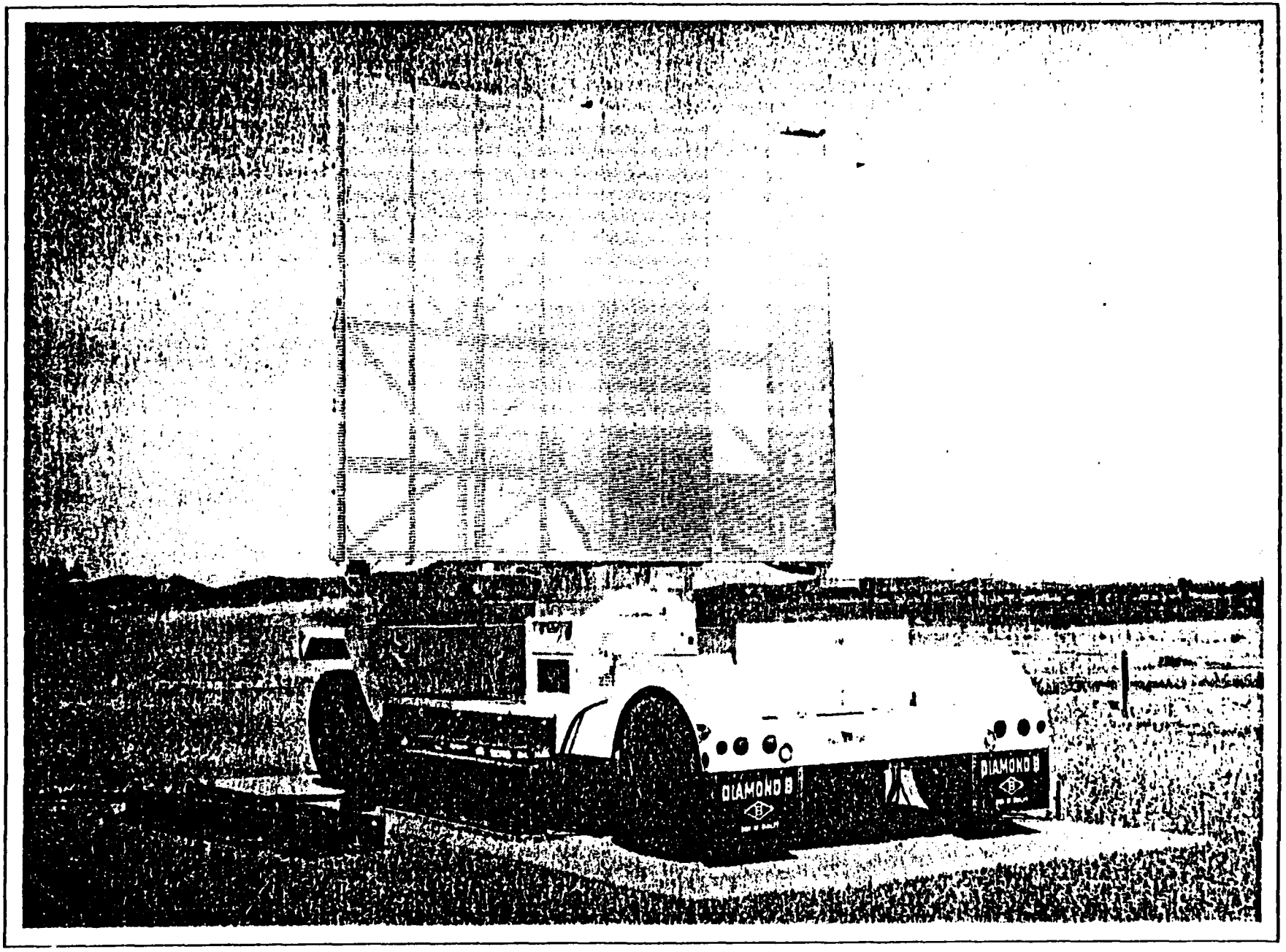

P14088-4

FIG. 3.3d ARBAT ANTENNA SUBSYSTEM (FRONT)

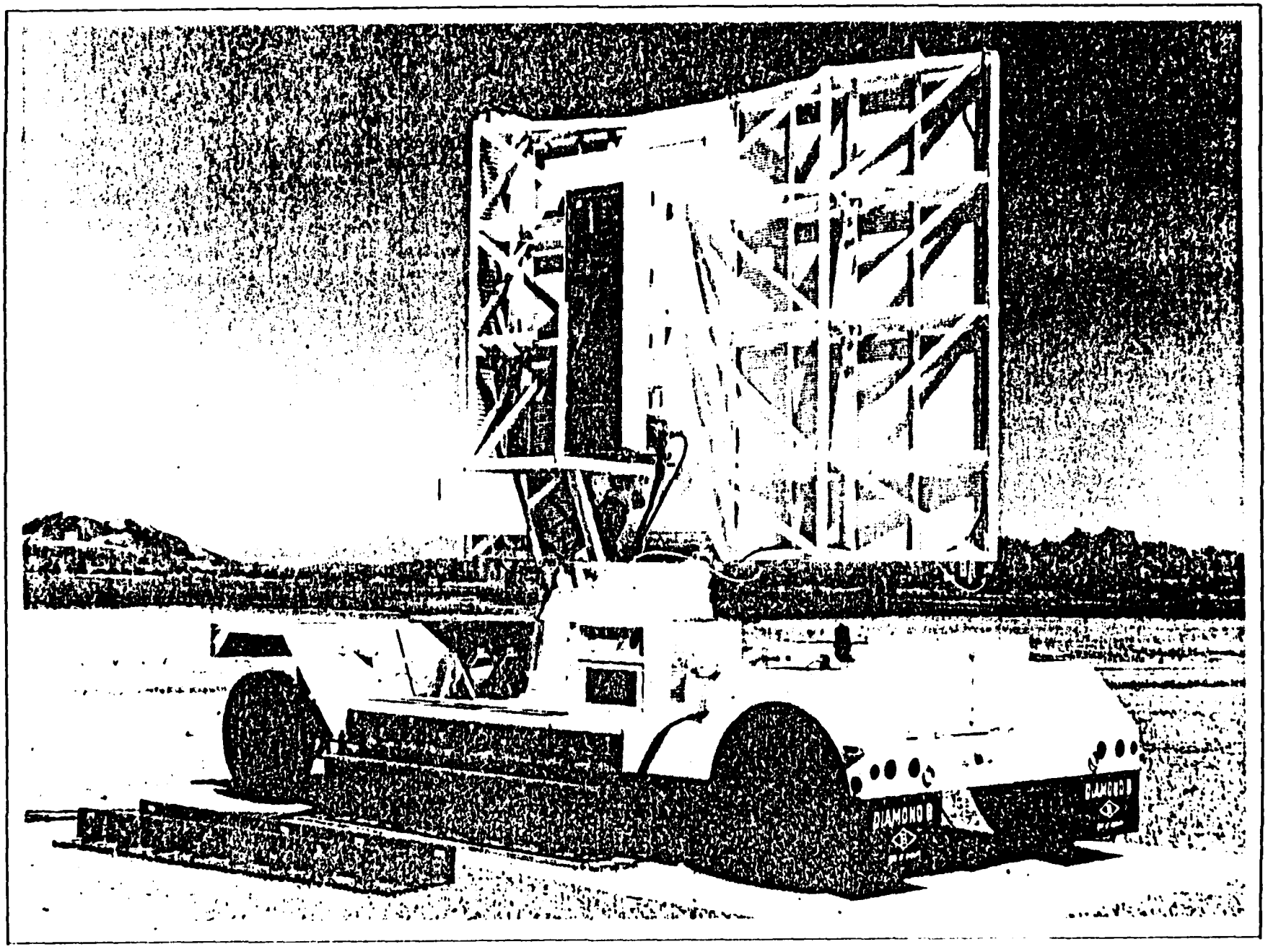

FIG. 3.3e ARBAT ANTENNA SUBSYSTEM (REAR)

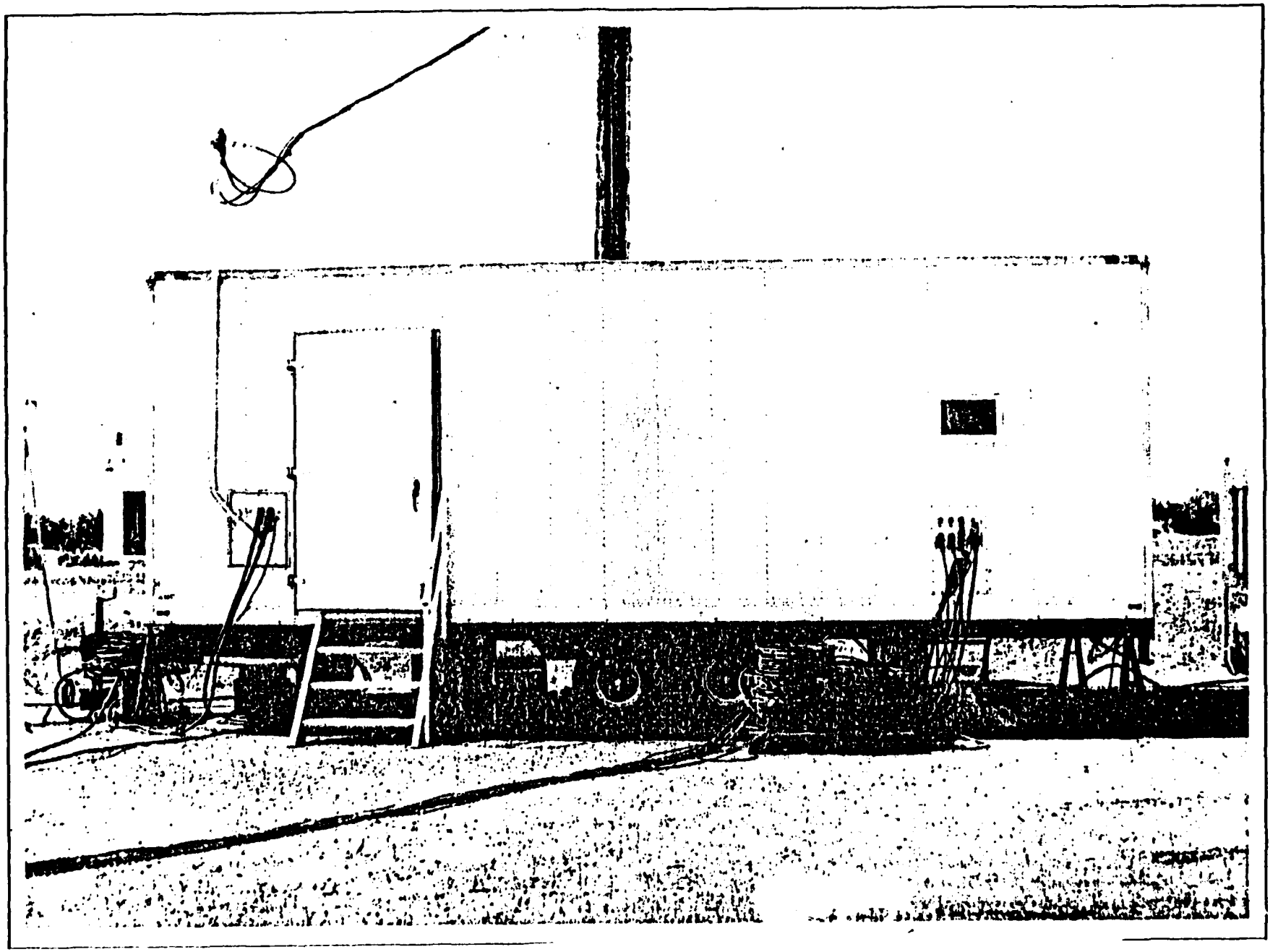

FIG. 3.3f ARBAT INSTRUMENTATION VAN

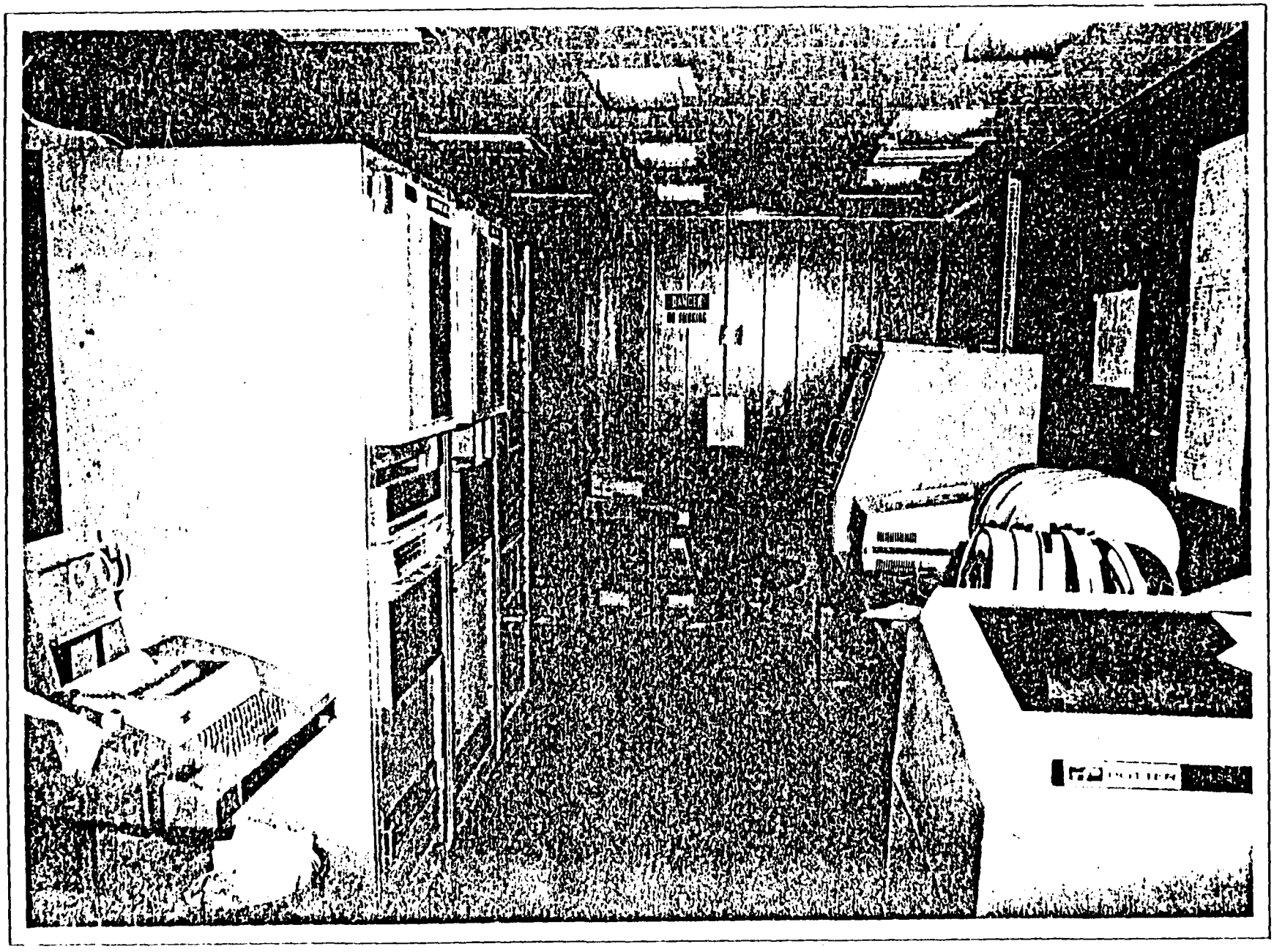

214088-3

3.39 ARBAT OPERATION CONTROL

APPENDIX F

DESCRIPTION OF THE RASIT 72A GROUND SURVEILLANCE RADAR

DESCRIPTION OF THE RASIT 72A GROUND-SURVEILLANCE RADAR

September 1976

TABLE OF CONTENTS

1 GENERAL INFORMATION

The RASIT is a mobile radar for battle-field surveillance. Its role is similar to that of a pair of binoculars of enormously increased range (20 km), whose vision is not affected by darkness or poor weather.

It can detect, acquire, recognize and locate, by directly reading, the polar or geographical coordinates moving objects on the ground or close to the ground, such as isolated infantrymen, infantry, vehicles, tanks, and low flying aircraft and helicopters.

The RASIT radar consists of four light, rugged, watertight, small units, each weighing less than 27 kg which are easily transportable, and can be set up on the ground very quickly. It is also easily installed on a vehicle or in an air-transportable shelter and operates from battery power.

Its operation does not require specially trained personnel, and it is fitted with an audible alarm which sounds as soon as a moving object is detected. It is difficult for the enemy to detect the use of the radar because the control console can be hidden up to 50m from the HF head, transmissions are short and infrequent, and the radar has special counter/counter-measures circuits.

Its integral test system and modular construction make test and maintenance both easy and rapid.

2 EMPLOYMENT

2.1 *PREPARATION FOR USE*

If the RASIT is installed in a vehicle:

> The only operation required is to turn on the equipment power, which raises the reflector from its folded travel position.

If the RASIT is installed on the ground:

Its preparation consists in mounting the three legs and the HF head on the rotating mechanism and plugging in the four connecting cables.

2.2 *OPERATION*

Provides surveillance by automatic antenna sector scanning over a sector of 30^{o} to 120^{o}, in any direction and up to a range of 20 km for general surveillance or over a 2.5 km range bracket for high-definition surveillance. An automatic alarm sounds as soon as a moving object enters the surveyed zone, thereby reducing operator fatigue during the automatic surveillance of an area.

Acquisition/Recognition – with the antenna stationary, the operator places the marker on a particular echo and can then read the target polar and geographical coordinates while the Doppler sound enables him to identify the target.

The track made by the target is plotted on the oscilloscope and can be transferred onto a plotting table.

3 CHARACTERISTICS AND PERFORMANCE

3.1 *TECHNOLOGY*

In order to improve the detection probability for low-level echoes, the RASIT uses:

The principle of coherent reception, which eliminates the need for fixed return close to the moving target to be detected,

The principle of fixed echo elimination by contiguous range gates associated with Doppler filters.

The RASIT operates with either linear polarization under most weather conditions, or with circular polarization in the event of atmospheric disturbances (rain, snow, etc.).

Integrated-circuit and micro-electronic technology is used. The only tubes are the magnetron and the scope.

3.2 PERFORMANCE

3.3 OPERATIONAL PERFORMANCE CHARACTERISTICS

Range (for a detection probability of 90 percent)

For pedestrian	12 to 14 km
For jeep	18 to 20 km

Accuracy

In range	±10m
In bearing	±10 mils

Discrimination between close targets

In range	40m
In bearing	45 mils

Sectors surveyed

Adjustable from ±200 to ±1100 mils about the sector center-line, the latter being positioned anywhere in a 360° circle by a control on the console.

Elevation angle

Adjustable from -200 to +400 mils by a control on the console.

Distance between the operator's console and the antenna

Maximum 50m

3.4 ENVIRONMENTAL CONDITIONS

a. Operating

Temperature	-40° to +55°C
Wind	70 kph with gusting up to 120 kph
Damp heat	+40°C with 95 percent humidity
HF head sealing	Tropical rain and sand storm
Console sealing	Dripping water

b. Transportation (radar switched off and reflector folded)

Vibration	5g from 10 to 55 Hz (installed on a tank)
Impact	40g for 6 msec (installed on a tank)

c. Storage

Temperature	-40^{o} to $+70^{o}$C

3.5 *TECHNICAL CHARACTERISTICS*

a. Transmitter

Frequency	Switchable from 9.5 to 9.7 GHz in order to evade jamming and interference
Peak power	3 kW

b. Receiver

Noise factor	10 dB
Sensitivity	Manually adjustable
Fixed-echo elimination factor	43 dB
Range gates	64
Range gate size	
normal mode	320m
expanded mode	40m
Doppler filters	
Bandwidth	either 180 to 1830 Hz or 60 to 250 Hz (selected by the operator)

c. Antenna

Beamwidth in azimuth	2.7^{o}
Beamwidth in elevation	4^{o}

d. Displays

All data required by the operator appear on the screen of a television type oscilloscope (daylight viewing):

Radar map on a type B screen (bearing/range), with digital storage of target coordinates:

- normal radar map (all echoes), or
- fast target display only, or
- slow target display only.

Numerical target data:

- bearing and range (polar coordinates),
- longitude and latitude (UTM coordinates).

Radar operating mode indications:

- operating mode,
- expanded display origin,
- antenna orientation.

All these data may be transmitted in encoded form to central intelligence by means of an optional interface equipment.

4 EQUIPMENT REQUIRED

4.1 *BASIC EQUIPMENT*

The HF head consisting of the transmitter/receiver, the antenna and the sighting telescope. The transmitter/receiver is housed in a sealed case. The assembly is mounted on the rotating part of a rotational mechanism by means of four quick-release fasteners.

The rotational mechanism is a sealed unit carrying a part rotating in bearing on which the HF head assembly is mounted.

The operator's console with a built-in loudspeaker, this console being in the form of a unit impervious to dripping water.

The power converter is a small sealed unit mounted on the right side of the console. It produces all the voltages required for operating the equipment from a primary 21 to 28 Vdc supply.

Set of interconnecting cables

Between the HF head and the mechanism	0.30m
Between the mechanism and console	3.50m

Between the console and converter	0.15m
Between the converter and external power supply	3m

4.2 *OPTIONAL EQUIPMENT*

Three legs to support the rotational mechanism when operated on the ground. 50-meter cable replacing the 3.50m cable mentioned above for operating the console away from the antenna. Head-set for operating the equipment silently when a radio link is in use.

5 DIMENSIONS AND WEIGHTS

		Length mm	Width mm	Height mm	Weight kg
HF Head	Reflector unfolded	800	600	750	28
	Reflector folded	800	600	370	28
Rotational mechanism		300	300	280	17
Console		570	305	235	23
Power converter		100	305	235	7
Set of cables		–	–	–	2
	Total	–	–	–	77

6 POWER SUPPLY

The power supply is provided by the user, which may be any of the following:

A 24 Vdc vehicle battery,

A 24 Vdc generator,

Any other 24 Vdc source.

The power source should have the following characteristics:

Voltage	21 to 30V
Load	6A at 25V
Power consumption	150W

7 TEST AND MAINTENANCE

Equipment tests are performed at two levels.

A 10-position switch on the front panel of the console enables the operator or technician to locate the defective function or subassembly (integral test system),

Another 10-position switch on the front panel of the power converter, associated with a built-in meter for checking all the RASIT power supplies.

Test sets are available for locating any defective module or board.

All equipment functions are performed by plug-in subassemblies in order to facilitate maintenance.

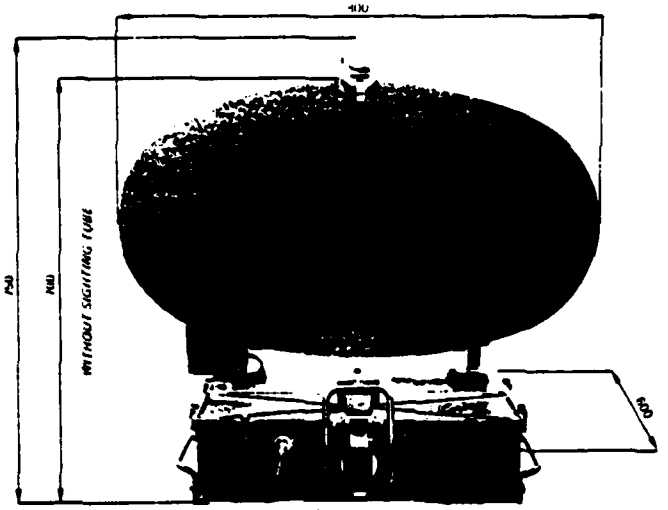

HF HEAD OPERATING POSITION

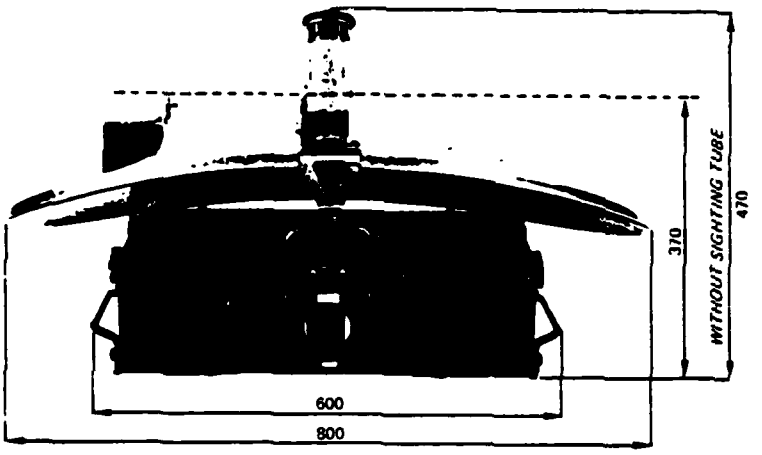

HF HEAD TRANSPORT POSITION

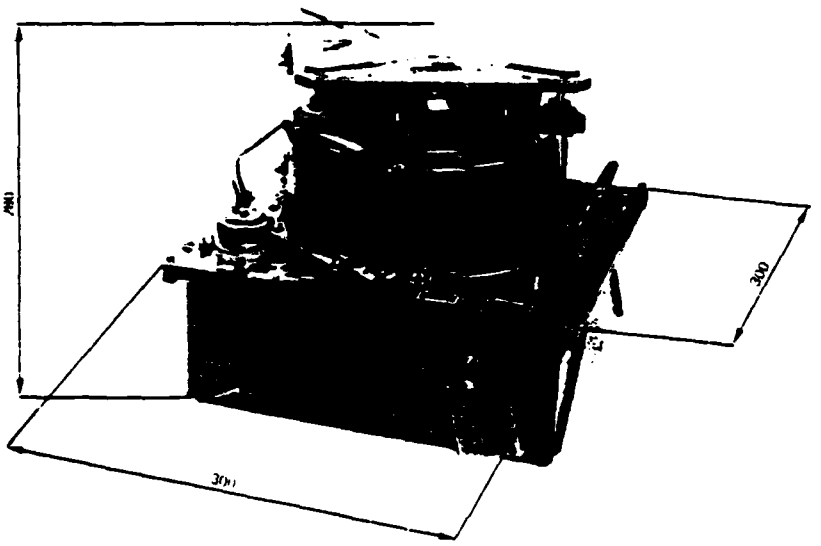

ROTATIONAL MECHANISM

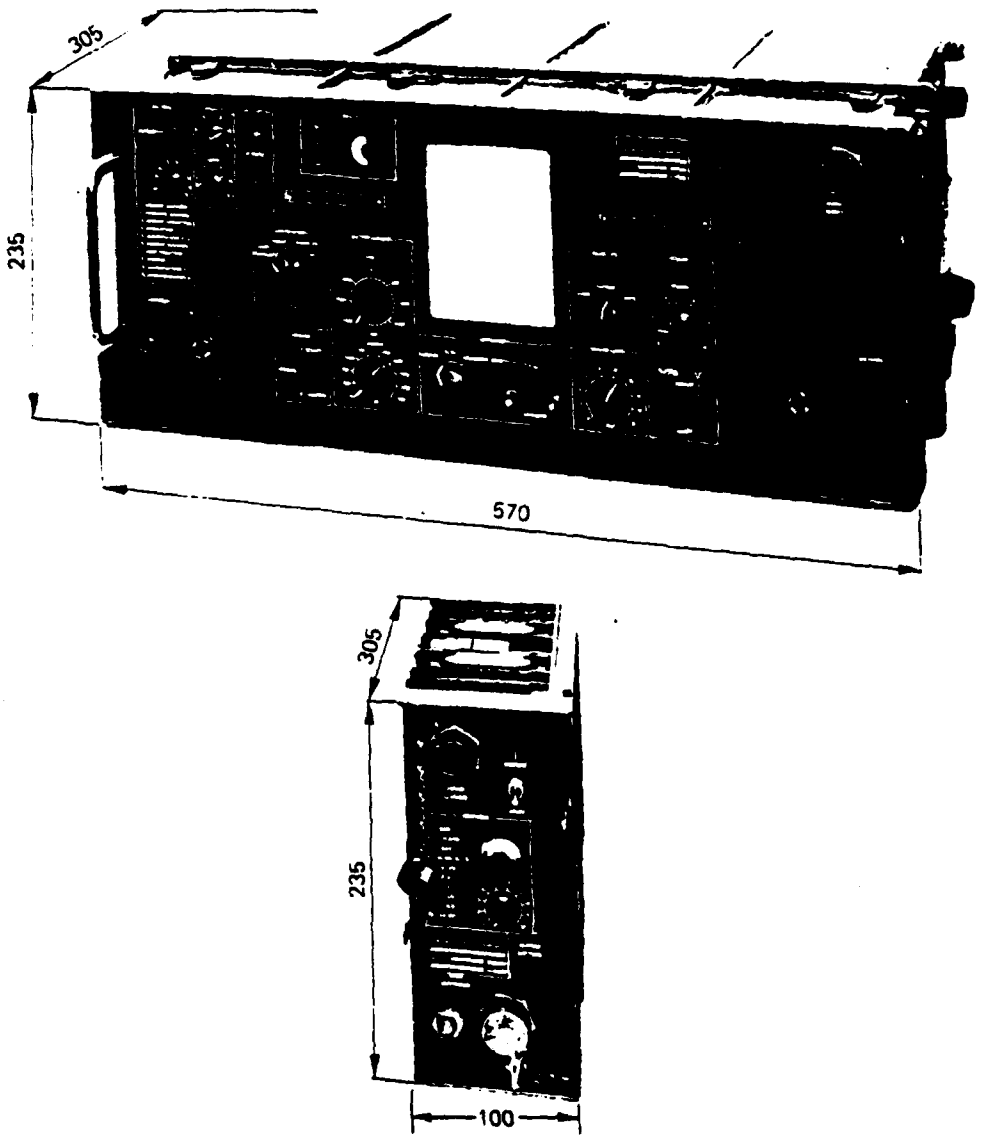

OPERATING CONSOLE AND POWER CONVERTER

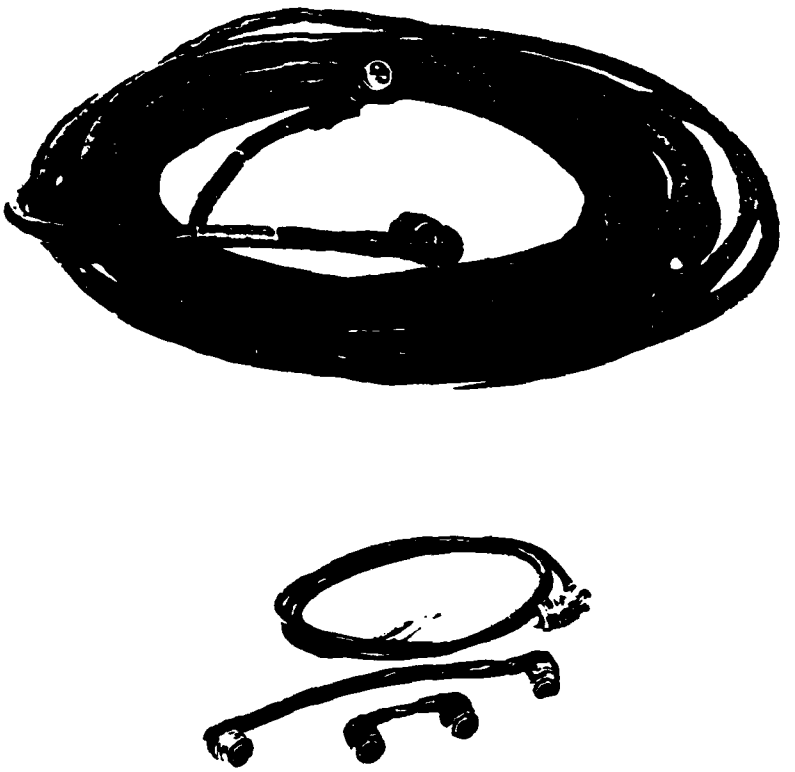

SET OF INTERCONNECTING CABLES

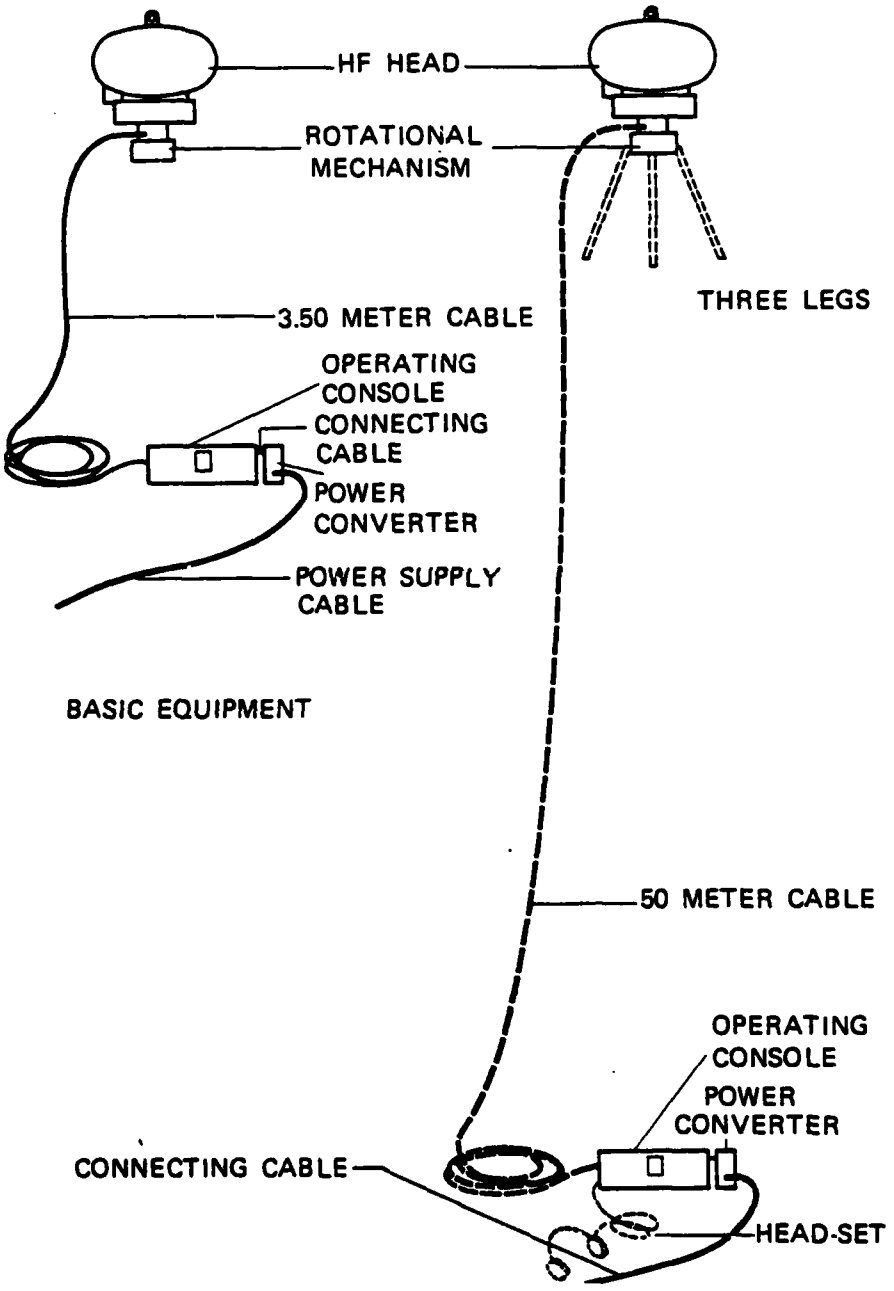
HF HEAD
ROTATIONAL MECHANISM
THREE LEGS
3.50 METER CABLE
OPERATING CONSOLE
CONNECTING CABLE
POWER CONVERTER
POWER SUPPLY CABLE
BASIC EQUIPMENT
50 METER CABLE
OPERATING CONSOLE
POWER CONVERTER
CONNECTING CABLE
HEAD-SET

EQUIPMENT IN OPERATION

ENTIRELY ON THE GROUND

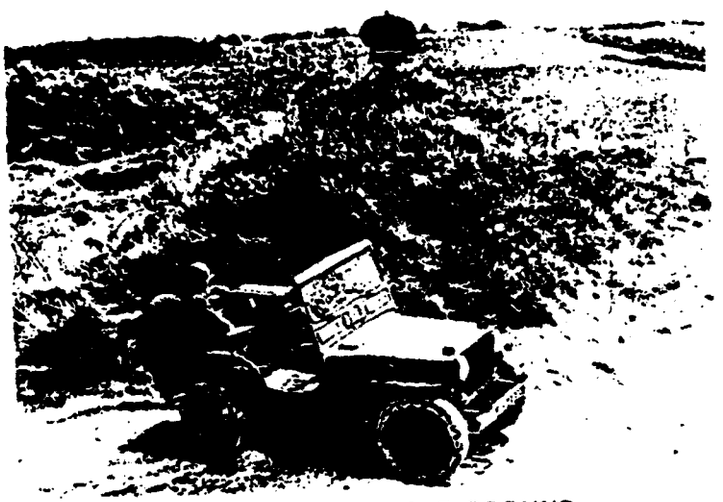

ANTENNA ON THE GROUND
CONSOLE ON A JEEP

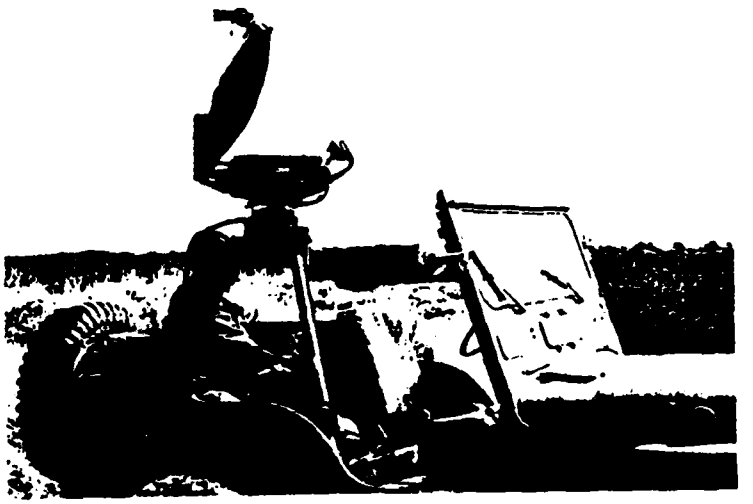

EQUIPMENT ENTIRELY ON A JEEP

APPENDIX G

COHERENT LASER RADAR

Coherent Laser Radar

Rationale:

Analyses, including the consideration of special processing techniques to negate the effects of multipath on low angle targets, have shown that the extraction of reliable and accurate elevation data on ground targets requires an optical adjunct. This conclusion was based on the smallest practical rf radar beamwidth capable of providing the total volumetric scan coverage required in an acceptable time period. As indicated in the previous report, an optical coherent laser radar based on either CO_2 or a dye laser head would be capable of providing the required data for low angle threats. It should be pointed out that millimeter rf radars to 93 gigahertz were considered before arriving at the conclusion that the optical subsystem would be required. The real differential is readily appreciated when, considering the fact that the same antenna gain and beamwidth relationships apply to optical and rf systems, that a CO_2 laser carrier frequency is around 30,000 gigahertz as compared to a 93 gigahertz millimeter wave rf radar. Basic relationships of frequency to beamwidth remaining, it will be noted that the CO_2 optical beamwidth can then be about 300 times (1/300) narrower than that of the 93 gigahertz rf radar and about 3000 times narrower than that of an X band rf radar. Doppler return frequencies from moving targets are correspondingly greater for the high carrier frequency of an optical radar which improves performance on slow moving targets and enables improved velocity resolution. In practice, such contrasting comparisons would not be implemented, rather the antenna (light radiator/receptor) would be far reduced in size to obtain the optimum balance between size, weight and gain/beamwidth. There is, of course, the obvious performance degradation common to all optical systems imposed by weather. It is worthwhile to note however, that the performance of a Neodynium YAG laser is slightly better than Ku band rf in rain, while it is much worse in terms of attenuation than the lower microwave frequencies. On the other hand, CO_2 is slightly inferior to Nd/YAG in rain, but it is much better in haze and light fog. In view of the same probable limitations on the weapon, the inclusion of a weather dependent subsystem to the prime system is not considered to constitute an unacceptable performance limiting factor. The high resolution and freedom from limiting multipath effects appears to fully offset the technical disadvantages in a weather limited subsystem. Because of the narrow beamwidth inherent in an optical system, the application in the FALW/FALW-D utilizes the optical radar only for limited area coverage after target detection by the

rf radar. This use avoids the relatively long search time which would be required if a large area was searched with the narrow optical beam.

Coherent Laser Configuration

The hardware requirements for a laser radar are shown in Figure 1, Laser Radar Block Diagram. The configuration shown is a "strapped down" system including the channels for multiple heads required for simultaneous illumination of up to five targets, however only a single head is shown to reduce diagram complexity. The additional laser heads if implemented duplicate the elements in the dotted line area labeled "optical head elements". If it is determined that a single or two simultaneous target capability is required, the hardware complement can be reduced by elimination of beam switches and optical heads. In this strapped down configuration the high power laser is located remotely from the radiating head by a mirror optical train and gimballed mirror radiator. Transmit/receive paths are implemented by means of a Brewster angle diplexer and return signal information enters the receiver after mixing with the LO signal via a mercury cadmium telluride quad detector. Three beam switching units are shown in the block diagram for the purpose of illustrating the hardware blocks necessary for multiple simultaneous target handling. The beam switchers may be either two or three channel devices. A single head is shown. The laser and beam switcher(s) will normally be located in dedicated equipment areas, the laser head(s) are located for unobstructed coverage of the surveillance volume and the remaining receiver elements, control and data output circuits are normally located for convenience in output interfacing. The specific type of laser has not been noted on the block diagram. Either a CO_2 or dye laser is compatible with this requirement. A major portion of the configuration shown has been built by ITT-G under a previous U.S. Navy program. The portions existing and the additional elements required for demonstration purposes are shown in the latter figure. The portion existing utilizes a lower power visible light HeNe laser for demonstration purposes.

FIGURE 1, LASER RADAR BLOCK DIAGRAM

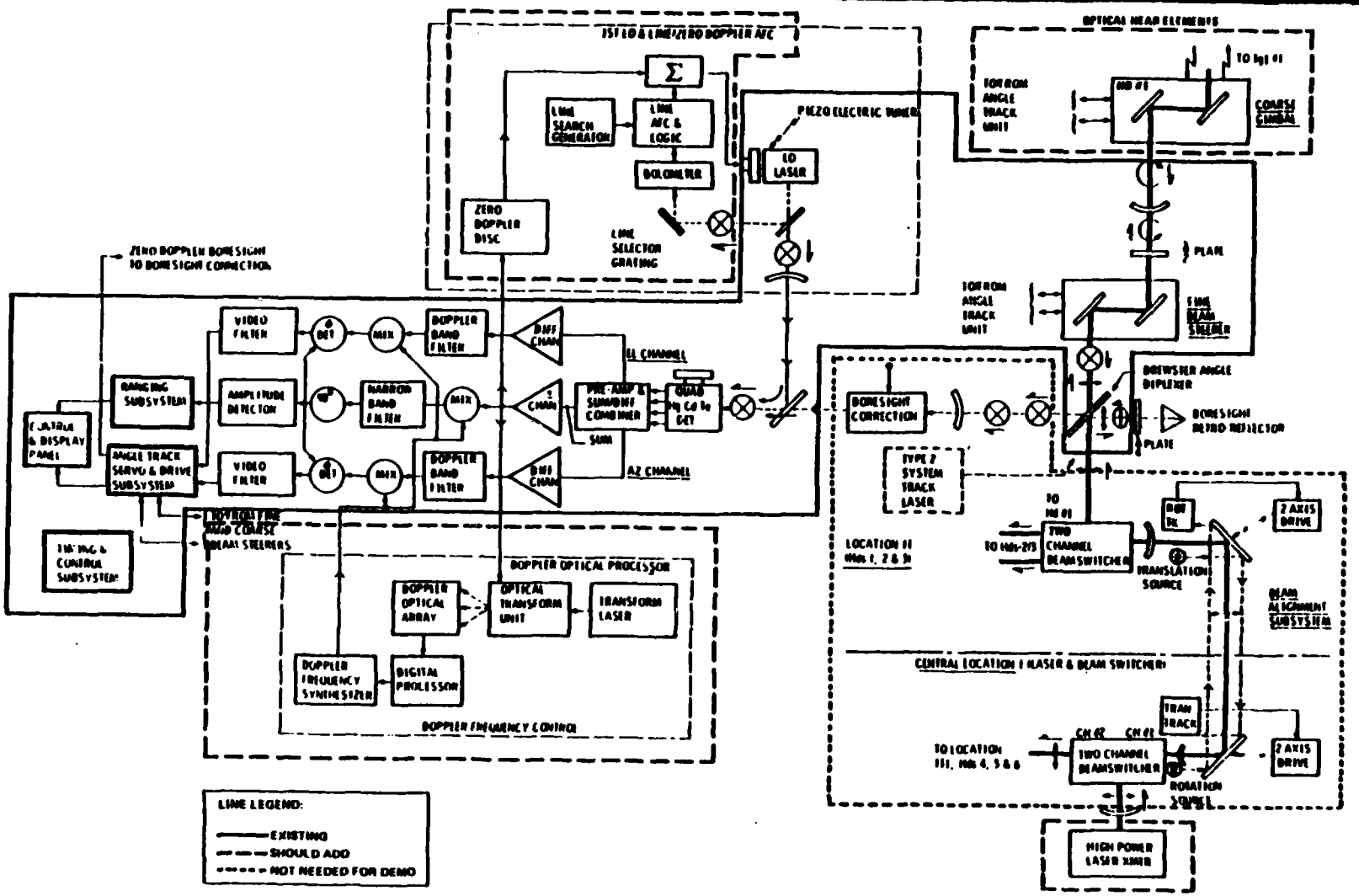

1057-34

ITT GILFILLAN

END

DATE
FILMED

11-82

DTIC